PALEOTEMPERATURE PROXIES: VALIDATION AND APPLICATIONS IN THE ATLANTIC AND PACIFIC OCEANS

A Dissertation

by

JENNIFER EVE HERTZBERG

Submitted to the Office of Graduate and Professional Studies of
Texas A&M University
in partial fulfillment of the requirements for the degree of

DOCTOR OF PHILOSOPHY

Chair of Committee,	Matthew W. Schmidt
Committee Members,	Ping Chang
	E. Brendan Roark
	Niall Slowey
Head of Department,	Deborah J. Thomas

August 2015

Major Subject: Oceanography

ABSTRACT

Paleotemperature proxies enable scientists to reconstruct past ocean temperatures from sediment recovered in deep-sea cores. This dissertation takes an in-depth look at two proxies, Mg/Ca ratios of planktonic foraminifera and the TEX_{86} index, and applies the Mg/Ca paleothermometer in a novel way to assess past changes in tropical Pacific climate.

Chapter II is a reinvestigation of a proposed large salinity effect on Mg/Ca ratios in the foraminifera *Globigerinoides ruber* based on a recent Atlantic core-top meridional transect study. Shell weight analyses and scanning electron microscopy are used to assess the preservation of similar *G. ruber* shells used in the core-top study. Shells from the equatorial Atlantic are highly dissolved compared to those from the subtropical gyres, impacting their Mg/Ca-temperatures. When Mg/Ca-temperature calibrations that account for dissolution differences are used, there is no longer an apparent large salinity effect, suggesting that regional differences in preservation, rather than salinity, significantly affect Mg/Ca-temperatures.

Chapter III investigates the TEX_{86} temperature proxy in the eastern Pacific by utilizing Mg/Ca paleothermometry on multiple species of planktonic foraminifera across the Holocene and Last Glacial Maximum (LGM) to determine the recording depth of the TEX_{86} proxy. Holocene TEX_{86} temperatures match sea surface temperatures, but during the LGM, there is a cold bias in TEX_{86} temperatures that are more representative of the

upper thermocline. The best explanation for the offset is a decrease in LGM nutrient availability. Therefore, caution should be applied when interpreting TEX_{86} records based solely on the relationship between core-top/Holocene TEX_{86} temperatures and modern observational temperatures.

Chapter IV reconstructs past changes in the tropical Pacific mean state across Marine Isotope Stage 3 by utilizing Mg/Ca paleothermometry on the thermocline dwelling foraminifera *Neogloboquadrina dutertrei* from an eastern equatorial Pacific sediment core. The thermocline temperature record reveals interstadials are characterized by a more El Niño-like mean state, with increases in thermocline temperatures up to 6°C. Thermocline warming events are more pronounced from 64-44 kyr when global climate was in a warmer state. From 44-32 kyr, the record shows cooler thermocline temperatures, suggesting a shift to a more La Niña-like mean state, as climate began transitioning into the LGM.

To my parents, for their never ending support of my dreams.

ACKNOWLEDGEMENTS

First and foremost, I would like to thank my advisor, Matthew Schmidt, for his unwavering support of my dissertation endeavors. His enthusiasm, mentorship, and friendship all made the last five years everything I had hoped for and more.

I would also like to thank my committee members, Ping Chang, Brendan Roark, and Niall Slowey for their guidance and support throughout the course of this research. Mitch Lyle also provided invaluable discussions on many aspects of my research, and I am grateful for that.

Many, many thanks also go to my friends for making my time in Texas memorable. I would especially like to thank Julia for the endless hours of cribbage and wine that went into the last five years. We were destined to become friends.

I would like to thank Teddy Them and Andrew Parker for their help and guidance in the lab. Without their assistance and camaraderie this dissertation would not have been possible. Luz Romero also provided valuable technical assistance with the running of the ICP-MS.

I also want to extend my gratitude to the Department of Oceanography, the College of Geosciences, Texas Sea Grant, the Cushman Foundation for Foraminiferal Research, and the National Science Foundation for their funding of my graduate degree.

Finally, thanks to my family, especially my parents, for their encouragement and support of my hopes and dreams. The sky is the limit.

Specific acknowledgements for Chapter II: We thank Dr. Michael Pendleton from the Microscopy and Imaging center at TAMU for assistance with SEM imaging. We acknowledge the LDEO core repository at Columbia University for providing samples. Reviews by Marcus Regenberg and an anonymous reviewer, and comments from the Editor improved the manuscript. We thank NSF (grant OCE-0823498 to M.W.S.) for partially funding this research. J.E.H. acknowledges support from a NSF S-STEM grant (DUE-0806926).

Specific acknowledgements for Chapter III: Richard Smith, Michael Shields, and Thomas Bianchi are thanked for their assistance with TEX_{86} measurements. We thank the captain, crew, and scientific party of MV1014 for assistance in obtaining the cores utilized in this study. We thank Mitch Lyle for valuable discussions, Luz Romero for technical support, and Noura Randle for laboratory assistance. The staff at the Oregon State University core repository is thanked for sampling assistance. JEH acknowledges support from the Cushman Foundation for Foraminiferal Research and an NSF S-STEM Scholarship.

Specific acknowledgements for Chapter IV: We thank the captain, crew, and scientific party of MV1014 for their assistance in obtaining the core utilized in this study. We thank Mitch Lyle for valuable discussions and providing the 17JC percent $CaCO_3$ data, Nathalie Dubois for providing the updated 24JC percent $CaCO_3$ data, and Luz Romero for technical support. The staff at the Oregon State University core repository is thanked for sampling assistance. JEH acknowledges support from the Cushman Foundation for Foraminiferal Research and an NSF S-STEM Scholarship.

TABLE OF CONTENTS

CHAPTER Page

I INTRODUCTION 1

II REFINING *Globigerinoides ruber* Mg/Ca PALEOTHERMOMETRY IN THE ATLANTIC OCEAN 10

- II.1 Introduction 10
- II.2 Materials and Methods 16
- II.3 Results 20
- II.4 Discussion 22
- II.5 Conclusions 39

III COMPARISON OF EASTERN TROPICAL PACIFIC TEX_{86} AND *Globigerinoides ruber* Mg/Ca DERIVED SEA SURFACE TEMPERATURES: INSIGHTS FROM THE HOLOCENE AND LAST GLACIAL MAXIMUM 41

- III.1 Introduction 41
- III.2 Oceanographic Setting 47
- III.3 Materials and Methods 50
- III.4 Results 57
- III.5 Discussion 62
- III.6 Conclusions 73

IV THERMOCLINE TEMPERATURE VARIABILITY REVEALS SHIFTS IN THE TROPICAL PACIFIC MEAN STATE ACROSS MARINE ISOTOPE STAGE 3 75

- IV.1 Introduction 75
- IV.2 Oceanographic Setting 78
- IV.3 Materials and Methods 84
- IV.4 Results 91
- IV.5 Discussion 97
- IV.6 Conclusions 105

V CONCLUSIONS 107

REFERENCES 112

LIST OF FIGURES

FIGURE Page

2.1 Mathien-Blard and Bassinot (2009) Data 13

2.2 Map of locations of core-tops analyzed by Arbuszewski et al. (2010) 15

2.3 SEM images 21

2.4 Map of SeaWiFS surface ocean color measurements and average shell weights 25

2.5 Observational and calibrated Mg/Ca temperatures 32

2.6 Comparison of isotopic calcification temperatures with Mg/Ca-SSTs 37

3.1 Locations of prior TEX_{86} studies and cores used in this study 44

3.2 Temperature profiles of the upper 200 m of the water column 49

3.3 Reconstructed TEX_{86}^{H} and multi species planktonic foraminiferal Mg/Ca temperatures 58

3.4 20° by 20° grid boxes used in the calculation of BAYSPAR TEX_{86} temperatures 65

3.5 Nitrite concentrations along the WOCE P19C line 68

4.1 Locations of cores referred to throughout this study 80

4.2 Monthly water column temperature profiles from the location of core 17JC 82

4.3 TAO array temperature data from 1992-2011 from the buoy located at 95°W 83

4.4 Percent calcium carbonate (% $CaCO_3$) records 86

4.5 Depth in 17JC versus age based on the age model created in this study 88

4.6 *N. dutertrei* Mg/Ca data and calibrated temperatures 92

4.7 Mn/Ca versus Mg/Ca ratios for each *N. dutertrei* analysis 95

FIGURE Page

4.8 Indicators of dissolution in 17JC 96

4.9 Comparison of thermocline temperatures and NGRIP ice core record 99

4.10 Comparison of thermocline temperature record with other temperature and hydrologic records 101

LIST OF TABLES

TABLE Page

2.1 Table of cores for which core-top samples were obtained for shell weight analyses 18

3.1 AMS-^{14}C data 52

3.2 Comparison of TEX_{86} calibrations and temperature proxies 63

4.1 17JC AMS-^{14}C data 85

CHAPTER I

INTRODUCTION

Understanding the temperature evolution of the oceans is key to understanding Earth's history, as the oceans play a fundamental role in Earth's climate In the past, ocean temperatures have varied in response to a number of factors, including atmospheric CO_2 concentrations, orbital parameters, solar output, ocean circulation, and even volcanic eruptions. All of these factors have the ability to change ocean temperatures, especially at the sea surface, which is in direct contact with the overlying atmosphere and receives the most direct insolation. Recent increases in greenhouse gas concentrations are increasing Earth's temperature, and thus, having constraints on past ocean temperatures can enable us to understand the sensitivity of the oceans to varying climate forcings.

As we do not have direct temperature measurements of the past oceans beyond the instrumental record, a number of proxies have been developed to act as 'paleothermometers', enabling scientists to reconstruct past ocean temperatures from sediment recovered in cores from the deep sea. For reconstructing sea surface and upper water column temperatures, these proxies include the $\delta^{18}O$ and Mg/Ca of planktonic foraminifera, alkenone and TEX_{86} biomarkers, Sr/Ca ratios in tropical corals, and the assemblages of varying species of foraminifera. This dissertation focuses on the use of the Mg/Ca paleothermometer to extract past ocean temperatures from planktonic

foraminifera. Planktonic foraminifera are unicellular zooplankton that secrete calcite ($CaCO_3$) shells, or tests, occurring in vast numbers in the water column. Currently, there are ~44 known species of planktonic foraminifera, of which approximately 21 species are most common in the world's oceans (Hemleben et al., 1989). These species not only vary in geographic range, varying with ocean properties such as temperature and salinity, but also vary in their habitat depth within the water column. Thus, planktonic foraminifera have the potential to provide information about temperatures at different depths of the water column.

The underlying basis for Mg/Ca paleothermometry is that the substitution of Mg^{2+} for Ca^{2+} in calcite is endothermic, and is favored at higher temperatures. Therefore, the Mg/Ca ratio of calcite, and thus foraminiferal tests, is expected to increase with increasing temperature. The temperature dependence on Mg uptake into planktonic foraminiferal tests has been determined using culture-based, sediment trap, and core-top calibrations. Culture-based calibrations rely on growing planktonic foraminifera under controlled laboratory conditions in which the temperature is fixed independently of other environmental parameters (e.g. Lea et al., 1999, Nürnberg et al., 1996 and Russell et al., 2004). These calibrations are advantageous because water temperature is known with great accuracy, however, test growth under laboratory conditions does not simulate the natural environment of foraminifera in the ocean. Sediment trap calibrations measure planktonic foraminifera collected in sediment trap time series from regions with high seasonal temperature variability (e.g. Anand et al., 2003). These calibrations are ideal because the conditions under which the foraminifera calcified are well constrained, and

the foraminifera grew in its natural conditions (Anand et al., 2003). The final calibration method, core-top calibrations, measure presumably modern, recently deposited planktonic foraminifera from the sea floor and are calibrated against the temperature in the water column overlying the sediment core site based on the foraminifera's depth habitat (e.g. Dekens et al., 2002, Lea et al., 2000 and Regenberg et al., 2009). The advantage to this calibration method is that the measured tests are the same as those that get buried deeper in the sediment, and may include any alteration the test underwent as it descended through the water column. Despite differences between calibration methods, most species of planktonic foraminifera have a temperature sensitivity of a ~9% change in Mg/Ca per degree Celsius (Anand et al., 2003, Dekens et al., 2002, Kisakürek et al., 2008 and Lea et al., 1999).

Although temperature is the primary control on Mg/Ca ratios in foraminiferal calcite, the Mg/Ca ratio of foraminifera tests can be altered by a number of secondary effects, such as dissolution, salinity, and carbonate ion concentration. Depth transect studies are the most useful in assessing the dissolution effect on foraminifera tests. It is assumed that tests with similar compositions, having grown under similar temperatures, rain down from overlying surface waters to sites at varying depths, and the observed differences in Mg/Ca must be due to postdepositional processes. These studies have shown that, in general, the Mg/Ca in the tests declines with water depth, especially once tests pass below the depth of the regional lysocline (Brown and Elderfield, 1996, Dekens et al., 2002 and Regenberg et al., 2014). The partial dissolution of foraminifera tests can significantly bias Mg/Ca ratios due to the heterogeneous distribution of Mg within

the test and the higher solubility of Mg-rich calcite (Brown and Elderfield, 1996 and Dekens et al., 2002). Several studies have developed methods to correct foraminiferal Mg/Ca ratios for the effect of dissolution by introducing correction terms into the Mg/Ca-temperature calibration equations (Dekens et al., 2002, Regenberg et al., 2006 and Rosenthan and Lohmann, 2002). For example, Dekens et al. (2002) developed separate calibration equations for three species of planktonic foraminifera from the Atlantic and Pacific oceans by adding a water depth-dependent dissolution correction term into the exponent of the calibration equation to account for the preferential dissolution of high-Mg foraminiferal calcite in undersaturated bottom waters. As long as one can assess independently the effect of dissolution on their tests, it is possible to correct for any potential loss of Mg that may have occurred.

Salinity has also been proposed as a potential secondary effect on the Mg/Ca ratios in formainiferal calcite. Culturing studies have suggested an influence of salinity on foraminiferal Mg/Ca ratios of up to a 5-8% increase per salinity unit (Hönisch et al., 2013, Kisakürek et al., 2008, Lea et al., 1999 and Nürnberg et al., 1996), however, a number of core-top studies have proposed a larger salinity effect of 15 to 30% per salinity unit (Arbuszewski et al., 2010, Ferguson et al., 2008 and Mathien-Blard and Bassinot, 2009). The most recent of these studies, Arbuszewski et al. (2010), found a 27% increase in Mg/Ca ratios per salinity unit increase for seawater salinities above 35.5 for the planktonic foraminifera *Globigerinoides ruber*. Based on an average sensitivity of Mg/Ca ratios to changes in temperature of 9% per degree Celsius, in the case of a large salinity effect, the use of foraminiferal Mg/Ca ratios as a temperature proxy would

be greatly hampered. The goal of Chapter II of this dissertation is to re-assess the study of Arbuszewski et al. (2010) to determine if there is an alternate explanation for their findings. The study measured Mg/Ca ratios from core-top foraminifera over a meridional transect from the Atlantic Ocean that spanned a wide range of salinities. However, the transect also spans regions with varying calcite preservation potential. Therefore, it is possible that dissolution may also be a strong secondary effect on the foraminiferal Mg/Ca ratios analyzed in their study. A careful analysis of test weights will be used to assess the degree of dissolution, with decreases in average test weights indicative of increased dissolution. In addition, scanning electron microscopy will be used to obtain highly magnified images of the microstructure of foraminiferal tests to visually inspect the tests for evidence of dissolution. If the findings of Arbuszewski et al. (2010) are correct, there would be a strong need to correct for this salinity effect, or avoid Mg/Ca temperature reconstructions in regions of high salinity.

Chapter III of this dissertation assesses the use of another paleotemperature proxy that has been recently proposed, known as TEX_{86}, by comparing temperature estimates derived from foraminiferal Mg/Ca ratios with temperatures derived from TEX_{86}. The TEX_{86} temperature proxy (TetraEther indeX of 86 carbons) is based on the degree of cyclization of isoprenoidal 86-carbon membrane lipids, known as glycerol dialkly glycerol tetraethers (GDGTs), produced by marine Thaumarchaeota (a phylum of the Archaea) (Schouten et al., 2002). The TEX_{86} index was first defined by Schouten et al. (2002), and its use a quantitative temperature proxy is based on observations that the number of cyclopentane rings in GDGTs increases with increasing growth temperature

(Wuchter et al., 2004). This response has been observed in a variety of culturing and mesocosm experiments (de Rosa et al., 1980, Schouten et al., 2007a, Uda et al., 2001 and Wuchter et al., 2004). Schouten et al. (2002) noted a relationship between the TEX_{86} index in marine surface sediments and overlying sea surface temperature, suggesting that the TEX_{86} index could be used as a sea surface temperature proxy. Subsequently, calibrations between the TEX_{86} index and sea surface temperature were developed based on hundreds of global core-top measurements (Kim et al., 2008, Kim et al., 2010, Schouten et al., 2002 and Tierney et al., 2014).

The use of the TEX_{86} sea surface temperature proxy is intriguing, as it has the potential to overcome some of the limitations of other temperature proxies. For example, foraminifera-based temperature reconstructions can be limited by the availability of tests, the geographic distribution of species, the effects of dissolution and other secondary influences, and are temporally limited by the use of modern foraminifera species for which temperature calibrations exist. Biomarker-based proxies, such as the TEX_{86} and alkenone $U^{k'}_{37}$ indices, can be advantageous due to the ubiquitous appearance of the associated biomarkers in marine sediments temporally and spatially, especially during times and in regions where calcareous fossils do not exist. Unfortunately, the $U^{k'}_{37}$ index saturates at temperatures around 28°C (Prahl and Wakeham, 1987), thus the newly developed TEX_{86} index holds promise for reconstructing a wider range of temperatures, notably during significantly warm periods in Earth's history (Schouten et al., 2007a). Unfortunately, a number of recent studies have arrived at differing conclusions as to whether the TEX_{86} index actually reflects sea

surface (e.g. Turich et al., 2013 and Wuchter et al., 2006) or subsurface temperatures (e.g. Huguet et al., 2007 and Lee et al., 2008). Planktonic foraminifera are ideally suited to resolve this issue due to their habitat depths within the upper water column. By pairing Mg/Ca analyses of multiple species of foraminifera that dwell within the upper water column with TEX_{86} measurements on the same samples, it is possible to determine the depth that the TEX_{86} temperatures are recording. This comparison is performed using sediments from the eastern equatorial Pacific, a location where the use of the TEX_{86} temperature proxy would be ideal, given the varying preservation states of foraminifera in the region, and the importance of the area for global climate and biogeochemical cycling. Lastly, the comparison is done for the late Holocene (the last 7 kyr), and the Last Glacial Maximum (LGM) (20 – 25 kyr) to further examine the influence of differing climate forcings and boundary conditions on the TEX_{86} temperature proxy. The LGM was a period in Earth's climate history when ice sheets were at their most recent maximum extension, and global oceanic circulation was believed to have been in a quiescent state (Lynch-Stieglitz et al., 2007).

Finally, chapter IV utilizes Mg/Ca paleothermometry to create a record of thermocline temperature variability in the eastern equatorial Pacific across Marine Isotope Stage 3 in an effort to understand how the mean climate state of the tropical Pacific varied during past periods of abrupt warming. The current climatic mean state of the tropical Pacific is characterized by trade wind induced upwelling of cold water in the east and the accumulation of warm surface waters in the west, resulting in a strong east-west sea surface temperature gradient. This gradient is reflected in the subsurface by a

deeper thermocline in the western Pacific that shoals to near the surface in the eastern Pacific. It has been hypothesized that the mean state may have been altered in the past, with periods characterized as more El Niño- or La Niña like during times with inferred weaker or stronger east-west sea surface temperature gradients, respectively (e.g. Koutavas et al., 2002 and Koutavas and Joanides, 2012). However, these records are somewhat ambiguous, as there is a strong imprint of the seasonal cycle on sea surface temperatures in the eastern Pacific, and thus, it is difficult to disentangle variations due to changes in the mean state versus changes in the seasonal cycle. Additionally, having constraints on past changes in the mean state may help climate modelers understand future changes in the El Niño-Southern Oscillation (ENSO), as changes in the tropical Pacific mean state can influence ENSO related processes and feedbacks and have the potential to modify ENSO properties.

Thermocline temperatures in the eastern Pacific are minimally influenced by the seasonal cycle, and instead, vary with ENSO conditions. During an El Niño, the easterly trade winds weaken, warm sea surface temperature anomalies migrate toward the eastern Pacific, upwelling in the eastern Pacific is drastically reduced, and the thermocline deepens. As a result, warm temperature anomalies are felt in the subsurface of the eastern Pacific upper-water column. The opposite effects are felt during a La Niña, when temperatures in the subsurface cool as a result of an intensification of the trade winds and the associated feedbacks. By extrapolating the hydrographic variability associated with individual events into longer-term mean state changes, periods characterized as more El Niño-like should record strong subsurface temperature

increases, with the opposite holding true for La Niña-like conditions. Therefore, reconstructing thermocline temperatures by measuring Mg/Ca ratios in the thermocline dwelling foraminifera *Neogloboquadrina dutertrei* is a novel way to reconstruct past changes in the tropical Pacific mean state.

To summarize, the layout of this dissertation is as follows:

- Chapter II is a reinvestigation of a proposed large salinity effect on Mg/Ca ratios in the planktonic foraminifera *Globigerinoides ruber* from sediment core-top samples from the Atlantic Ocean. Foraminifera test weights and scanning electron microscopy are used to examine the potential effects of dissolution on test Mg/Ca ratios.
- Chapter III investigates the TEX_{86} temperature proxy in the eastern tropical Pacific Ocean by utilizing Mg/Ca paleothermometry on multiple species of planktonic foraminifera across the Holocene and LGM. This will enable the determination of the depth that the TEX_{86} temperature proxy is recording.
- Chapter IV attempts to reconstruct past changes in the tropical Pacific Ocean mean state across Marine Isotope Stage 3 by measuring Mg/Ca ratios in the thermocline dwelling foraminifera *Neogloboquadrina dutertrei* from a sediment core in the eastern equatorial Pacific Ocean. The changes are interpreted in terms of El Niño- or La Niña-like mean states.
- Chapter V concludes the dissertation with a summary of the findings of three major studies.

CHAPTER II

REFINING *Globigerinoides ruber* Mg/Ca PALEOTHERMOMETRY IN THE ATLANTIC OCEAN*

II.1. Introduction

Numerous culturing, core-top, and sediment trap studies have shown that temperature is the primary control on Mg/Ca ratios in foraminiferal calcite (e.g. Anand et al., 2003, Barker et al., 2005, Cléroux et al., 2008, Dekens et al., 2002, Hastings et al., 1998, Kisakürek et al., 2008, Lea et al., 1999 and Nürnberg et al., 1996), and calibrations of this relationship have been applied successfully to the paleo-record to reconstruct ocean temperatures across a wide range of time periods (e.g. Koutavas et al., 2002, Lea et al., 2000, Oppo et al., 2009 and Schmidt et al., 2012a). In addition, paired Mg/Ca temperatures and $\delta^{18}O_{calcite}$ ($\delta^{18}O_c$) measurements on surface-dwelling planktonic foraminifera are often used to reconstruct past $\delta^{18}O_{seawater}$ ($\delta^{18}O_{sw}$) variability, a robust proxy for sea surface salinity (e.g. Schmidt et al., 2006, Schmidt and Lynch-Stieglitz, 2011 and Weldeab et al., 2007). A number of secondary controls on foraminiferal Mg/Ca ratios have been identified from culturing experiments, including pH, carbonate ion concentration, and salinity; however, these studies suggest that their influence is

*Reprinted from *Earth and Planetary Science Letters*, 383, Jennifer E. Hertzberg and Matthew W. Schmidt, Refining *Globigerinoides ruber* Mg/Ca Paleothermometry in the Atlantic Ocean, 123-133, 2013, with permission from Elsevier.

small in comparison to temperature (Hönisch et al., 2013, Kisakürek et al., 2008, Lea et al., 1999, Nürnberg et al., 1996 and Russell et al., 2004).

While laboratory culturing studies have suggested an influence of salinity on foraminiferal Mg/Ca ratios of up to 5–8% per salinity unit (Hönisch et al., 2013, Kisakürek et al., 2008, Lea et al., 1999 and Nürnberg et al., 1996), recent studies on core-top foraminifera from high-salinity regions suggest an influence of salinity ranging from 15 to 30% per salinity unit (Arbuszewski et al., 2010, Ferguson et al., 2008 and Mathien-Blard and Bassinot, 2009). As the average sensitivity of Mg/Ca ratios to changes in temperature is ~9% per degree Celsius (Anand et al., 2003, Dekens et al., 2002 and Lea et al., 1999), in the case of a large salinity effect, the use of foraminiferal Mg/Ca ratios as a temperature proxy may be greatly hampered, as the salinity effect would overshadow any temperature change.

Ferguson et al. (2008) measured Mg/Ca ratios on planktonic foraminifera from the high salinity Mediterranean Sea and noted a significant bias on Mg/Ca ratios for seawater salinities above 36. For the surface-dwelling planktonic foraminifera *Globigerinoides ruber* (white), they determined an influence of salinity on Mg/Ca ratios of ~15–30% per salinity unit increase, depending on the size fraction measured (Ferguson et al., 2008). However, subsequent studies have concluded that foraminifera shells from the Mediterranean Sea appear to be affected by post-depositional diagenetic alteration, adding high-Mg overgrowths under $CaCO_3$-supersaturated conditions in pore-waters (Boussetta et al., 2011, Hoogakker et al., 2009, Kontakiotis et al., 2011 and Sabbatini et al., 2011).

A second study by Mathien-Blard and Bassinot (2009) measured Mg/Ca ratios on *G. ruber* (white) across a wide range of salinities from the Atlantic, Pacific, and Indian Oceans and noted a salinity bias on Mg/Ca ratios of ~15% per salinity unit increase. For samples from the high salinity regions of the Atlantic Ocean, Mathien-Blard and Bassinot (2009)'s calculated Mg/Ca-sea surface temperatures (SSTs) were significantly elevated above isotopic calcification temperatures, in some cases by as much as ~2.5°C (Figure 2.1). However, the difference between their calculated Mg/Ca-SSTs and isotopic calcification temperatures is only weakly correlated with sea surface salinity. In addition, prior to Mg/Ca analysis, their *G. ruber* samples were cleaned using the method of Barker et al. (2003), which includes only an oxidative step for removal of organic matter. Cleaning protocols that also include a reductive step to remove metal oxides have been shown to reduce shell Mg/Ca ratios by ~7–15% (e.g. Arbuszewski et al., 2010, Barker et al., 2003, Pena et al., 2005 and Rosenthal et al., 2004). Reducing the Atlantic Mg/Ca ratios measured by Mathien-Blard and Bassinot (2009) by 10% (a value commonly applied when comparing reductively vs. non-reductively cleaned samples, e.g. Arbuszewski et al., 2010 and Schmidt et al., 2012b) puts most of their calculated Mg/Ca-SSTs within a ±~1°C range of isotopic calcification temperatures (Figure 2.1), similar to their reported ±1°C uncertainty on calculated Mg/Ca-SST estimates. Therefore, it does not appear that there is a large salinity bias on the Atlantic core-tops studied by Mathien-Blard and Bassinot (2009).

Most recently, a study by Arbuszewski et al. (2010) found a 27% increase in *G. ruber* (white) Mg/Ca ratios per salinity unit increase for seawater salinities above 35.5.

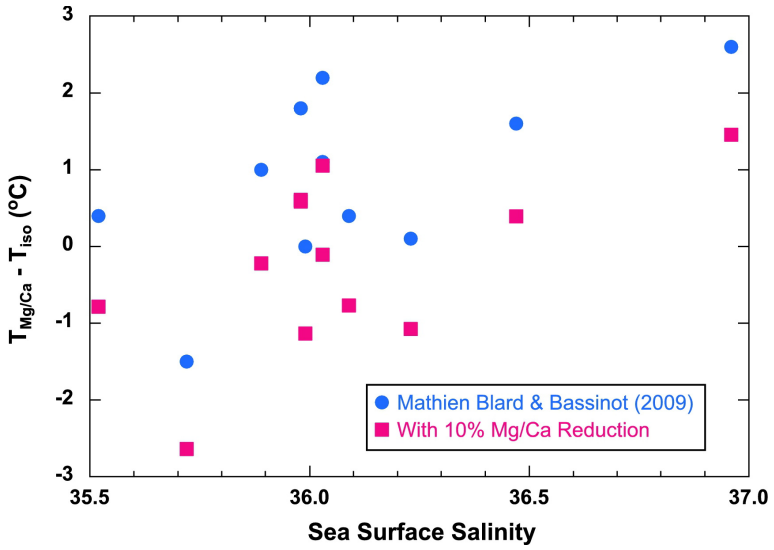

Figure 2.1 Mathien-Blard and Bassinot (2009) Data. Plot of the difference between calculated Mg/Ca-SSTs and isotopic calcification temperatures versus sea surface salinity for the Atlantic Ocean core-tops used in the study by Mathien-Blard and Bassinot (2009). The original data are plotted in blue, while the data with a 10% Mg/Ca reduction are plotted in pink. Note that the 10% Mg/Ca reduction puts most of their calculated Mg/Ca-SSTs within a ±1°C range of isotopic calcification temperatures, similar to their reported ±1°C uncertainty on calculated Mg/Ca-SST estimates (Mathien-Blard and Bassinot, 2009).

Their study is based on measurements of 64 core-top *G. ruber* (white) Mg/Ca ratios across an Atlantic meridional transect spanning from 43°N to 25°S, including samples from both the high salinity subtropical Atlantic gyre regions and the lower salinity Equatorial Atlantic region (Figure 2.2). Arbuszewski et al. (2010) found that *G. ruber* Mg/Ca ratios from the high salinity subtropical gyres are significantly elevated above values expected from observed and isotopic calcification temperatures. In addition, they noted that their calculated core-top Mg/Ca-SSTs were weakly correlated with observed temperatures across the transect ($r^2 = 0.19$), attributing the poor correlation to elevated Mg/Ca ratios in the high salinity subtropical gyre regions, resulting in excessively high SST estimates for the northern and southern subtropics (Arbuszewski et al., 2010).

In this paper, we closely examine the study of Arbuszewski et al. (2010), focusing on a number of assumptions that were made that led to their conclusions. In their study, Arbuszewski et al. (2010) converted all of their measured Mg/Ca ratios to SST using a single dissolution-corrected Mg/Ca:SST calibration equation (Dekens et al., 2002) that includes a water-depth correction factor to account for the loss of high-Mg foraminiferal calcite due to dissolution. Here, we use shell weight analyses and scanning electron microscope (SEM) imaging to assess the assumption that all of the *G. ruber* shells used in the study by Arbuszewski et al. (2010) were subject to dissolution, and whether or not a single calibration equation should be used across the range of latitudes and depths of the core-tops used by Arbuszewski et al. (2010). In addition, we evaluate the observational data chosen by Arbuszewski et al. (2010) that was used to compare with their calculated Mg/Ca-SSTs, as this data assesses how well calculated core-top

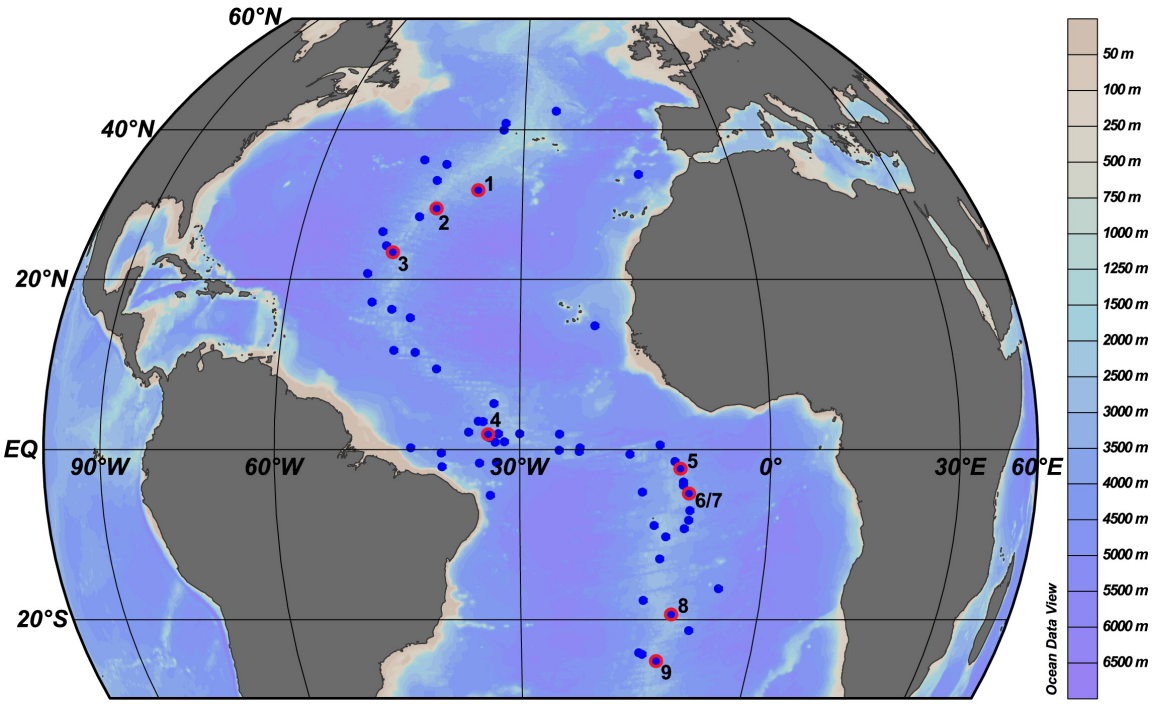

Figure 2.2 Map of locations of core-tops analyzed by Arbuszewski et al. (2010). Map indicating the locations of core-tops analyzed by Arbuszewski et al. (2010) (blue dots). Locations outlined in red indicate core-tops analyzed in the current study for shell weights and SEM imaging. Numbers next to outlined locations correspond to core names as follows: (1) VM27-261, (2) VM19-301, (3) VM16-206, (4) RC13-188, (5) RC24-11, (6) RC24-16, (7) RC24-17, (8) VM16-36, (9) RC8-23. Latitudes, longitudes, and core depths can be found in Table 2.1. Map created with Ocean Data View (Schlitzer, 2013).

Mg/Ca-SSTs reconstruct modern oceanographic conditions. Taking all of these factors into account, we conclude with a re-evaluation of the proposed large salinity effect on *G. ruber* Mg/Ca ratios that was determined by Arbuszewski et al. (2010).

II.2. Materials and Methods

II.2.1. Description of Geochemical Data

The previously published geochemical data referred to throughout this paper were reported by Arbuszewski et al. (2010). In the Arbuszewski et al. (2010) study, a suite of 64 core-top sediment samples spanning from 43°N to 25°S along the Mid-Atlantic Ridge were analyzed for $\delta^{18}O$ and Mg/Ca ratios (Figure 2.2). In brief, 80–100 specimens of *G. ruber* (white, sensu stricto) were picked from each sample from the 250–355 μm size fraction, crushed, and split into aliquots for Mg/Ca and $\delta^{18}O$ analyses (Arbuszewski et al., 2010). After removal of clays, and full reductive and oxidative cleaning steps, samples were analyzed for Mg/Ca ratios on an ICP-OES (Arbuszewski et al., 2010). Samples for $\delta^{18}O$ analyses were also cleaned in rinses of ultra-pure water prior to analysis (Arbuszewski et al., 2010).

Stratigraphic quality for each core-top was assessed using a variety of methods, including radiocarbon dating, age control from the CLIMAP, GLAMAP, SPECMAP, EPILOG, or MARGO databases, or $\delta^{18}O$, $CaCO_3$ or *Globorotalia menardii* stratigraphies (Arbuszewski et al., 2010).

II.2.2. Core Selection and Sample Processing

To examine the preservation differences of the foraminifera in the core-tops analyzed by Arbuszewski et al. (2010), we performed shell weight analyses and SEM

imaging on *G. ruber* (white), the same species of planktonic foraminifera used for the Mg/Ca and $\delta^{18}O$ analyses, on a subset of the same cores used by Arbuszewski et al. (2010). We obtained a different set of core-top samples from cores across a narrow depth range (~3.2 to ~3.7 km) from the North, Equatorial, and South Atlantic (Table 2.1). This depth range was chosen as it contained the greatest number of cores in the three regions, and the range is above the ~4 km lysocline depth (Berger, 1968 and Jones et al., 1984), enabling us to examine preservation differences that may be driven by factors other than the ΔCO_3^{2-} (defined as $[CO_3^{2-}]_{in\ situ} - [CO_3^{2-}]_{saturation}$) of bottom waters. Three cores from the North Atlantic, four cores from the Equatorial Atlantic, and two cores from the South Atlantic satisfied these constraints and had enough sample material remaining close to the top of the cores. Samples were first rehydrated with deionized water, disaggregated on an orbital shaker table for 6 hours, and then wet-sieved through a 63μm mesh. The remaining >63 μm fraction was then dried in an oven overnight at 50°C.

II.2.3. Shell Weight Analyses

Shell weight analyses were performed on the core-top samples following the procedure outlined in Broecker and Clark (2002). When available, 50 shells of *G. ruber* (white, sensu stricto) were picked from the 300–355μm size fraction and weighed in triplicate on a Mettler Toledo MX5 microbalance. To avoid potential bias in shell selection, *G. ruber* shells were picked upon first encounter on a gridded picking tray. Performing shell weight analyses on a narrow size fraction of foraminifera minimizes size related weight differences (e.g. Barker et al., 2004, Beer et al., 2010a, Beer et al.,

Core	Latitude	Longitude	Core depth (m)	# of shells weighed	Avg. weight/shell (μg)	Bottom water ΔCO_3^{2-} (μmol/kg)
VM27-261	31.37	−35.98	3253	50	23.0	27.1
VM19-308	29.02	−41.4	3197	42	21.3	29.0
VM16-206	23.33	−46.48	3733	50	23.1	17.5
RC13-188	1.80	−33.70	3450	50	19.6	25.6
RC24-11	−2.18	−11.25	3445	50	16.4	21.7
RC24-16	−5.03	−10.18	3559	50	18.4	20.3
RC24-17	−5.05	−10.18	3559	50	17.0	20.3
VM16-36	−19.37	−11.43	3329	49	20.6	23.8
RC8-23	−25.15	−12.77	3338	50	21.4	23.6

Table 2.1 Table of cores for which core-top samples were obtained for shell weight analyses. In addition to latitude, longitude, and core depth, the number of shells used for shell weight analyses and the average weight per shell is also given. Bottom water ΔCO_3^{2-} values were originally determined by Arbuszewski et al. (2010) using the GLODAP database.

2010b and Broecker and Clark, 2001). Therefore, simply reporting average shell weights on samples used for geochemical analyses, which are often from a ~100μm size fraction range (e.g. Arbuszewski et al., 2010), is insufficient for assessing potential dissolution using this method. In addition, when picking foraminifera for geochemical analyses, there is a bias to select only the 'best-looking' shells (i.e. those that might not have any evidence of dissolution), thereby influencing the average shell weights reported for foraminifera used for geochemical analysis. We attempted to sonicate samples prior to shell weight analyses to remove any residual fine debris; however, due to the frail nature of the samples from the tropical Atlantic, the foraminifera broke up or were damaged immediately upon sonication. As even minor loss of shell material during sonication would have major implications for the shell weights, the decision was made to not sonicate any of the samples. We assume that as all samples underwent the same initial sample washing process, any offset due to residual fine debris would be constant among samples.

II.2.4. Scanning Electron Microscopy Imaging

Representative shells of *G. ruber* were selected from the same subset of samples used for shell weight analyses to obtain SEM images. Shells were mounted on SEM stubs using adhesive tape and sputter-coated with gold. Images were obtained using a JEOL JSM-6400 with a 5 kV accelerating voltage at the Microscopy and Imaging Center at Texas A&M University.

II.3. Results

II.3.1. Shell Weight Analyses

The results from the shell weight analyses on *G. ruber* are summarized in Table 2.1. Average shell weights from the North Atlantic sites range from 21.3µg to 23.1µg, with an average of 22.5µg, while average shell weights from the South Atlantic sites range from 20.6 to 21.4µg, with an average of 21.0µg. Average shell weights from the Equatorial Atlantic are significantly lower, ranging from 16.4µg to 19.6µg, with an average of 17.9µg. Triplicate measurements of each core-top sample yielded the same weight each measurement, indicating that the reported average shell weights are highly precise. We estimate the standard error of our measurements to be about ±0.5–0.7µg, in agreement with a prior study of the natural variability of a population of *G. ruber* (white) shells from the South China Sea (Regenberg et al., 2013), and the average shell weights obtained from cores RC24-16 and RC24-17, recovered from nearly identical locations (Table 2.1). In comparison to the North Atlantic sites, South Atlantic sites are on average 6% lower, while Equatorial Sites are 20% lower than North Atlantic sites. Broecker and Clark (2002) found only a ~4% reduction in average shell weights due to sonication of samples to remove residual fine debris. Therefore, it is unlikely that the shell weight differences between the three regional sites are an artifact of not sonicating the samples prior to weighing them.

II.3.2. SEM Imaging

SEM images were obtained for whole shells of *G. ruber* from a subset of the core-tops used in the shell weight study (Figure 2.3, Panel I). Overall, shells from the

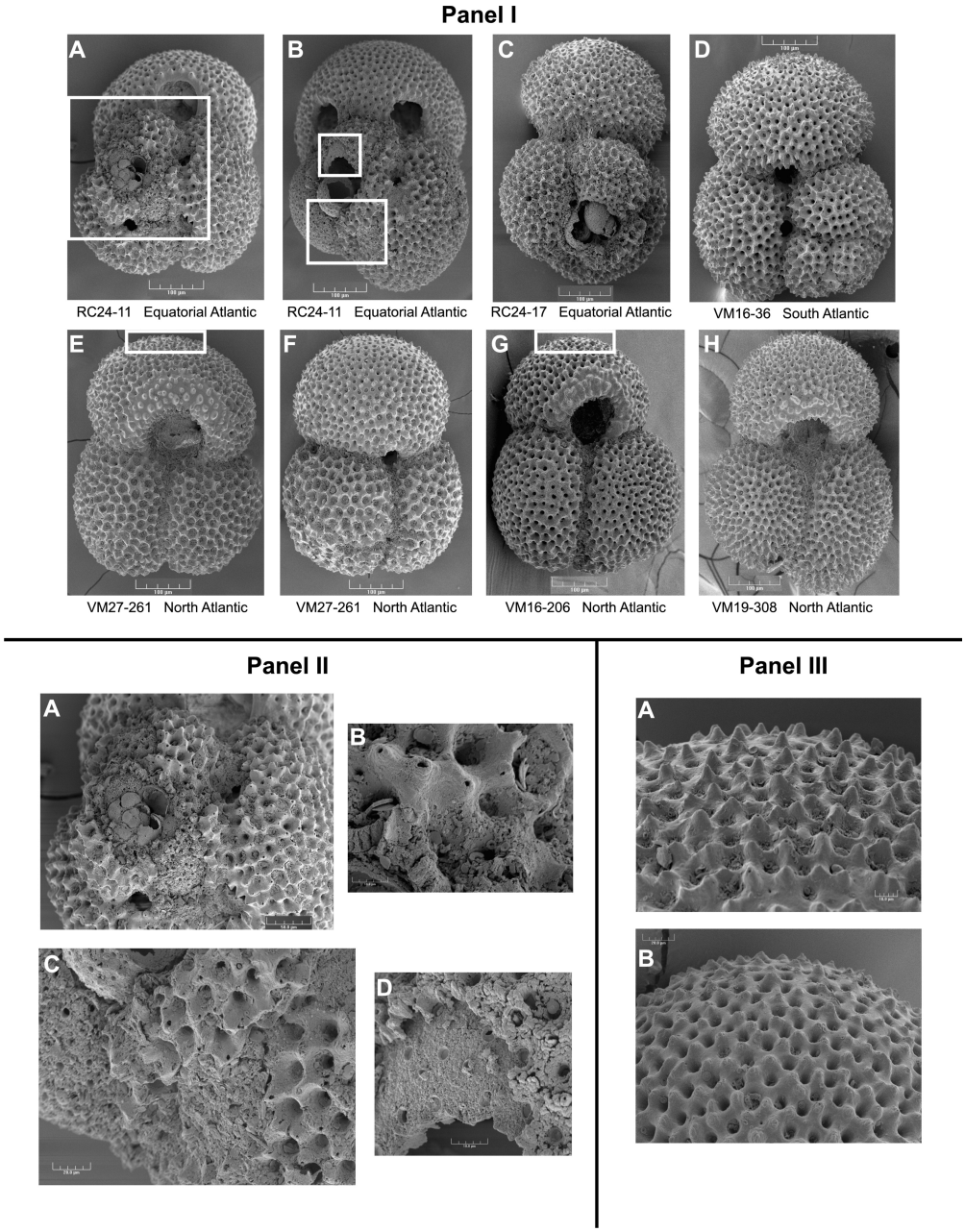

Figure 2.3 SEM images. SEM images of representative *Globigerinoides ruber* (white) shells from the North, Equatorial, and South Atlantic. Panel I: Whole shell images of *G. ruber* (white) from the Equatorial Atlantic (A&B from core RC24-11, C from core RC24-17), South Atlantic (D from core VM16-36), and North Atlantic (E&F from core VM27-261, G from core VM16-206, H from core VM19-308). Panel II: Further magnified images of features from shells from the Equatorial Atlantic (A&B correspond to region outlined in Panel I-A image; C&D correspond to regions outlined in Panel I-B image; all are from core RC24-11). Panel III: Further magnified images of shell surface images from shells from the North Atlantic (A corresponds to region outlined in Panel I-E image, core VM27-261; B corresponds to region outlined in Panel I-G image, core VM16-206). Overall, shells from the North and South Atlantic exhibit much better overall preservation than those from the Equatorial Atlantic.

North and South Atlantic exhibit excellent preservation, while those from the Equatorial Atlantic display significant loss of shell material. Further magnified images show evidence of dissolution pits and loss of surface structure on shells from the Equatorial Atlantic (Figure 2.3, Panel II), especially in comparison to those from the North and South Atlantic (Figure 2.3, Panel III). Although the three study regions exhibit some range of shell preservation, the shells chosen for SEM imaging exhibit features common to most of the *G. ruber* shells in each sample.

II.4. Discussion

II.4.1. Preservation Differences Across the Atlantic Basin

Based on the results of our core-top shell weight study, and as indicated by the SEM images on the same *G. ruber* shells, *G. ruber* shells from the North and South Atlantic exhibit a much higher degree of preservation than those from the Equatorial Atlantic across the same range of depths between the three regions. These findings are in line with previous studies from the Equatorial Atlantic that found evidence for significant dissolution of *G. ruber* along depth transects from the Caribbean and Western and Eastern Equatorial Atlantic at sites well above the lysocline depth (Dekens et al., 2002, Regenberg et al., 2006, Rosenthal et al., 2000 and Rosenthal and Lohmann, 2002). There have been fewer studies examining preservation along depth transects in the North and South Atlantic; however, Dekens et al. (2002) found no evidence for dissolution of *G. ruber* shells above the lysocline on the Rio Grande Rise in the South Atlantic. Given that our shell weights from the North Atlantic are slightly higher than those from the

South Atlantic, we interpret our results to indicate that *G. ruber* shells from the North and South Atlantic sites have undergone little dissolution.

Dissolution of foraminiferal calcite can occur within the water column, at the sediment–water interface, and/or within the sediment column as a result of low in situ carbonate ion concentrations (Berger et al., 1982). Based on $CaCO_3$ budgets for the global open ocean, Milliman et al. (1999) estimated that as much as 60–80% of calcite dissolution can occur in the upper 500–1000 m of the water column, well above the lysocline depth. Within the water column and at the sediment–water interface, the rain rate of organic matter (Jahnke et al., 1994 and Martin and Sayles, 2006) and the ΔCO_3^{2-} of deep water (Berger, 1968), which is primarily a function of the relative age of bottom waters, are the main controls on calcite dissolution. At and below the seafloor, dissolution is controlled by the flux and rain rate of calcium carbonate, bottom water chemistry, and the metabolic respiration of organic carbon within sediments (e.g. Archer et al., 1989, de Villiers, 2005 and Emerson and Bender, 1981). Martin and Sayles (2006) created a model of coupled organic matter oxidation and calcite dissolution and showed that metabolic dissolution is likely to be significant at all bottom water carbonate saturation levels and can result in dissolution of up to 50% of the $CaCO_3$ rain at the depth of the calcite saturation horizon. Most of these factors affecting dissolution vary not only spatially with latitude and depth within the water column, but they can also change temporally.

For all nine locations where shell weight analyses were performed, bottom water ΔCO_3^{2-} values are roughly equal (Table 2.1), yet the large differences in shell weights

between the three regions indicate that there is likely another factor controlling the dissolution differences between the sites. A number of studies have shown that even for locations where bottom waters are supersaturated with respect to carbonate ion concentration, significant calcite dissolution can occur at the sediment–water interface and within the sediment column due to enhanced productivity in the overlying water column (Archer et al., 1989, de Villiers, 2005 and Emerson and Bender, 1981). Metabolic CO_2 generated from the oxidation of organic carbon can drive porewater carbonate ion values below calcite saturation levels, leading to dissolution (Archer et al., 1989, Emerson and Bender, 1981, Hales and Emerson, 1996 and Hales and Emerson, 1997).

To assess the possibility that productivity differences may be the cause of the dissolution differences among the three regions, we plotted the average shell weights for the nine sites on a map of surface chlorophyll concentrations inferred from ocean color measurements from the SeaWiFS project (http://seawifs.gsfc.nasa.gov) (Figure 2.4). A number of studies have shown that surface chlorophyll concentrations correlate well with primary productivity, and thus are a good first order approximation of primary productivity by marine phytoplankton (e.g. Frazel and Berberian, 1990 and Huot et al., 2007). Although not all of the organic matter produced in the upper water column will descend to the sediments, the general pattern of regions with high (low) surface chlorophyll concentrations match locations for which prior studies have measured high (low) surface sediment organic carbon concentrations (e.g. Mollenhauer et al., 2004 and Premuzic et al., 1982). Sites in the North and South Atlantic with the highest average

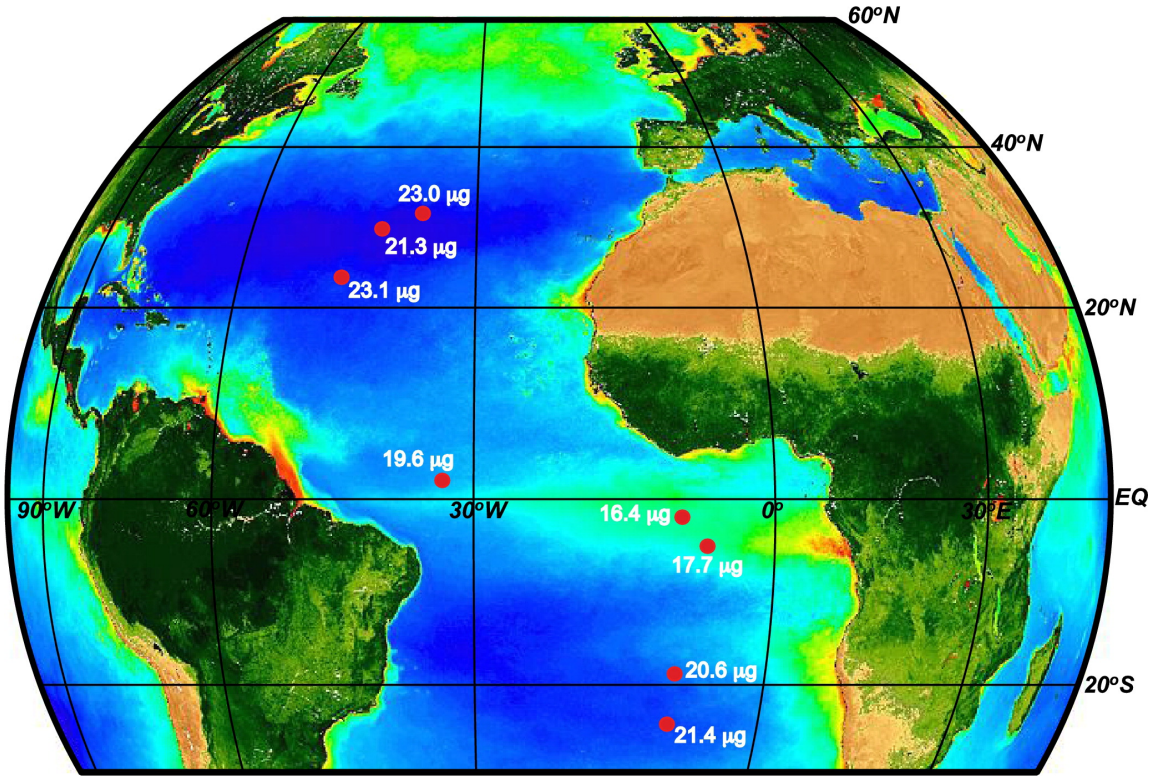

Figure 2.4 Map of SeaWiFS surface ocean color measurements and average shell weights. Average *Globigerinoides ruber* (white) shell weights plotted next to locations of cores used for shell weight study. Locations and weights are plotted on surface chlorophyll concentrations inferred from ocean color measurements from the SeaWiFS project, a good first order approximation of primary productivity by marine phytoplankton. SeaWiFS map created on the NASA Ocean. Color website http://oceancolor.gsfc.nasa.gov.

shell weights fall within the oligotrophic gyre regions, while the Equatorial sites fall within the high-productivity equatorial upwelling zone (Figure 2.4). Additionally, between the core-tops from the Equatorial Atlantic, those with the lowest average shell weights fall directly within the regions of highest surface water productivity. Therefore, it is likely that productivity differences are the main discriminating factor of preservation differences between the three sites. While the North and South Atlantic sites are both within the low productivity oligotrophic gyre regions, South Atlantic sites have lower average shell weights than North Atlantic regions. This is likely due to the location of South Atlantic sites closer to older, more corrosive southern sourced water masses (Berger, 1968).

II.4.2. Dissolution and Mg/Ca Ratios in *Globigerinoides ruber*

G. ruber is one of the most susceptible species of planktonic foraminifera to dissolution (e.g. Adelseck, 1978, Berger, 1968 and Thunell and Honjo, 1981), an issue that has major implications for using the Mg/Ca ratio of this species to estimate past SST. The partial dissolution of *G. ruber* shells can significantly bias Mg/Ca ratios due to the heterogeneous distribution of Mg within the shell and the higher solubility of Mg-rich calcite (Brown and Elderfield, 1996 and Dekens et al., 2002). Laser ablation and electron microprobe mapping studies have shown that *G. ruber* shells contain Mg-enriched surface veneers (Bolton et al., 2011, Eggins et al., 2003, Sadekov et al., 2005 and Sadekov et al., 2008), so any loss of the surface structure of the shell due to dissolution would considerably impact the shell's Mg/Ca ratio, yielding calibrated SSTs lower than they should be. This is likely true for the Equatorial Atlantic sites in our

study, as the SEM images we obtained on shells from these locations show significant loss of surface layers (Figure 2.3, Panel I-A–B, Panel II-A–D).

Several studies have developed methods to correct foraminiferal Mg/Ca ratios for the effect of dissolution by introducing correction terms into Mg/Ca:SST calibration equations. Dekens et al. (2002) developed separate calibration equations for *G. ruber* from the Atlantic and Pacific Oceans by adding a water depth-dependent dissolution correction term into the exponent of the calibration equation to account for the preferential dissolution of high-Mg foraminiferal calcite in undersaturated bottom waters. In the Atlantic, their study was based on three core-top depth transects: two sites from the Equatorial Atlantic and one from the South Atlantic. They found no evidence of dissolution at locations on the Rio Grande Rise in the South Atlantic where all cores were taken from above the lysocline (~4 km, Jones et al., 1984), but did find that dissolution significantly impacted *G. ruber* shells deeper than 3 km at their Equatorial Atlantic sites on the Ceara and Sierra Leone Rises (Dekens et al., 2002). Interestingly, Mg/Ca ratios from the Ceara Rise were offset to higher values than those from the Sierra Leone Rise even though modern observational SSTs at both sites are nearly identical. Dekens et al. (2002) speculated that this offset may be due to differences in the amount of organic matter in the sediments at the two locations, which would lead to differences in the degree of metabolically-induced dissolution. Indeed, the Sierra Leone Rise is located directly within the main high-productivity equatorial upwelling region off Northwest Africa, while the Ceara Rise is further west, away from the high-productivity region. This lends support to our hypothesis that metabolic CO_2 generated from the

oxidation of organic carbon in sediments is an important, and often times overlooked, driver of calcite dissolution. Based on the limited number of depth transects in the Atlantic, and the core-depths covered within their study, Dekens et al. (2002) concluded that the depth corrections in their calibration equations should only be applied to sediment deeper than ~2.8 km in the Equatorial Atlantic. Regenberg et al. (2006) extended the depth coverage of the Dekens et al. (2002) study to include core-tops from shallower depths from the Caribbean, but came to a similar conclusion regarding the depth at which a water-depth corrected calibration equation for *G. ruber* should be used (between 2.5 and 3 km).

Rosenthal and Lohmann (2002) developed a calibration equation for *G. ruber* containing a correction term where the preexponential constant is a function of size-normalized shell weights. Their study was based on a depth-transect from the Sierra Leone Rise in the eastern Equatorial Atlantic, one of the same locations used in the Dekens et al. (2002) study. The main difference between the approaches taken by Dekens et al. (2002) and Rosenthal and Lohmann (2002) is that the correction term developed by Rosenthal and Lohmann (2002) is not static and instead, can change temporally. This is important, especially for productivity-induced diagenetic dissolution, as the factors controlling dissolution in this manner can change with time under different nutrient and upwelling regimes. In addition, correcting for dissolution in this way is a culmination of all dissolution factors, as the final shell weight is the product of any dissolution that may have impacted the shell.

II.4.3. Conversion of Mg/Ca Ratios to Sea Surface Temperature

In their study, Arbuszewski et al. (2010) convert all of their core-top Mg/Ca values (spanning from 43°N to 25°S) to SST using the Dekens et al. (2002) dissolution-corrected Atlantic *G. ruber* equation:

$$T\ (°C) = ln\ (Mg/Ca\ /\ 0.38)\ /\ 0.09 + 0.61\ *\ \text{core depth (km)} \qquad \text{Eq. (2.1)}$$

However, as discussed in Section II.4.2, the study by Dekens et al. (2002) was only able to constrain depth-induced dissolution in the equatorial Atlantic region, cautioning against the use of their dissolution-corrected calibration equation elsewhere. The results of our *G. ruber* shell weight analyses and SEM imaging of a number of the same cores used in the Arbuszewski et al. (2010) study indicate that there are large preservation differences between sites in the North and South Atlantic versus the Equatorial Atlantic within the same range of core depths. Sites in the North and South Atlantic appear to be only minimally affected by dissolution, at least for the range of core depths we have analyzed here. Therefore, the application of a calibration equation containing a constant dissolution correction results in artificially higher SSTs in the better preserved North and South Atlantic. Across the latitudinal transect of core-tops analyzed by Arbuszewski et al. (2010) from 43°N to 25°S, our results suggest that surface productivity may serve as a good latitudinal indicator of where a dissolution correction should be applied to sediments from cores above the lysocline. If we base our cutoff latitudes on the map of surface chlorophyll concentrations, inferred from ocean color measurements from the SeaWiFS project, as an indicator of regions that should experience a high rain of organic carbon to the sediments, this would fall between 15°N and 7°S (Figure 2.4). Thus, we

convert all Mg/Ca ratios for core-tops within this latitudinal band to SST using the Dekens et al. (2002) dissolution-corrected calibration equation for *G. ruber* (Eq. (2.1)), the same equation that was originally used by Arbuszewski et al. (2010). It is important to note that use of the Dekens et al. (2002) dissolution-corrected calibration equation (Eq. (2.1)) may not be the best equation to apply in situations where diagenetic dissolution appears to be the controlling dissolution factor, rather than the ΔCO_3^{2-} of bottom waters. However, as we were not able to obtain samples for all of the core-tops used in the Arbuszewski et al. (2010) study, use of the calibration equation developed by Rosenthal and Lohmann (2002) was not possible as application requires shell weight measurements for each sample, but this is an issue that should be explored in future work.

Unfortunately, we are unable to constrain the degree of preservation for cores deeper than ~3.7 km in the North Atlantic and ~3.6 km in the South Atlantic. Instead, if we assume that the main control on dissolution in these regions is the ΔCO_3^{2-} of bottom waters, we can use the depth of the lysocline (~4 km in the Atlantic Ocean, Jones et al., 1984) as the depth below which dissolution is likely going to impact the *G. ruber* shells in these regions. For core depths above the lysocline north of 15°N and south of 7°S, we convert the Mg/Ca ratios obtained by Arbuszewski et al. (2010) to SST using the multi-planktonic species calibration equation developed by Anand et al. (2003):

$$T\ (°C) = ln\ (Mg/Ca / 0.38) / 0.09 \qquad \text{Eq. (2.2)}$$

that is based on a sediment trap study from the Sargasso Sea in the subtropical North Atlantic. This equation has been used in many studies to convert *G. ruber* Mg/Ca ratios

to SST, as calibrated core-top Mg/Ca-SSTs using this equation often best reflect modern surface water conditions (e.g. Lund and Curry, 2006, Schmidt and Lynch-Stieglitz, 2011, Schmidt et al., 2012a and Schmidt et al., 2012b). Interestingly, this calibration equation is identical to the equation developed by Dekens et al. (2002) without the water-depth dissolution correction term, so in a sense, we are simply using Eq. (2.1) with no depth correction. For core-top depths that fall below the lysocline, we convert Mg/Ca ratios to SST using the Dekens et al. (2002) calibration Eq. (2.1). Thus, the main difference between our Mg/Ca-SST conversion and that done by Arbuszewski et al. (2010) is that we do not use a dissolution correction for core-tops above the lysocline north of 15°N and south of 7°S, as we have shown that the *G. ruber* shells from these areas have been only minimally affected by dissolution.

II.4.4. Comparison of Mg/Ca-SSTs with Observational Data

In order to determine how well the calibrated core-top Mg/Ca-SSTs track modern SST, modern observational data must be chosen that best represent the habitat in which the foraminifera calcified. In the study by Arbuszewski et al. (2010), all core-top Mg/Ca-SSTs (calibrated using Eq. (2.1), Dekens et al., 2002) were compared to mean annual SST at 0 m water depth derived from the World Ocean Atlas, yielding a poor correlation with an r^2 of 0.19 (Figure 2.5A). Arbuszewski et al. (2010) noted excessively high SST estimates in the northern and southern subtropics, and attributed this to the high salinities of the subtropical gyres. An "excess Mg/Ca" term was calculated, defined as the difference between the measured shell Mg/Ca ratio and the expected Mg/Ca ratio at the $\delta^{18}O_{sw}$-corrected $\delta^{18}O$ calcification temperature (Arbuszewski et al., 2010). The

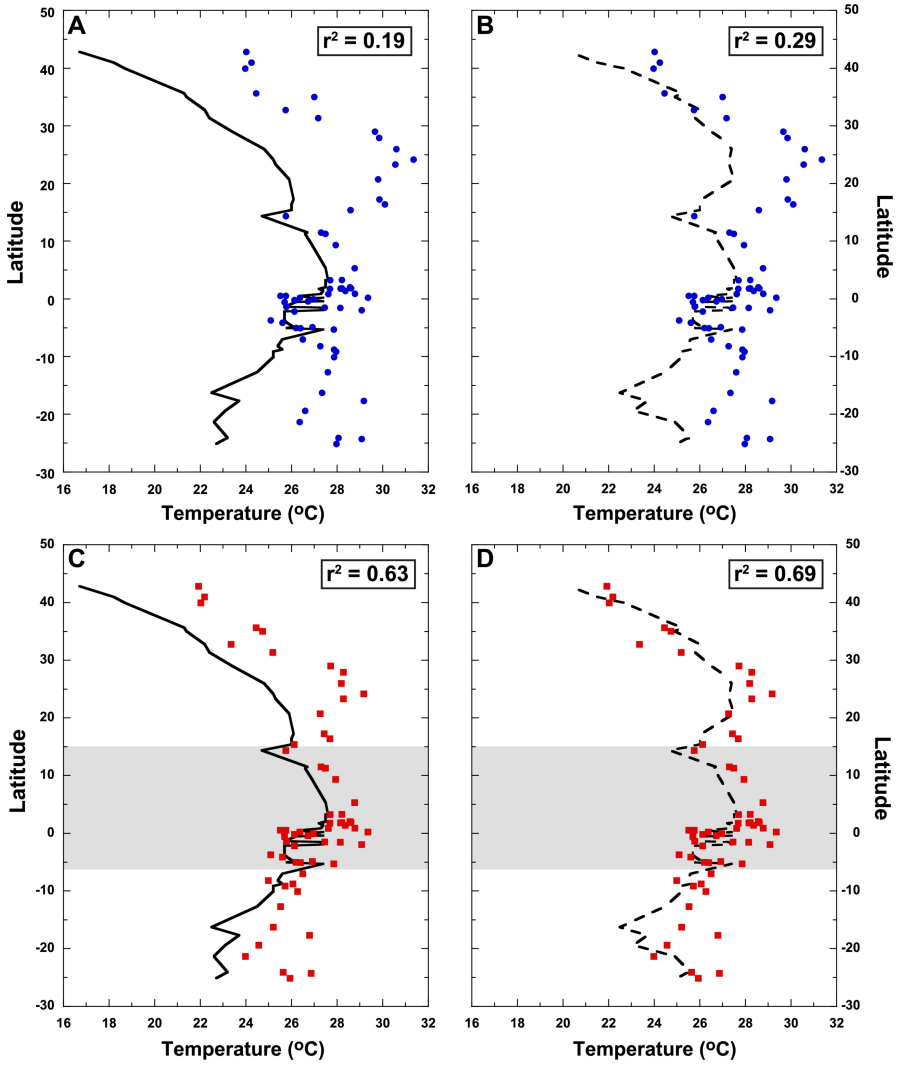

Figure 2.5 Observational and calibrated Mg/Ca temperatures. Combinations of observational and calibrated Mg/Ca temps. for core-tops in Fig. 2.2. (A) Mean annual temps. (MAT) at 0 m depth (black, solid line) plotted with Mg/Ca temps. calibrated using *G. ruber* Atlantic dissolution-corrected calibration of Dekens et al. (2002) (blue circles). This is the original comparison of Arbuszewski et al. (2010). (r^2 = 0.19). (B) MAT at 30 m depth between 23°N / 23°S and mean temps. of 3 warmest months of year at 30 m depth N of 23°N / S of 23°S (black, broken line) plotted with Mg/Ca temp. calibrated using *G. ruber* (white) Atlantic dissolution-corrected calibration of Dekens et al. (2002) (blue circles). (r^2 = 0.29). (C) MAT at 0 m depth (black, solid line) plotted with re-calibrated Mg/Ca temps. (red squares) using original Mg/Ca ratios of Arbuszewski et al. (2010). Mg/Ca ratios for core-tops between 15°N / 7°S (gray shaded) and core-tops below lysocline depth outside of this region were calibrated using Dekens et al. (2002) *G. ruber* (white) Atlantic dissolution-corrected calibration. For core-tops above lysocline N of 15°N / S of 7°S, Mg/Ca ratios were calibrated using the Anand et al. (2003) multi- species calibration. (r^2 = 0.63). (D) MAT at 30 m water depth between 23°N / 23°S and mean temps. of three warmest months of year at 30 m depth N of 23°N / S of 23°S (black, broken line) plotted with re-calibrated Mg/Ca temps. (red squares). (r^2 = 0.69). Observational data from WOA 2005 (Locarnini et al., 2006).

expected Mg/Ca ratios were determined by substituting calculated isotopic temperatures into the Dekens et al. (2002) Mg/Ca-SST calibration equation. Isotopic temperatures were determined with the Bemis et al. (1998) low-light isotopic temperature equation, using measured $\delta^{18}O_c$ values and $\delta^{18}O_{sw}$ values estimated from a $\delta^{18}O_{sw}$:salinity relationship derived from the global $\delta^{18}O_{sw}$ database (Schmidt et al., 1999). When the "excess Mg/Ca" values were compared with mean annual salinity for each core site, a much higher correlation was noted, with an r^2 of 0.77 (Arbuszewski et al., 2010). While the "excess Mg/Ca" values were nearly zero in the equatorial region, the highest "excess Mg/Ca" values were found in the higher salinity subtropical gyre regions, with Mg/Ca ratios elevated by up to 1–2 mmol/mol above values expected from $\delta^{18}O$ calcification temperatures (Arbuszewski et al., 2010). This would lead to Mg/Ca-temperature estimates that can be biased by several degrees of Celsius (Arbuszewski et al., 2010). It is this logic that led Arbuszewski et al. (2010) to conclude that there is a large salinity effect on *G. ruber* Mg/Ca ratios for *G. ruber* from regions where salinities are in excess of 35.5.

Here we investigate the assumptions that led to these conclusions by Arbuszewski et al. (2010), and explore an alternative scenario which can greatly improve the correlation between the Mg/Ca-SSTs and modern observational data without a significant influence of salinity on the Mg/Ca ratios. The first assumption, as we have discussed in Section II.4.3, is in regards to the calibration equation used by Arbuszewski et al. (2010) to convert their measured Mg/Ca ratios to SST. The second has to do with the observational data chosen to compare their Mg/Ca-SSTs with, mainly

in regards to the depth habitat and calcification seasons for *G. ruber* (white). As stated earlier, Arbuszewski et al. (2010) compared their Mg/Ca-SSTs to the average annual SST at 0 m water depth. However, a number of studies have shown that the preferred depth habitat of *G. ruber* is ~30 m, although they can be found in shallower depths, or even depths up to ~100 m (Bé, 1960, Fairbanks et al., 1980, Fairbanks et al., 1982 and Schmuker and Schiebel, 2002). Therefore, comparing core-top *G. ruber* Mg/Ca-SSTs to temperatures at 0 m depth is not appropriate, and instead, should be compared to temperatures slightly deeper in the water column (30 m).

In addition, sediment trap studies have shown that the largest (and in some cases, only) flux of *G. ruber* occurs during the warmest months of the year in temperate latitudes (Bé, 1960, Deuser, 1987 and Tolderlund and Bé, 1971). This makes sense, as *G. ruber* is predominantly a tropical species, calcifying throughout the year in the tropics. Thus, given the latitudinal extent of the transect used by Arbuszewski et al. (2010) spanning from 43°N to 25°S, not every core-top *G. ruber* Mg/Ca-SST value should be compared to average annual temperatures. As the temperate latitudes experience a wider annual range of temperatures, *G. ruber* Mg/Ca-SSTs for core-tops from these latitudes may appear too warm. Instead, we argue that *G. ruber* Mg/Ca-SSTs for core-tops from temperate latitudes should be compared to the average temperature of the 3 warmest months of the year, using ~23°N/S as a cutoff for the temperate latitudes.

Taking these factors into account, we compute correlations between different combinations of the originally calibrated Mg/Ca-SSTs and average annual temperatures at 0 m depth of Arbuszewski et al. (2010), and our re-calibrated Mg/Ca-SSTs and a

combination of average annual temperatures at 30 m depth in the tropics and average temperature of the 3 warmest months of the year at 30 m depth in the temperate latitudes (Figure 2.5). Correlation of the Mg/Ca-SSTs calculated from only the Dekens et al. (2002) calibration equation with average annual temperatures at 0 m depth yields an r^2 of 0.19 (the correlation reported by Arbuszewski et al., 2010) (Figure 2.5A), while correlation with our seasonal/depth weighted temperatures is slightly stronger, yielding an r^2 of 0.29 (Figure 2.5B). Instead, the correlations are greatly improved when using our re-calibrated Mg/Ca-SSTs. We calculated an r^2 of 0.63 when comparing our re-calibrated Mg/Ca-SSTs with the average annual temperatures at 0 m depth (Figure 2.5C), but the strongest correlation is noted (r^2 of 0.69) when comparing our re-calibrated Mg/Ca-SSTs with seasonal/depth weighted temperatures (Figure 5.5D). Thus, using a combination of calibration Eq. (2.1) (Dekens et al., 2002) and Eq. (2.2) (Anand et al., 2003) is the single factor that has the greatest increase in correlation with observational temperatures. Comparison of our re-calibrated Mg/Ca-SSTs with seasonal/depth weighted observational temperatures further improves the correlation. Although the correlation is not perfect, given the uncertainty in our proposed latitudinal and depth constraints for choice of calibration equation, the uncertainty in stratigraphic control of the core-tops used by Arbuszewski et al. (2010) described in Section II.2.1, and the error uncertainty on the measured, Mg/Ca ratios and calibrated Mg/Ca-SSTs (±1.2°C, Dekens et al., 2002; ±1.1°C, Anand et al., 2003), we feel that *G. ruber* Mg/Ca ratios are a robust proxy for SST, and are not significantly altered in regions of high salinity. In addition, the "excess Mg/Ca" term calculated by Arbuszewski et al. (2010) is

based on the assumption that calculated isotopic calcification temperatures are perfect recorders of surface ocean conditions, yet our re-calibrated Mg/Ca-SSTs are more strongly correlated with surface ocean conditions than isotopic calcification temperatures ($r^2 = 0.69$ versus an $r^2 = 0.65$ on their isotopic calcification temperatures, Arbuszewski et al., 2010). Therefore, we believe that the large salinity effect on *G. ruber* Mg/Ca ratios determined by Arbuszewski et al. (2010) was an artifact of the choice of calibration equation used, whereby using a dissolution-corrected calibration equation for samples that were not affected by dissolution led to artificially high Mg/Ca-SSTs in the subtropical regions. As these samples were from regions with significantly higher sea surface salinities, it appeared that the high Mg/Ca-SSTs were related to salinity. In addition, comparison of the Mg/Ca-SSTs from the higher-salinity regions to annual, rather than seasonal SSTs, led these samples to appear even warmer.

II.4.5. Comparison of Mg/Ca-SSTs with $\delta^{18}O_c$-SSTs

Although we have resolved the issue reported by Arbuszewski et al. (2010) of elevated Mg/Ca-SSTs in the Atlantic subtropics, the offset between Mg/Ca-SSTs and isotopic calcification temperatures ($\delta^{18}O_c$-SSTs) along the transect that was described by Arbuszewski et al. (2010) (Figure 2.6A) also requires closer examination. In order to translate *G. ruber* $\delta^{18}O_c$ measurements into temperature, Arbuszewski et al. (2010) used the equation of Bemis et al. (1998):

$$T\ (°C) = 16.5 - 4.90 * (\delta^{18}O_c - \delta^{18}O_{sw} - 0.27‰) \qquad \text{Eq. (2.3)}$$

that is based on culturing experiments of the foraminifera *Orbulina universa* grown under low-light conditions. In Eq. (2.3), $\delta^{18}O_c$ is the measured *G. ruber* isotopic

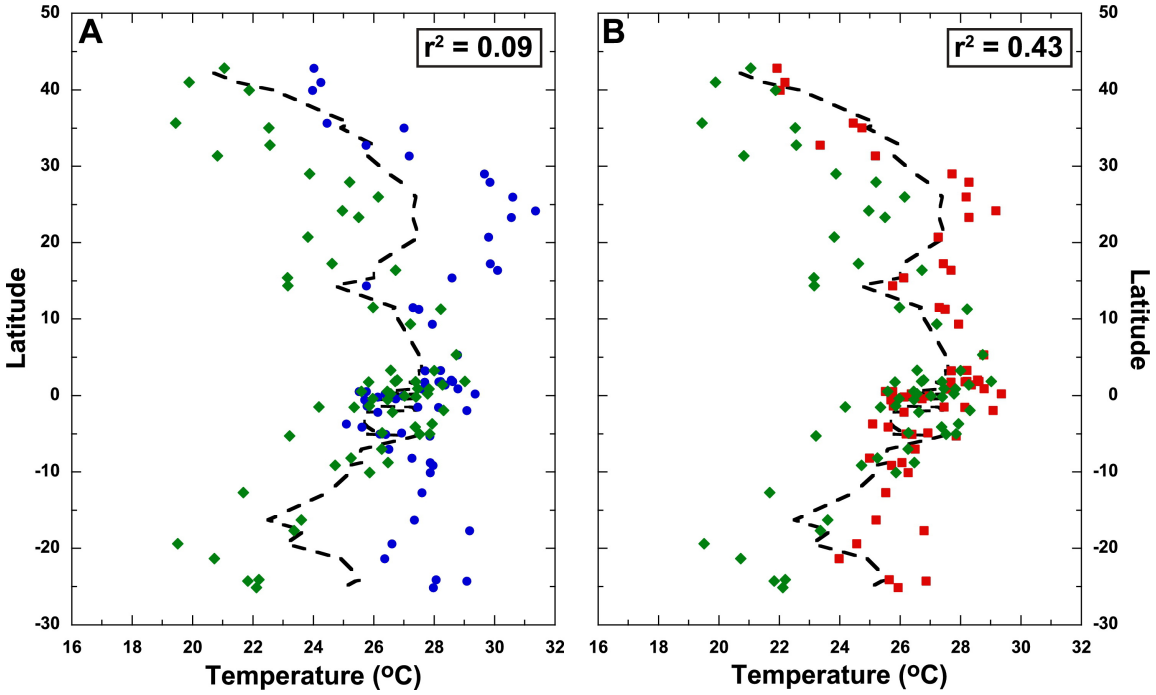

Figure 2.6 Comparison of isotopic calcification temperatures with Mg/Ca-SSTs. (A) Isotopic calcification temperatures $\delta^{18}O_c$-SSTs) (green triangles) calculated by Arbuszewski et al. (2010) plotted with Mg/Ca temperatures calibrated using the *Globigerinoides ruber* (white) Atlantic Ocean dissolution-corrected calibration equation of Dekens et al. (2002) (blue circles). Correlation between isotopic and Mg/Ca temperatures yields an r^2 of 0.09 (Arbuszewski et al., 2010). (B) Isotopic calcification temperatures ($\delta^{18}O_c$-SSTs) (green triangles) calculated by Arbuszewski et al. (2010) plotted with re-calibrated Mg/Ca temperatures (red squares) (see Figure 2.5C caption for description). Correlation between isotopic and Mg/Ca temperatures yields an r^2 of 0.43. Also shown are seasonal/depth weighted observational temperatures (black, broken line).

composition relative to Pee-Dee Belemnite (PDB), $\delta^{18}O_{sw}$ is the seawater isotopic composition relative to standard mean ocean water (SMOW), with the −0.27‰ term correcting for the $\delta^{18}O$ difference between SMOW and PDB (Hut, 1987). In their calculation of $\delta^{18}O_c$-SSTs along the meridional transect, Arbuszewski et al. (2010) estimated $\delta^{18}O_{sw}$ based on a single relationship between surface ocean salinity and $\delta^{18}O_{sw}$ (0–50 m) of $\delta^{18}O_{sw}$ = 0.238 * salinity – 7.69, created from the NASA global seawater $\delta^{18}O_{sw}$ database (Schmidt et al., 1999). Mean annual salinity values at 0 m in the water column were then used to compute $\delta^{18}O_{sw}$ for each core site along the transect (Arbuszewski et al., 2010).

Comparison of the resulting calcification temperatures with mean annual surface (0 m) temperatures yields an r^2 of 0.65, as reported by Arbuszewski et al. (2010). As noted earlier, our re-calibrated Mg/Ca-SSTs are more strongly correlated with surface ocean conditions than isotopic calcification temperatures (r^2 = 0.69). More importantly, our re-calibrated Mg/Ca-SSTs are more strongly correlated to $\delta^{18}O_c$-SSTs, with r^2 of 0.43 (Figure 2.6B), significantly higher than the r^2 of 0.09 reported by Arbuszewski et al. (2010), when comparing $\delta^{18}O_c$-SSTs with their Mg/Ca-SSTs that were calculated using only the Dekens et al. (2002) Mg/Ca-SST calibration equation (Figure 2.6A).

It is worth noting that correlation of the Arbuszewski et al. (2010) $\delta^{18}O_c$-SSTs with our combination of seasonal/annual temperatures at 30 m depth along the transect yields an r^2 value of 0.44, lower than the r^2 of 0.65 between calcification temperatures and mean annual surface (0 m) temperatures. This is in contrast to the stronger correlation between Mg/Ca-SSTs and seasonal/annual temperatures at 30 m depth than

mean annual temperatures at 0 m depth. We hypothesize that this discrepancy is due to calculation of $\delta^{18}O_{sw}$ values based on a single $\delta^{18}O_{sw}$:salinity relationship across the entire transect that may have removed distinct latitudinal differences in the slope and fresh water end member of the relationship (Fairbanks et al., 1992), and/or may have removed regional seasonal and depth differences in the relationship. See Hönisch et al. (2013) for additional factors that may affect the correlation between the Arbuszewski et al. (2010) $\delta^{18}O_c$-SSTs and observational and Mg/Ca-SSTs.

II.5. Conclusions

Our results suggest that application of a single dissolution-corrected Mg/Ca-SST calibration equation for *G. ruber* (Dekens et al., 2002) is not valid across the entire Atlantic Basin given the excellent preservation of shells in the oligotrophic gyre regions. Basin-wide application of a dissolution-corrected calibration equation leads to artificially high Mg/Ca-SSTs in the subtropical gyre regions. However, a dissolution-corrected calibration equation for *G. ruber* is needed in the high-productivity equatorial upwelling region where there is evidence for significant shell dissolution, even at core depths above the lysocline. In addition, for core depths below the lysocline in the subtropics, a dissolution-corrected calibration equation for *G. ruber* still appears to be required. It is important to note that the boundaries for application of different calibration equations that we have discussed are a first attempt to do this, and additional work needs to be done to better define the oceanographic locations and conditions under which different calibration equations should be used. Therefore, taking into account usage of appropriate calibration equations and comparison to temperatures based on realistic *G.*

ruber growth seasons and depth habitats, we find invoking a large salinity effect on *G. ruber* Mg/Ca ratios is unnecessary. We thus are able to reconcile the core top Mg/Ca data reported in Arbuszewski et al. (2010) with culturing experiments that found salinity has only a minor influence on foraminiferal Mg/Ca ratios.

CHAPTER III

COMPARISON OF EASTERN TROPICAL PACIFIC TEX_{86} AND *Globigerinoides ruber* Mg/Ca DERIVED SEA SURFACE TEMPERATURES: INSIGHTS FROM THE HOLOCENE AND LAST GLACIAL MAXIMUM

III.1. Introduction

Numerous paleothermometers have been developed to reconstruct sea surface temperatures (SSTs) on timescales ranging from the last decade and century back to hundreds of millions of years ago. Early foraminifera-based SST reconstructions relied on transfer functions and oxygen isotopes, and recent work has utilized the Mg/Ca ratio of surface dwelling planktonic foraminifera (Erez and Luz, 1983, Imbrie and Kipp, 1971 and Nürnberg et al., 1996). However, foraminifera-based SST reconstructions can be limited by availability of materials, the geographic distribution of species, and the effects of dissolution and other secondary influences (Dekens et al., 2002 and Russell et al., 2004). In addition, Mg/Ca reconstructions are temporally limited by the use of modern foraminifera species for which Mg/Ca-SST calibrations exist (Anand et al., 2003). Biomarker-based SST proxies, such as the TEX_{86} and alkenone $U^{k'}_{37}$ indices, can be advantageous due to the ubiquitous appearance of the associated biomarkers in marine sediments temporally and spatially, especially during times and in regions where calcareous fossils do not exist (Brassell et al., 1986 and Schouten et al., 2002). Unfortunately, the alkenone $U^{k'}_{37}$ index saturates at temperatures around 28ºC (Prahl and

Wakeham, 1987), thus the newly developed TEX_{86} index holds promise for reconstructing a wider range of temperatures, notably during significantly warm periods in Earth's history (Schouten et al., 2007a and Tierney, 2014).

The TEX_{86} temperature proxy (TetraEther indeX of 86 carbons) is based on the degree of cyclization of isoprenoidal 86-carbon membrane lipids, known as glycerol dialkyl glycerol tetraethers (GDGTs), produced by marine Thaumarchaeota (formerly Group 1 Crenarchaeota) (Schouten et al., 2002). The TEX_{86} index was first defined by Schouten et al. (2002) as:

$$TEX_{86} = \frac{[GDGT-2]+[GDGT-3]+[Cren']}{[GDGT-1]+[GDGT-2]+[GDGT-3]+[Cren']} \qquad \text{Eq. (3.1)}$$

where GDGTs 1-3 indicate lipids containing 1-3 cyclopentyl moieties, respectively, and Cren' designates the regioisomer of crenarchaeol, a distinct biomarker for marine Thaumarchaeota (Sinninghe Damsté et al., 2002a). The use of the TEX_{86} index as a quantitative temperature proxy is based on observations that the number of cyclopentane rings in GDGTs increases with increasing growth temperature (Wuchter et al., 2004). This response has been observed in a variety of culturing and mesocosm experiments (de Rosa et al., 1980, Schouten et al., 2007a, Uda et al., 2001 and Wuchter et al., 2004). It is thought that the addition of rings into the GDGTs raises the melting point of the cell membrane and alters membrane packing (Gliozzi et al., 1983 and Uda et al., 2001), thus enabling Thaumarchaeota to adjust membrane stability in response to temperature changes (Chong, 2010).

Schouten et al. (2002) were the first to note a relationship between the degree of cyclization in marine surface sediments and overlying SST, thereby developing the

TEX_{86} index (Eq. (3.1)) as the ratio expressing the degree of cyclization that best correlated with SST. In addition, Schouten et al. (2002) developed the first TEX_{86} temperature calibration based on 40 sediment core top samples from 15 locations. This calibration equation and subsequent calibrations involving the addition of hundreds of core-top samples (Kim et al., 2008 and Kim et al., 2010) all note the highest correlation between the TEX_{86} index and SSTs. However, recent studies have arrived at differing conclusions as to whether the TEX_{86} index actually reflects sea surface (Ho et al., 2011, Rueda et al., 2009, Turich et al., 2013, Wei et al., 2011, Wuchter et al., 2006 and Zhu et al., 2011) or subsurface temperatures (Chen et al., 2014, Huguet et al., 2007, Lee et al., 2008, Lopes dos Santos et al., 2010, Richey et al., 2011 and Wuchter et al., 2006). As the distribution of these studies would suggest (Figure 3.1), there does not appear to be a single factor controlling the distribution of regions where the TEX_{86} index reflects surface or subsurface temperatures (i.e. within one ocean basin, high versus low latitude, coastal versus open ocean, etc.).

A growing body of evidence from water column studies of GDGT lipids and archaeal genetic material suggests that Thaumarchaeota preferentially reside in the mesopelagic zone, below the surface photic zone (Herndl et al., 2005, Huguet et al., 2007, Ingalls et al., 2006, Karner et al., 2001, Massana et al., 1997, Turich et al., 2007, Wakeham et al., 2003, Wuchter et al., 2005 and Wuchter et al., 2006). These studies align well with a recent study suggesting that Thaumarchaeota are aerobic ammonia oxidizers (Könneke et al., 2005), and would thus dwell in the subsurface nitrite maximum below the photic zone (Meeder et al., 2012 and Wada and Hattori, 1971).

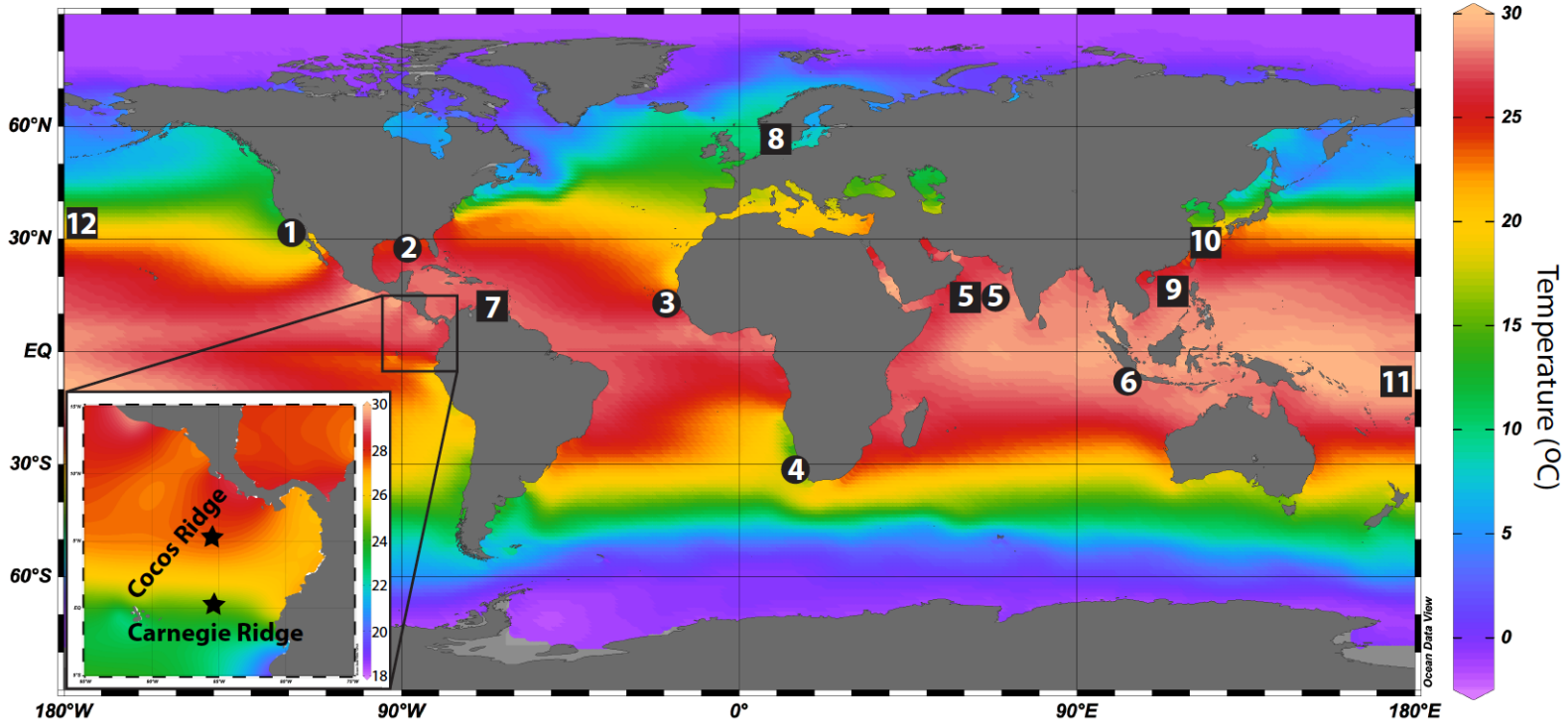

Figure 3.1 Locations of prior TEX_{86} studies and cores used in this study. Locations of previous studies finding that TEX_{86} temperatures were representative of subsurface conditions (black circles) or surface conditions (black squares). Numbers correspond to references as follows: (1) Hughet et al., 2007 (2) Richey et al., 2011 (3) Lopes dos Santos et al., 2010 (4) Lee et al., 2008 (5) Wuchter et al., 2006 (6) Chen et al., 2014) (7) Turich et al., 2013 (8) Rueda et al., 2009 (9) Wei et al., 2011 (10) Zhu et al., 2011 (11) Ho et al., 2011 (12) Wuchter et al., 2006. Note that this is not an exhaustive list of all available TEX_{86} studies, but rather a sampling of studies to exemplify the distributions of surface and subsurface findings. Studies are plotted on a surface map of average annual sea surface temperatures from the World Ocean Atlas 2013 (Locarnini et al., 2013). Inset: Location of the Cocos Ridge and Carnegie Ridge study areas. 07MC (6°14.037'N, 86°2.613'W; 1,995 m depth) and 08JC (6°14.038'N, 86°2.613'W; 1,993 m depth) were recovered from the Cocos Ridge location shown with black star and 09MC (0°41.630'S, 85°19.995'W; 2,452 m depth) and 17JC (0°10.832'S, 85°52.004'W; 2,867 m depth) were recovered from the Carnegie Ridge location shown with black star. Map created with ODV (Schlitzer, 2013).

While these studies would indicate a subsurface signal for the TEX_{86} temperature proxy, they are at odds with sediment calibration studies that find the highest correlation between the TEX_{86} index and SST (Kim et al., 2008, Kim et al., 2010 and Schouten et al., 2002). One explanation for this disagreement comes from the 'surface export hypothesis' (Tierney, 2014), which speculates that grazers play an important role in exporting GDGTs from the surface waters to the sediments in fecal pellets, and the absence of grazers in deeper waters prohibits the export and preservation of GDGTs from these depths in sediments (Wakeham et al., 2003). Another explanation involves the 'correlation hypothesis' in which subsurface temperatures are highly and significantly correlated with SSTs, and thus, while TEX_{86} may actually record subsurface temperatures, a high correlation with SSTs is also noted (Tierney, 2014). This may be compounded by the fact that SSTs are known to a higher precision than subsurface temperatures, resulting in artificially higher correlations between TEX_{86} and SSTs than TEX_{86} and subsurface temperatures (Tierney, 2014).

Regardless of the explanation for how the TEX_{86} index can reflect surface or subsurface temperatures, it appears certain that this issue must be addressed for each study region where the TEX_{86} index will be applied. The eastern tropical Pacific (ETP) is a key paleoceanographic region, given the importance of the region to global climate. Through its role in the El Niño-Southern Oscillation (ENSO), the ETP exerts a major influence on tropical climate dynamics and climate in other regions around the globe through teleconnections (Wang and Fiedler, 2006). The ETP is also a crucial region for the global carbon cycle, responsible for up to 10% of global primary productivity

(Pennington et al., 2006). Therefore, understanding the past climatic evolution of the ETP is a key concern to paleoceanographers. Use of the TEX_{86} temperature proxy in the ETP is enticing, given its ability to reconstruct temperatures further back in time than foraminiferal proxies and to a higher degree than the alkenone $U^{k'}_{37}$ index. In addition, the preservation of foraminifera can change significantly over time, as can seawater Mg/Ca ratios, leading to uncertainties in Mg/Ca temperature reconstructions on longer time scales (Brown and Elderfield, 1996 and Medina-Elizalde et al., 2008).

The use of the TEX_{86} temperature proxy in the ETP has thus far yielded conflicting results as to whether the proxy reflects surface or subsurface temperatures. A study of eight core-top sediment samples along 95ºW in the ETP from 8ºN to 8ºS resulted in TEX_{86} temperatures ranging from 4.4º cooler than mean annual SST to 2.4º warmer than mean annual SST (Ho et al., 2011). However, the majority of samples returned TEX_{86} temperatures that were cooler than mean annual SST (Ho et al., 2011). A subsequent study by Seki et al. (2012) compared TEX_{86} temperatures to alkenone $U^{k'}_{37}$ temperatures over the past 10 myr from ODP Site 1241 (5º50'N, 86º26'W), noting that TEX_{86} temperatures were consistently cooler than $U^{k'}_{37}$ temperatures. In addition, TEX_{86} temperatures were cooler than Mg/Ca temperatures of the surface dwelling foraminifera *Globigerinoides sacculifer* that were calculated for the time period from 2 to 5 myr (Seki et al., 2012). Further south along the equator at ODP Site 1240 (0º41'S, 82º5'W), bin Shaari et al. (2013) interpreted a TEX_{86} temperature record for the past 450 kyr as a mixed temperature signal from the surface mixed layer and the thermocline, using the difference between TEX_{86} temperatures and $U^{k'}_{37}$ temperatures as an upwelling

index. Most recently, a study by Zhang et al. (2014) utilized TEX_{86} and $U^{k'}_{37}$ temperatures to determine long term trends in the gradient between the western and eastern equatorial Pacific for the last 12 myr. Although their TEX_{86} temperatures were consistently cooler than $U^{k'}_{37}$ temperatures, the authors averaged the two temperature proxies to create a SST record for the eastern equatorial Pacific (Zhang et al., 2014).

In this study, we take a unique approach to investigating the TEX_{86} temperature proxy in the ETP by comparing TEX_{86} temperatures to Mg/Ca temperatures of multiple species of planktonic foraminifera for two sites in the ETP. One location is on the Carnegie Ridge (0.5°S, 85°W) directly within the cold tongue upwelling region, and the other is on the Cocos Ridge (6°N, 86°W) within the East Pacific Warm Pool (EPWP) (Figure 3.1, inset). These locations with differing oceanographic conditions are ideal to study the effects of regional hydrography on the TEX_{86} temperature proxy. Our multi-proxy approach enables us to determine the depth of GDGT export given the known depth habitats of the planktonic foraminifera. In addition, we perform this comparison for the Holocene and Last Glacial Maximum (LGM) to further examine the influence of differing climate forcings and boundary conditions on the TEX_{86} temperature proxy.

III.2. Oceanographic Setting

The ETP is a highly dynamic oceanographic region characterized by strong vertical and meridional gradients. The easterly trade winds blowing along the equator result in Ekman induced divergence of surface waters and consequent upwelling along the equator. The resultant shallow thermocline leads to the upwelling of cool, nutrient rich waters, giving rise to the eastern Pacific equatorial cold tongue, extending east of

120ºW to the South American continent (Fiedler and Talley, 2006). Just beneath the surface along the equator, lies the strong, eastward flowing Equatorial Undercurrent (EUC). The EUC lies at the base of the equatorial thermocline between 30 – 300 m and is the source of the water that upwells into the thermocline (Kessler, 2006). As the source waters of the EUC are derived from sub-Antarctic Mode Water/Antarctic Intermediate Waters that form in the Southern Ocean off Antarctica, the ETP serves as an important region linking the tropics to the high-latitudes (Toggweiler et al., 1991). The three main surface currents of the ETP are the eastward flowing North Equatorial Countercurrent between 5 and 10ºN and the westward flowing North and South Equatorial Currents, which flow on either side of the countercurrent (Kessler, 2006). The equatorial front, located at around 3ºN, separates the cold tongue region to the south from the EPWP to the north. The EPWP is centered along the coast of southwestern Mexico and Guatemala, and is the result of seasonally large net heat flux and weak wind mixing (Wang and Enfield, 2001).

The Cocos Ridge study area (6°N, 86°W) is located within the EPWP, with higher surface temperatures and lower surface salinity than the Carnegie Ridge region. Surface temperatures range annually from 26.9°C (November) to 29.0°C (April), with an average annual temperature of 27.8°C (Locarnini et al., 2013) (Figure 3.2A). The average annual surface salinity is 32.7, driven by increased precipitation in the region (Zweng et al., 2013). The surface mixed layer extends down to ~20 m, with the thermocline between 20 and 75 m. The thermocline in the EPWP is stronger than the equatorial upwelling region (Fiedler and Talley, 2006). Due to the stronger thermocline

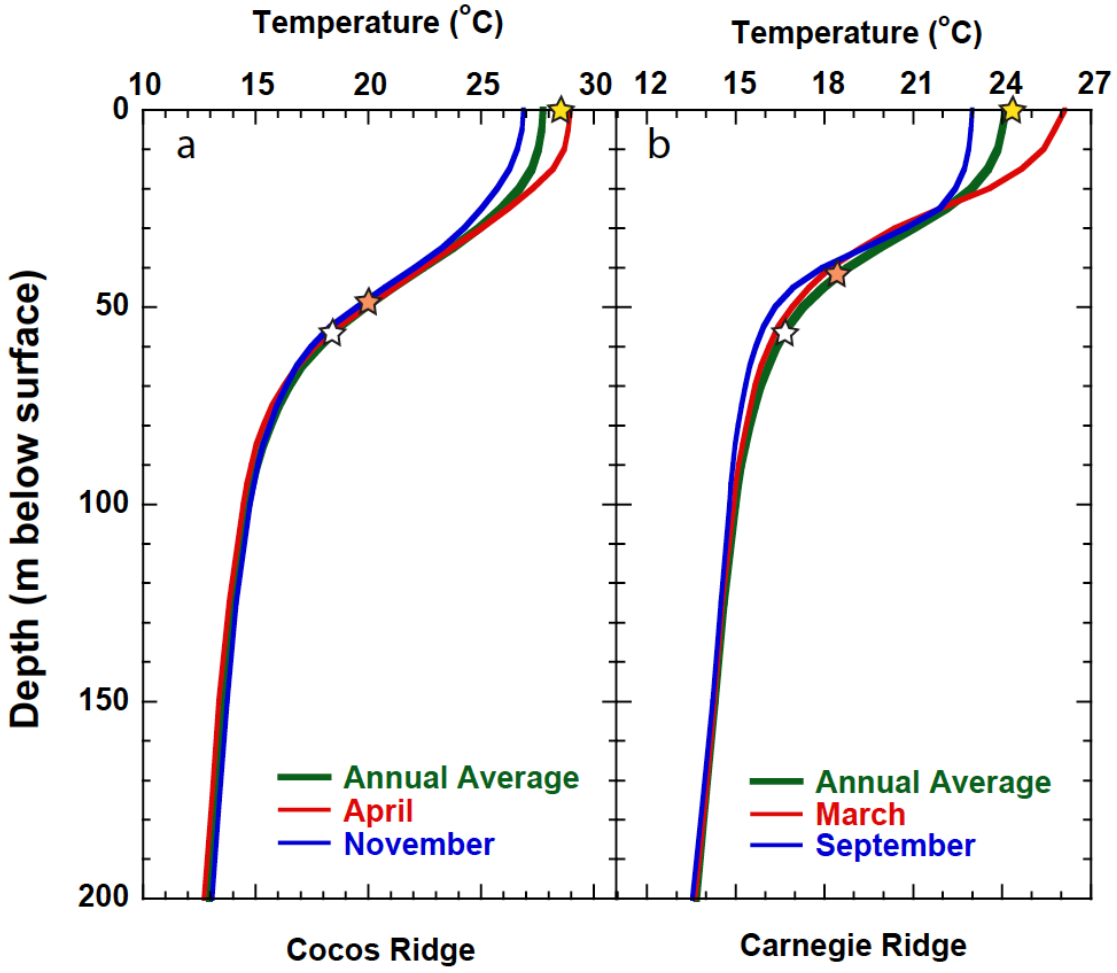

Figure 3.2 Temperature profiles of the upper 200 m of the water column. (a) Cocos Ridge (6.5°N, 86.6°W) and (b) Carnegie Ridge (0.5°S, 85.5°W). Average annual temperatures (green) and the month with the highest sea surface temperature (red) and lowest sea surface temperature (blue) are plotted. Values are from the World Ocean Atlas 2013 (Locarnini et al., 2013). Also plotted are the core top *Globigerinoides ruber* Mg/Ca temperature (yellow star), and the average Holocene Mg/Ca temperatures from *Globorotalia menardii* (orange star) and *Neogloboquadrina dutertrei* (white star). Mg/Ca temperature calibrations used can be found in section III.3.4. Values for *G. menardii* and *N. dutertrei* are plotted where the Mg/Ca temperatures intersect with the average annual temperature profiles for both study areas.

and weaker winds in the EPWP, the nutricline is deeper than in the equatorial upwelling region, and primary productivity is low (Pennington et al., 2006).

The Carnegie Ridge (0.5°S, 85°W) study area is located directly within the cold tongue equatorial upwelling region (Fiedler and Talley, 2006). At the surface, temperatures range annually between 23.0°C (September) and 26.1°C (March), with an average annual temperature of 24.1°C (Locarnini et al., 2013) (Figure 3.2B). The surface mixed layer extends down to ~15 m, with the thermocline between 15 and 50 m. Average annual salinity at the surface is 34.1 (Zweng et al., 2013). The region is characterized by high concentrations of nutrients brought to the surface from upwelling, which fuels high primary productivity along the equator (Pennington et al., 2006). As a result, the nutricline is this area is relatively shallow with high nitrate levels near the surface (Pennington et al., 2006).

III.3. Materials and Methods

The sediment cores utilized in this study were recovered from the ETP in 2010 aboard the R/V *Melville* on cruise MV1014. Multi-core 07MC (6°14.037'N, 86°2.613'W; 1,995 m depth) and piston core 08JC (6°14.038'N, 86°2.613'W; 1,993 m depth) were recovered from the Cocos Ridge, while multi-core 09MC (0°41.630'S, 85°19.995'W; 2,452 m depth) and piston core 17JC (0°10.832'S, 85°52.004'W; 2,867 m depth) were recovered from the Carnegie Ridge (Figure 3.1, inset). Samples for the Holocene portion of this study were taken from different multi-cores from the same deployment in both regions to ensure high sampling resolution with enough material for both foraminiferal and GDGT analyses. Only samples from the multi-core used for

GDGT analyses were freeze dried prior to processing. Once age models were established for the piston cores (see below), samples were taken from the targeted LGM sections of the cores covering 20 – 25 ka. These samples were freeze dried and then split into two separate aliquots for foraminiferal and GDGT analyses.

III.3.1. Age Model Development

The age models for all cores (multi and piston cores) are based on radiocarbon dates determined from the planktonic foraminifera *Neogloboquadrina dutertrei*. Radiocarbon ages were converted to calendar age using Calib 7.1 most probable age distributions with a marine reservoir correction 400 years (www.calib.qub.ac.uk). A summary of radiocarbon dates obtained for this study can be found in Table 3.1. For multicores 07MC and 09MC, radiocarbon dates were measured for the upper and bottom intervals and then linearly interpolated. The age models yield sedimentation rates of 2.8 cm/kyr and 4.1 cm/kyr for 07MC and 09MC, respectively. Holocene sample intervals analyzed in this study span 1.24 – 3.53 kyr for 07MC, and 2.58 – 6.94 kyr for 09MC. The radiocarbon dates for the multi-cores were previously published by Marcantonio et al. (2014), but we updated the dates using the most recent Calib 7.1 program, as they were originally calibrated using Calib 7.0.

The age model for piston core 08JC is based on three radiocarbon-dated intervals spanning the LGM interval of the core. Linear interpolation between these age control points results in an average sedimentation rate of 6.7 cm/kyr across the interval. The age model for piston core 17JC is based on two calibrated radiocarbon dates bracketing the LGM and linearly interpolating between them. Based on this age model, the average

Core	Depth (cm)	Accession #	F_m	F_m error	$\delta^{13}C$	^{14}C Age (yr)	SD (yr)	Calendar Age (yr BP)	Error - (yr BP)	Error + (yr BP)
07MC	0.25	OS-88113	0.8369	0.0031	assumed	1430	30	970	70	80
07MC	21	OS-94597	0.3771	0.0023	assumed	7830	45	8300	110	80
08JC	61	OS-97832	0.1628	0.0016	1.67	14600	80	17300	260	250
08JC	81	OS-97822	0.1098	0.0015	1.84	17750	110	20900	310	350
08JC	101	OS-97823	0.0806	0.0015	2.01	20200	150	23800	380	380
09MC	0.25	OS-88117	0.7329	0.0028	assumed	2490	30	2200	100	130
09MC	34	OS-88108	0.3072	0.0017	assumed	9480	45	10300	110	140
17JC	220	OS-98923	0.16710	0.00120	1.26	14350	60	16900	290	230
17JC	356.5	OS-117129	0.05160	0.00110	2	23800	180	27600	270	260

Table 3.1 AMS-^{14}C data

sedimentation rate across the LGM in 17JC is 12.7 cm/kyr. The LGM samples analyzed from 08JC range from 20.20 – 24.55 kyr, and from 20.37 – 24.73 kyr for 17JC.

III.3.2. Foraminiferal Analyses

Sediment from the core intervals designated for foraminiferal analyses were disaggregated in ultra-pure water, wet-sieved through a 63 μm sieve, and dried in an oven at 50°C. To minimize intraspecific variations in the geochemistry of each species, specimens of *Globigerinoides ruber* (white, sensu stricto), *Globorotalia menardii* and *N. dutertrei* were collected from the 250–350, 600-850, and 315-355 μm size fractions, respectively. All tests were measured against a calibrated reticle to verify the size restrictions. These species of foraminifera were chosen due to their habitat depth preferences, thus enabling us to reconstruct surface and thermocline temperature profiles. *G. ruber* is a species known to live in the upper mixed layer of tropical and subtropical waters between 0 and 50 m (Bé, 1977, Fairbanks et al., 1982 and Ravelo and Fairbanks, 1992). *G. ruber* does not migrate to deeper waters to add a layer of gametogenic calcite crust at the end of its life cycle (Bé, 1980 and Caron et al., 1990), so it is ideal for reconstructing tropical surface water conditions in the past (Elderfield and Ganssen, 2000, Lea et al., 2000, Lea et al., 2002, Nürnberg et al., 2000 and Ravelo and Fairbanks, 1992). *G. menardii* lives in the upper thermocline between 25 and 85 m and *N. dutertrei* dwells in the lower thermocline between 60 and 150 m (Faul et al., 2000 and Spero et al., 2003) (Figure 3.2). Spero et al. (2003) found that while *G. ruber* maintains an upper mixed layer habitat in the ETP over the last three glacial cycles, *G. menardii* and *N. dutertrei* consistently record thermocline properties in this region.

Approximately 60, 25, and 10 shells per trace metal analysis were picked for *G. ruber*, *N. dutertrei*, and *G. menardii*, respectively, providing enough material to run duplicates (~600 μg). For intervals where not enough material was available for duplicate analyses, every effort was made to use the greatest number of shells available for single analysis. The foraminifera from each interval were gently crushed between glass plates under a microscope, homogenized, and then split into aliquots for duplicate analyses (when applicable). To maintain trace metal clean conditions, the samples were then cleaned according to the procedures described by Schmidt et al. (2012b) in a laminar flow clean bench. The cleaning process included sonication in both ultra clean water and methanol to remove clays, a hot water bath in reducing agents to remove metal oxides, and a hot water bath in an oxidizing solution to remove organic matter. Finally, the samples were transferred to new acid-leached micro-centrifuge vials and leached with a dilute ultra-pure nitric acid solution. The samples were dissolved and analyzed at Texas A&M University on a Thermo Scientific Element XR High Resolution Inductively Coupled Plasma Mass Spectrometer (HR-ICP-MS) using isotope dilution, as outlined in Lea and Martin (1996). A suite of elements including Na, Mg, Ca, Sr, Ba, U, Al, Fe and Mn, were analyzed. Analyses with anomalously high (>100 μmol/mol) Al/Ca, Fe/Ca, or Mn/Ca ratios were rejected. High Al/Ca ratios indicate the presence of detrital clays that were not removed during the cleaning process, while elevated levels of Fe/Ca or Mn/Ca indicate the presence of diagenetic coatings that were not removed during the cleaning process.

III.3.3. GDGT Analyses

GDGTs were analyzed at Texas A&M University (a contributing member to the TEX_{86} interlaboratory study (Schouten et al., 2009)) according to Schouten et al. (2002) as modified by Smith et al. (2010). Approximately 1 to 5 g of freeze-dried sediment were extracted (3 times, 5 minutes each) in 9:1 CH_2Cl_2:CH_3OH using a Dionex accelerated solvent extractor (ASE) at 100°C and $7.6x10^6$ Pa. The extracts were loaded onto an activated (2 hours, 150°C) alumina pipet column. Hexane:CH_2Cl_2 (9:1 vol:vol) was used to elute the apolar fraction and CH_2Cl_2:MeOH (1:1) to elute the polar fraction, which contained the GDGTs. Polar extracts were dissolved in hexane/isopropanol (99:1; % vol.:vol.) at a concentration of 2 mg mL^{-1}, and filtered through a 0.2 μM PTFE syringe-tip filter into silanized 150 μL vial inserts. Analysis was performed with a Shimadzu 2010A Series liquid chromatography–mass spectrometry (LC–MS) instrument with LC-MS solution software. Separation was achieved with a Prevail Cyano column (4.2 x 150 mm, 3 μm; Alltech) maintained at 30°C. GDGTs were eluted at a flow rate of 1 mL $min.^{-1}$, first isocratically with hexane/isopropanol (99:1; %vol.:vol.) for 5 minutes, then with a linear gradient up to 1.8% isopropanol over 40 minutes. To clean the column after each run, the gradient was increased to 75% 2-propanol over a period of three minutes, and held for ten minutes. After cleanup, the system was re-equilibrated for five minutes with 99:1 hexane/isopropanol. Analysis was achieved using atmospheric pressure chemical ionization–mass spectrometry (APCI–MS) using the following conditions: nebulizer pressure 65 psi, vaporizer temperature 400°C, N_2 drying gas flow 2.5 L $min.^{-1}$, capillary voltage of 4.5 kV. Single ion monitoring (SIM) was used instead

of full scanning to increase the reproducibility and signal-to-noise ratio (Schouten et al., 2007b). SIM was set to scan the $[M + H]^+$ parent ions of isoprenoidal GDGTs (m/z 1302, m/z 1300, m/z 1298, m/z 1296, m/z 1292) with a dwell time of 200 ms for each ion.

III.3.4. Mg/Ca Temperature Calculations

In order to calculate calcification temperatures for *G. ruber*, the Pacific Ocean dissolution corrected species-specific Mg/Ca:SST calibration from Dekens et al. (2002) was used:

$$Mg/Ca = 0.39 \exp 0.09 [SST - 0.61 (\text{core depth (km)}) - 1.6°C] \quad (\text{error} \pm 1.2°C) \quad \text{Eq. (3.2)}$$

The dissolution correction is based on the depth of the sediment core to account for the preferential loss shell Mg/Ca that increases with increasing seawater carbonate ion concentration and thus, depth. This calibration has been shown to work well in the ETP (Lea et al., 2006). To calculate upper-thermocline temperatures (T) from *G. menardii*, the species-specific calibration from Regenberg et al. (2009) was used:

$$Mg/Ca = 0.36 \exp 0.091(T) \quad \text{Eq. (3.3)}$$

However, this calibration equation was developed using core-top samples from the tropical Atlantic, where foraminiferal tests are better preserved than those in the tropical Pacific. Therefore, we employed a method similar to that used by Steph et al. (2010) and added a dissolution correction developed by Dekens et al. (2002) that was developed for *G. sacculifer* to Eq. (3.3):

$$Mg/Ca = 0.36 \exp 0.091 [T - 0.36 (\text{core depth (km)}) - 2.0°C] \quad (\text{error} \pm 1.2°C) \quad \text{Eq. (3.4)}$$

This depth-based dissolution correction has been applied successfully to reconstructions for the species *Globorotalia tumida*, a species with similar dissolution potential to *G. menardii* (Ford et al., 2012). Finally, the Pacific Ocean dissolution corrected *N. dutertrei* calibration from Dekens et al. (2002) was used to calculate lower thermocline temperatures from *N. dutertrei* Mg/Ca ratios:

$$Mg/Ca = 0.60 \exp 0.08 [SST - 2.8 (\text{core depth (km)}) - 5.4°C] \quad (\text{error} \pm 1.6°C) \quad \text{Eq. (3.5)}$$

III.3.5. TEX_{86} Temperature Calculations

The TEX_{86} index described in Eq. (3.1) was calculated based on the GDGTs analyzed in the sediment samples. From this, we calculated the TEX_{86}^{H} index that was developed by Kim et al. (2010) for reconstructing oceanic temperatures above 15°C:

$$TEX_{86}^{H} = \log (TEX_{86}) \qquad \text{Eq. (3.6)}$$

Lastly, TEX_{86}^{H} values were converted to temperature using the core-top calibration developed by Kim et al. (2010):

$$T = 38.6 + 68.4 (TEX_{86}^{H}) \quad (\text{error} \pm 2.5°C) \quad \text{Eq. (3.7)}$$

Our choice of TEX_{86} temperature calibration equation is explored further in Section III.5.1.

III.4. Results

The results for all foraminiferal and TEX_{86} analyses are summarized in Figure 3.3. Also shown in Figure 3.3 are the standard deviations for individual samples for which duplicate analyses were performed.

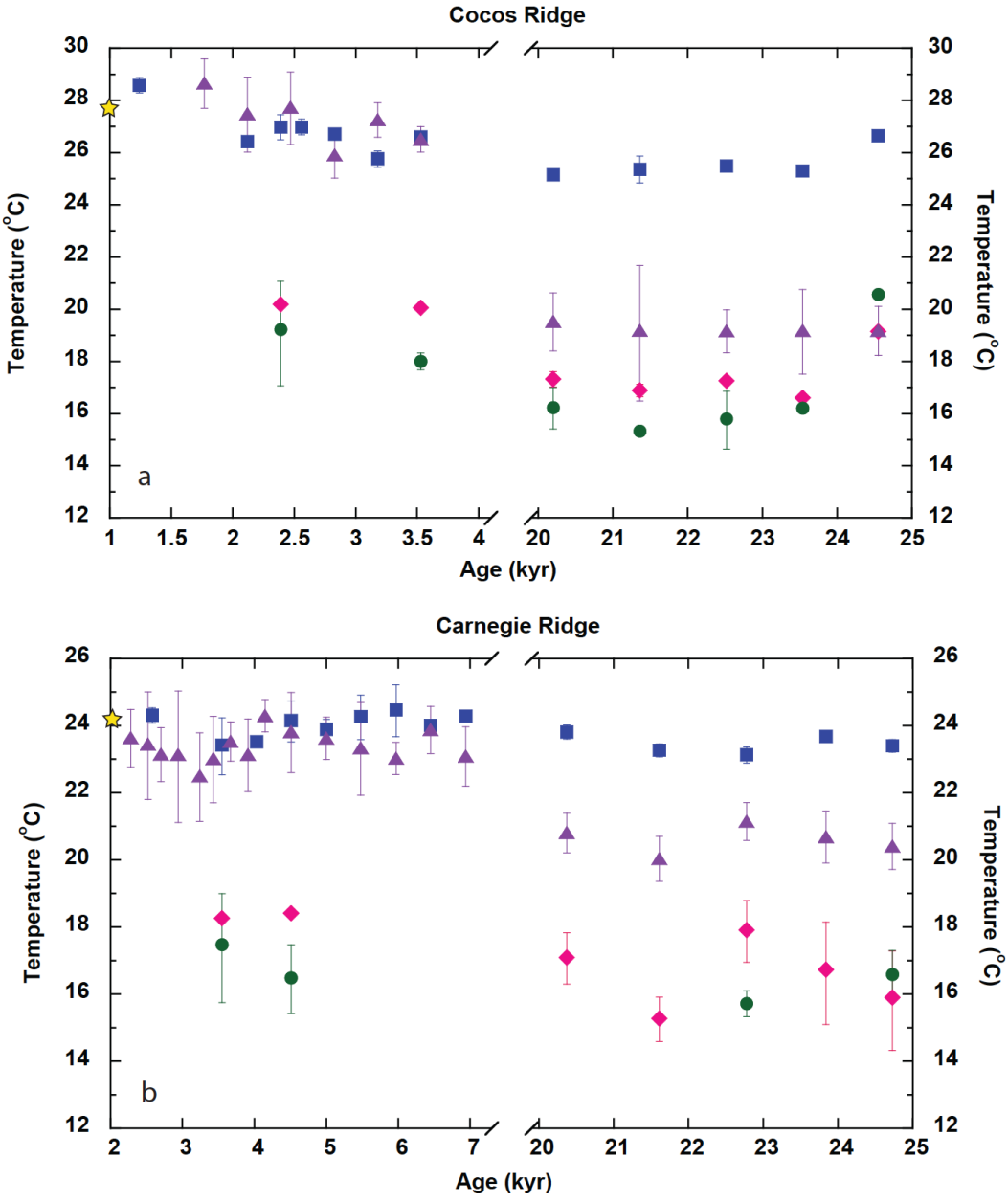

Figure 3.3 Reconstructed TEX_{86}^{H} and multi species planktonic foraminiferal Mg/Ca temperatures. (a) Cocos Ridge and (B) Carnegie Ridge. For the (a) Cocos Ridge, Holocene and Last Glacial Maximum values are from 07MC and 08JC. For the (b) Carnegie Ridge, Holocene and Last Glacial Maximum values are from 09MC and 17JC, respectively. Plotted are *Globigerinoides ruber* Mg/Ca temperatures (blue squares), *Globorotalia menardii* Mg/Ca temperatures (pink diamonds), *Neogloboquadrina dutertrei* Mg/Ca temperatures (green circles), and TEX_{86}^{H} temperatures (purple triangles). Also plotted are the 2-sigma standard deviations on replicate analyses (for samples containing enough material for replicate analyses). Observational modern average annual sea surface temperatures for both study sites are plotted on the temperature axes with yellow stars. Note the x-axis breaks between Holocene and Last Glacial Maximum temperatures, and the differing temperature scales between the Cocos and Carnegie Ridges. See the text for the calibration equations used to compute all Mg/Ca and TEX_{86}^{H} temperatures.

III.4.1. Holocene Results

For 07MC, the measured core-top *G. ruber* Mg/Ca temperature of 28.6°C is in good agreement with the modern average annual SST at the Cocos Ridge site of 27.8°C (Figure 3.3A). In addition, the measured core-top TEX_{86}^{H} temperature of 28.7°C is also in good agreement with the modern average annual SST (Figure 3.3A). Similarly, for 09MC, the measured core-top *G. ruber* Mg/Ca and TEX_{86}^{H} temperatures of 24.3°C and 23.6°C, respectively, are both in good agreement with the modern average annual SST at the Carnegie Ridge site of 24.1°C (Figure 3.3B). It is important to note that some of the uppermost intervals of the multicores do not have both TEX_{86}^{H} and Mg/Ca temperatures on the same intervals. This is due to the high-resolution shipboard sampling scheme of the uppermost layers of the multicores, resulting in some samples needing to be combined to allow for enough sample material for analyses. Slight discrepancies between the core-top values and modern SST values may result from age deviations of the core-top samples from modern (1.24 and 2.58 kyr for 07MC and 09MC, respectively). The close agreement between proxies continues down-core for the Holocene, with *G. ruber* Mg/Ca and TEX_{86}^{H} temperatures at both sites matching well, within error. For 07MC, average Holocene Mg/Ca and TEX_{86}^{H} temperatures are 26.9°C and 27.3°C, respectively (Figure 3.3A), and 24.0°C and 23.4°C, respectively for 09MC (Figure 3.3B). While TEX_{86}^{H} temperatures are slightly warmer than Mg/Ca temperatures on the Cocos Ridge, they are slightly cooler on the Carnegie Ridge. Thus, there does not appear to be a consistent offset to warmer or cooler temperatures between the two proxies during the Holocene.

Mg/Ca temperatures of *G. menardii* and *N. dutertrei* were obtained for two intervals from each multi-core to compare the modern depth habitats with the depth habitats inferred from the Mg/Ca temperatures. The intervals were chosen based on those with the greatest number of shells available for analysis. For 07MC on the Cocos Ridge, *G. menardii* Mg/Ca temperatures averaged 20.1°C and *N. dutertrei* Mg/Ca temperatures averaged 18.6°C (Figure 3.3A). Based on the modern thermocline at the study area, these temperatures would correspond to a depth habitat for *G. menardii and N. dutertrei* of 50 m and 60 m (based on annual average temperature profiles), respectively, well in line with previous studies (Fairbanks et al., 1982 and Faul et al., 2000) (Figure 3.2A). On the Carnegie Ridge, results from 09MC returned average Mg/Ca temperatures for *G. menardii and N. dutertrei* of 18.3°C and 17.0°C, respectively (Figure 3.3B), corresponding to depths of 45 m and 55 m, respectively (Figure 3.2B). These results also agree well with previous studies (Fairbanks et al., 1982; Faul et al., 2000), giving us confidence that the Mg/Ca calibration equations used for each of these species can be used to determine thermocline temperatures during the LGM.

III.4.2. Last Glacial Maximum Results

Unlike the close agreement between Mg/Ca and TEX_{86}^{H} temperatures for both study regions for the Holocene, results for the LGM suggest TEX_{86}^{H} temperatures are representative of subsurface, upper thermocline temperatures during this time period. For piston core 08JC on the Cocos Ridge, *G. ruber* Mg/Ca temperatures average 25.6°C at the LGM from 20 – 25 kyr, while TEX_{86}^{H} temperatures yield an average of 19.3°C over the same time interval (Figure 3.3A). The average difference between *G. ruber*

Mg/Ca temperatures and TEX_{86}^{H} temperatures is 6.3°C, ranging from 5.6°C to 7.5°C over the time interval. TEX_{86}^{H} temperatures remain relatively constant, and changes in the offset between the proxies are driven by variability in *G. ruber* Mg/Ca temperatures. The average *G. menardii* and *N. dutertrei* Mg/Ca temperatures at the LGM are 17.4°C and 16.8°C, respectively (Figure 3.3A), indicating that the TEX_{86}^{H} temperatures are more representative of thermocline temperatures than upper mixed layer temperatures, suggesting a deeper GDGT export depth during the LGM.

On the Carnegie Ridge, we also find an offset between *G. ruber* Mg/Ca and TEX_{86}^{H} temperatures at the LGM, although not as large as the offset on the Cocos Ridge. For piston core 17JC, *G. ruber* Mg/Ca temperatures average 23.5°C, while TEX_{86}^{H} temperatures yield an average of 20.6°C from 20 – 25 kyr (Figure 3.3B). TEX_{86}^{H} temperatures are cooler than *G. ruber* Mg/Ca temperatures by an average of 2.9°C, although this offset ranges from 2.0°C to 3.2°C over the time period. Average *G. menardii* and *N. dutertrei* Mg/Ca temperatures on the Carnegie Ridge at the LGM are 16.6°C and 16.2°C, respectively (Figure 3.3B). TEX_{86}^{H} and *G. menardii* temperatures display similar trends of cooling and warming over the interval, indicating that both may be influenced by changes in thermocline properties, as *G. ruber* temperatures do not display the same trend. Therefore, it appears that TEX_{86}^{H} temperatures are also representative of subsurface temperatures at the LGM on the Carnegie Ridge as well.

III.5. Discussion

III.5.1. TEX_{86} Temperature Calibrations

Since the development of the first TEX_{86} temperature calibration (Schouten et al., 2002), subsequent temperature calibrations have been developed based on the addition of core-tops to the global core-top database (Kim et al., 2008) and the separation of calibrations into temperature ranges (TEX_{86}^{L} for -3° to 30°C, TEX_{86}^{H} for 5° to 30°C) (Kim et al., 2010). Most recently, Tierney and Tingley (2014) developed a temperature calibration using a Bayesian regression model approach that varies spatially (termed BAYSPAR), and utilizes previously published core-top data (Kim et al., 2010) along with the addition of 155 core-top sites. We compare results from four of these calibration equations in Table 2, excluding the TEX_{86}^{L} calibration, as it is not recommended for temperatures above 15°C (Kim et al., 2010). Using each calibration equation, we compare temperatures for three intervals of our study regions: the multicore core-top values, the average Holocene value, and the average LGM value (Table 3.2). Also shown are the World Ocean Atlas 13 average annual SST (0 m) at both study regions (Locarnini et al., 2013), and the corresponding *G. ruber* Mg/Ca SSTs for the same three intervals.

Overall, the TEX_{86}^{H} calibration (Kim et al., 2010) shows the greatest agreement between core-top temperatures and average annual SSTs at both sites. When applying the BAYSPAR calibration (Tierney and Tingley, 2014), there is a significant warm bias at the Cocos Ridge study area for the core-top value (6.2°C warmer than *G. ruber* Mg/Ca SST, 6.1°C warmer than TEX_{86}^{H} temperature) that propagates through the Holocene.

	Multi-Core Core Top		Holocene Average		LGM Average	
	Cocos Ridge	Carnegie Ridge	Cocos Ridge	Carnegie Ridge	Cocos Ridge	Carnegie Ridge
Schouten et al. (2002)	29.0	21.6	26.9	21.3	16.1	17.7
Kim et al. (2008)	29.4	23.2	27.6	22.9	18.5	19.9
Kim et al. (2010)	28.7	23.6	27.3	23.4	19.3	20.6
Tierney & Tingley (2014)	34.8	25.5	32.1	25.0	18.6	20.6
G. ruber Mg/Ca SST	28.6	24.3	26.9	24.0	25.6	23.5
WOA13 SST (0 m)	27.8	24.1				

All values in °C

Table 3.2 Comparison of TEX_{86} Calibrations and Temperature Proxies

The core-top BAYSPAR value of 34.8°C is well above even the maximum seasonal SST at the Cocos Ridge site of 29.0°C (Figure 3.2A, April). The BAYSPAR calibration also yields core-top temperatures warmer than annual average and *G. ruber* Mg/Ca SSTs on the Carnegie Ridge, although the differences are not nearly as great as on the Cocos Ridge. The unique aspect of the BAYSPAR calibration model is that it varies spatially, deriving 'local' TEX_{86}-SST calibrations based on regression parameters from 20° by 20° grid boxes (Tierney and Tingley, 2014). The 20° by 20° grid boxes used for the calculation of BAYSPAR temperatures on the Cocos and Carnegie Ridges are shown in Figure 3.4. We hypothesize that the disagreement between BAYSPAR temperatures and the other TEX_{86} calibrations stems from the integration of parameters in the regression grid box from a region of strong oceanographic gradients, and the spread of core-top data within the grid box across these gradients that is influencing the 'local' regression. The Cocos Ridge cores used in this study were retrieved from the EPWP region, and those from the Carnegie Ridge are from the cold-tongue upwelling region. The thermocline in the EPWP is stronger than that in the cold-tongue region, which may influence the water column distribution of GDGTs. In addition, it is still unclear whether nutrient availability can affect the production of certain GDGTs (Turich et al., 2007) or even GDGT production by Marine Group II Euryarchaeota that may be more present than Thaumarchaeota in shallow water (Lincoln et al. 2014). Thus, the differing nutrient regimes of our two study areas incorporated into one 20° by 20° grid box may be a cause of the offsets between the BAYSPAR and other TEX_{86} calibrations that rely on global calibrations.

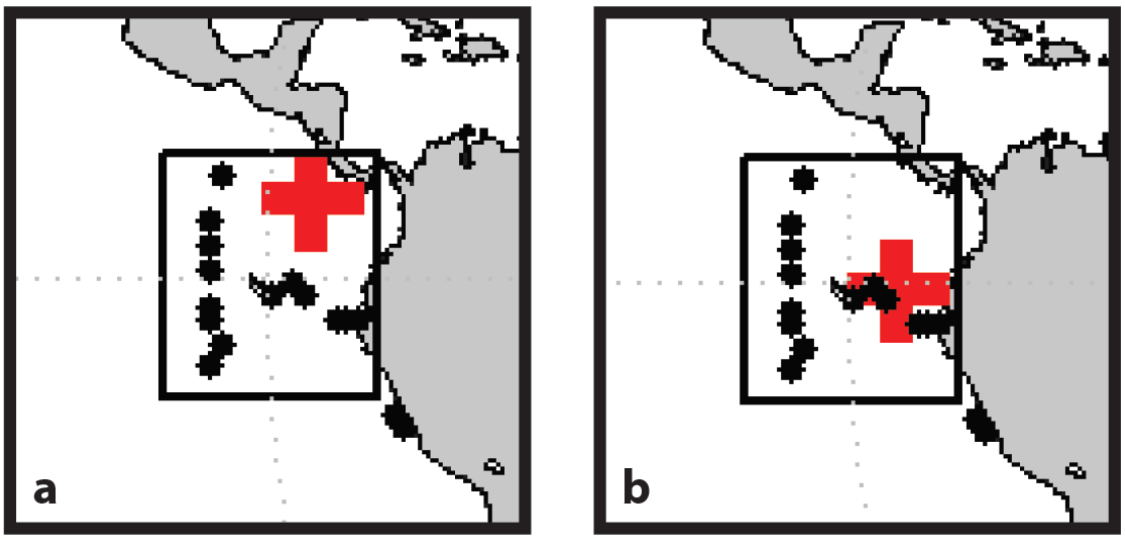

Figure 3.4 20° by 20° grid boxes used in the calculation of BAYSPAR TEX_{86} temperatures. Grid boxes are outlined in black squares, red crosses show the location of cores used in this study on the (a) Cocos Ridge and (B) Carnegie Ridge. Shown with black stars are the locations of core-top TEX_{86} data that are used in the calculation of local parameters for the BAYSPAR calibration. The standard prediction mode with default settings was used on the web interface (www.whoi.edu/bayspar). Values were calculated in April, 2015 (noted as the core-top database is subject to updating).

The use of different TEX_{86} temperature calibrations also does little to improve the offset between TEX_{86} temperatures and *G. ruber* Mg/Ca temperatures at the LGM (Table 3.2). The BAYSPAR calibration model (Tierney and Tingly, 2014) is in better agreement with the other TEX_{86} temperature calibrations at the LGM, returning the same average LGM temperature as the Kim et al. (2010) TEX_{86}^{H} calibration for the Carnegie Ridge. As there is little difference between the TEX_{86} temperature calibrations at the LGM, and the Kim et al. (2010) TEX_{86}^{H} core-top temperatures agrees best with both *G. ruber* Mg/Ca temperatures and modern average annual temperatures at both study sites, we utilize TEX_{86}^{H} temperatures for the remainder of our discussion.

III.5.2. Implications for the Use of the TEX_{86} Temperature Proxy

If our first order assumption is that TEX_{86}^{H} temperatures should reflect SSTs based on studies finding higher correlations between core-top TEX_{86} indices and temperatures at 0 m ($r^2 = 0.94$) than depth averaged temperatures from 0 – 200 m ($r^2 = 0.87$) (Kim et al., 2008), then our core-top and Holocene results would suggest that the TEX_{86} proxy could be used reliably to reconstruct SSTs in the ETP. However, the assumption that TEX_{86}^{H} temperatures reflect SSTs may not hold further back in time. As we do not have observational SST data for the LGM, we must rely on the *G. ruber* Mg/Ca SSTs to assess the reliability of TEX_{86}^{H} temperatures to reflect SSTs at the LGM. *G. ruber* has a well-established depth habitat in the upper mixed layer and is thus well suited for this purpose. Based on our findings that TEX_{86}^{H} temperatures were on average 6.3°C and 2.9°C cooler than *G. ruber* Mg/Ca SSTs at the LGM for the Cocos and Carnegie Ridges, respectively, it is evident that the assumption that TEX_{86}^{H}

temperatures reflect SSTs does not hold with time. Therefore, caution should be taken when interpreting TEX_{86} records based solely on the relationship between core-top/Holocene TEX_{86} temperatures and modern observational temperatures.

We hypothesize that the differing depth that TEX_{86}^{H} temperatures reflect is due to variability in GDGT export depth with time. Recent studies have suggested that Thaumarchaeota are aerobic ammonia oxidizers (Könneke et al., 2005), and thus their position in the water column should coincide with the subsurface primary nitrite maximum, located toward the base of the euphotic zone. Under modern conditions in the ETP, the subsurface nitrite maximum is centered around ~40 m depth (Figure 3.5), however, values elevated above 0 can be found as shallow as ~10 m, well within the depths of the surface mixed layer. The shallow depth of the nitrite maximum is likely due to high concentrations of degradable organic material in the upper water column where oxygen levels are still high enough for aerobic ammonia oxidation. The shallow nitrite maximum may explain the close match between TEX_{86}^{H}, *G. ruber* Mg/Ca, and modern SSTs at both of our study sites in the ETP. However, in modern oligotrophic regions, such as the Sargasso Sea, the subsurface nitrite maximum typically occurs much deeper, around 120 – 150 m depth and is decoupled from the thermocline (Brzezinski 1988 and Lomas and Lipschultz, 2006). Thus, the colder TEX_{86}^{H} temperatures at the LGM in the ETP may reflect a deepening of the nitrite maximum under differing nutrient availability, and by association, a deeper depth habitat for Thaumarchaeota. Loubere and Fariduddin (2008) used benthic foraminiferal abundances from ETP sediment cores to reconstruct productivity, based on transfer functions between

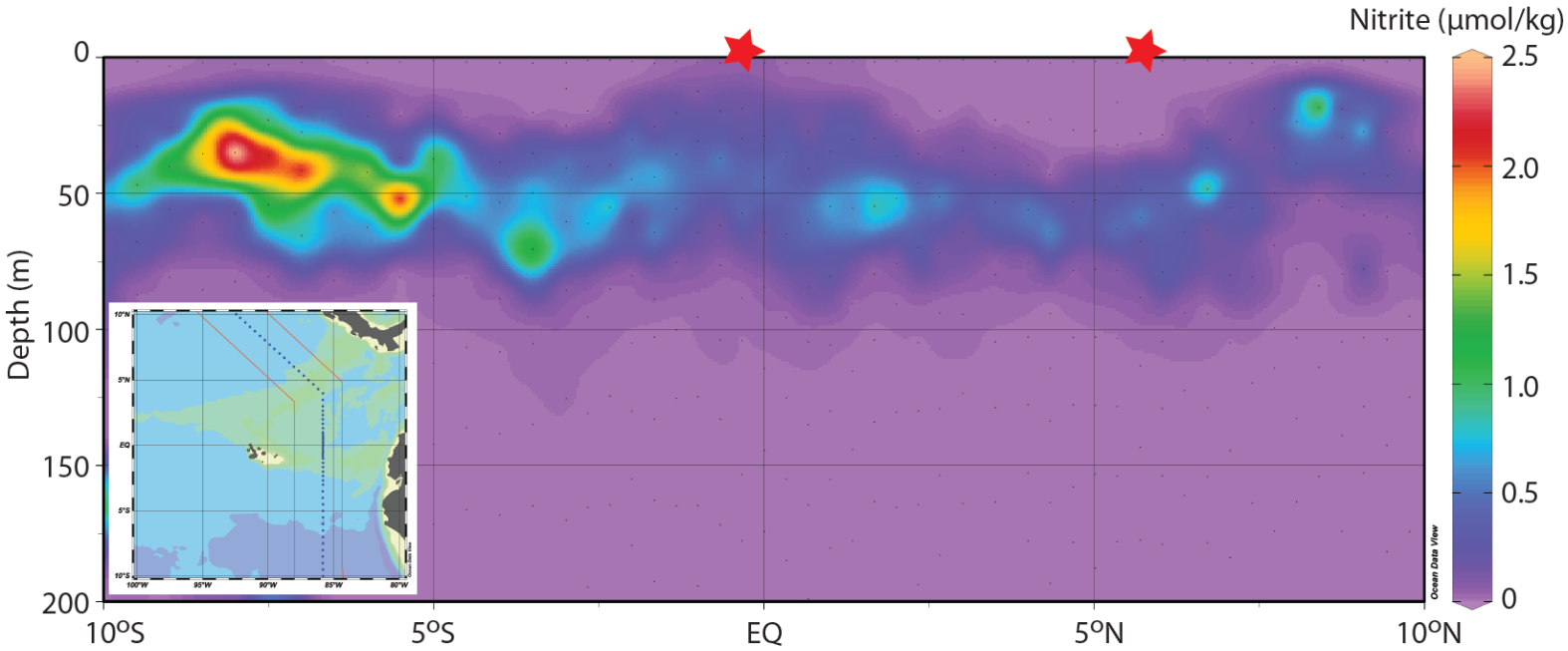

Figure 3.5 Nitrite concentrations along the WOCE P19C line. Nitrite concentrations in the Eastern Tropical Pacific along the WOCE P19C survey line (inset). Shown are the bottle data from 10°N to 10°S in gridded section plotted with Ocean Data View (Schlitzer, 2013). Red stars along the 0 m depth show the approximate locations of the Cocos Ridge study area at 6°N and the Carnegie Ridge study area at .0°S.

abundances and surface ocean biological productivity. Their results, along with measurements of the $\delta^{13}C$ of the thermocline dwelling planktonic foraminifera *N. dutertrei*, suggest reduced export production during the LGM likely driven by a reduction in thermocline nutrient concentrations (Loubere and Fariduddin, 2008). Robinson et al. (2009) used bulk sediment $\delta^{15}N$ and total nitrogen concentration data to also show that the LGM was a period of reduced nutrient supply in the ETP. The cause of the reduced LGM nutrient supply to the ETP has been suggested to be a reduction in nutrients of the EUC supplied by Subantarctic Mode Water and Antarctic Intermediate Water (Spero et al., 2003). In addition, the nitrification of ammonium to nitrite requires oxygen, and a reduction in surface water productivity during the LGM may have increased the availability of oxygen at deeper depths in the water column. Support for this idea comes from a study by Cartapanis et al. (2011) who measured redox-sensitive trace metal concentrations in a sediment core from the Northeastern Pacific. Although further north from our study sites, the study suggested that the LGM was a period of reduced strength of the regional oxygen minimum zone as a result of either decreased export productivity or enhanced delivery of oxygenated subsurface waters to the area (Cartapanis et al., 2011). If TEX_{86}^{H} temperatures in this region can track vertical changes in the depth of nitrification with time, the proxy might have a use as a productivity and nutrient proxy.

The interpretation of a decrease in LGM export productivity would be at odds with studies that have suggested that the LGM was a period of increased export productivity (e.g. Lyle, 1988, Pederson, 1983 and Pederson et al., 1991). It is interesting

to note that these studies predominantly find that export production was greater in the *equatorial* Pacific during the LGM, while studies further to the north suggest the LGM was less productive (e.g. Dean et al., 1997 and Ganeshram and Pedersen, 1998). Based on the differing cold biases between the Cocos Ridge and the Carnegie Ridge at the LGM, it is possible that while the Cocos Ridge was experiencing a decrease in export productivity, the Carnegie Ridge was not experiencing the same conditions. The average offset between *G. ruber* and TEX_{86}^{H} temperatures at the LGM on the Carnegie Ridge is 2.9°C, minimally outside of the ± 2.5°C error on TEX_{86}^{H} temperatures. In addition, as *G. ruber* is predominantly a tropical species of foraminifera, it is possible that LGM SSTs were at the cold end for the preferred temperature habitat of *G. ruber*, and thus, they were only living during (and therefore recording) the warmest months of the year at the LGM. This interpretation suggests that there may have been large spatial differences in productivity during the LGM, with sites north of the equatorial cold tongue upwelling area experiencing a decrease in productivity, and the equatorial region experiencing no change, or an increase in productivity.

Alternatively, if our first order assumption is incorrect, and the agreement between TEX_{86}^{H} core-top temperatures and *G. ruber* Mg/Ca temperatures and modern average annual temperatures at both study sites is merely a function of issues stemming from the TEX_{86} temperature calibration, it is possible that TEX_{86}^{H} temperatures should always represent subsurface temperatures. If in fact GDGT production depths did not vary temporally and TEX_{86}^{H} temperatures are always representative of subsurface temperature, then changes in TEX_{86}^{H} between the LGM and Holocene may solely reflect

changes in subsurface temperature conditions. Although more research needs to be done to fully understand the environmental controls on Thaumarchaeota depth habitats, based on the currently available research on Thaumarchaeota as aerobic ammonia oxidizers (Könneke et al., 2005), we favor our first scenario of changing GDGT export depths due to varying nutrient levels between the Holocene and LGM. Lastly, we do not believe the offset between proxies at the LGM is due to differences in preservation of GDGTs between the Holocene and LGM. Although GDGTs are relatively refractory compounds, they do degrade over time (Huguet et al., 2008). However, studies have shown that diagenetic degradation does not affect the TEX_{86} index within analytical error (Huguet et al., 2009, Kim et al., 2009a, Schouten et al., 2004 and Sinninghe Damsté et al., 2002b). Similarly, studies have shown that GDGTs are minimally impacted by lateral transport, and are primarily influenced by local conditions (Kim et al., 2009b and Mollenhauer et al., 2008).

III.5.3. Implications for Calculating the Magnitude of LGM Cooling

Understanding the magnitude of LGM SST cooling is a key question for paleoceanographers, as it provides constraints on climate sensitivity under different forcings and boundary conditions. In turn, climate modelers can use these constraints on climate sensitivity to better predict future climate change (Schmittner et al., 2011). The earliest estimations of LGM cooling were compiled by the CLIMAP project (CLIMAP Project Members, 1976) based on temperature transfer functions of planktonic foraminiferal abundances. More recently, the MARGO project (MARGO Project Members, 2009) took a multi-proxy approach, integrating microfossil and geochemical

reconstructions of SST to understand the magnitude of LGM SST cooling. Unfortunately, the distribution of records used by the MARGO project does not cover large areas of the Pacific Ocean, likely due to the absence of calcareous microfossils in sediments and areas approaching the upper limit of the $U^{k'}_{37}$ SST proxy. The MARGO project did not include estimates of cooling based on TEX_{86} temperatures, as the proxy was still in the early stages of its uses during that time. However, the TEX_{86} proxy is enticing to use as it overcomes many of the shortfalls of the other SST proxies and could potentially fill in large spatial gaps in the MARGO data set.

If we define the degree of LGM cooling (LGM ΔT) as the average LGM (20 – 25 kyr) temperature minus the multi-core core-top temperature (1.24 and 2.58 kyr for 07MC and 09MC, respectively), we can compare the magnitude of LGM cooling based on both TEX_{86}^{H} and *G. ruber* Mg/Ca temperatures at both of our study sites. LGM ΔT values based on *G. ruber* Mg/Ca temperatures are -2.99°C and -0.85°C for the Cocos Ridge and Carnegie Ridge, respectively, while LGM ΔT values based on TEX_{86}^{H} temperatures are -9.4°C and -3.0°C. The LGM ΔT values based on *G. ruber* Mg/Ca temperatures are in line with other studies from the ETP (e.g. Lea et al., 2000), averaging no more than 3.0°C of LGM cooling. Although the LGM ΔT value based on TEX_{86}^{H} temperatures for the Carnegie Ridge is within this range, there is a marked offset between the LGM ΔT values between the two proxies. This may be due to a summer season bias on *G. ruber* Mg/Ca temperatures, as sediment trap studies suggest that on average *G. ruber* abundances in the tropical Pacific peak in boreal summer (Thunell et al. 1983). On the Cocos Ridge, the LGM ΔT value based on TEX_{86}^{H} temperatures is

over three times greater than that based on *G. ruber* Mg/Ca temperatures, and is well outside of any LGM ΔT reported for the ETP (MARGO Project Members, 2009). Our findings agree well with a recent compilation of LGM TEX_{86} and $U^{k'}_{37}$ records by Ho and Laepple (2015). The study calculated LGM ΔT values based on TEX_{86} and $U^{k'}_{37}$ proxies for a number of tropical and subtropical sites, and found that TEX_{86}^{H} based LGM ΔT values consistently averaged ~two times greater than those values based on $U^{k'}_{37}$ values (Ho and Laepple, 2015). Based on our findings and the results of the Ho and Laepple (2015) study, we would not recommend including TEX_{86}^{H} based LGM ΔT values in global compilation studies.

III.6. Conclusions

We have compared TEX_{86} temperatures and Mg/Ca temperatures of three species of planktonic foraminifera that inhabit the upper mixed layer and thermocline for two regions of the ETP over the Holocene and LGM. While TEX_{86}^{H} temperatures agree well, within error, with *G. ruber* Mg/Ca temperatures for the Holocene, there is a significant cold bias in TEX_{86}^{H} temperatures at the LGM for both study regions whereby TEX_{86}^{H} temperatures are more representative of upper thermocline temperatures than SSTs. The offset between *G. ruber* Mg/Ca temperatures and TEX_{86}^{H} temperatures cannot be reconciled with the use of different TEX_{86} temperature calibrations. The best explanation for the offset between proxies is a decrease in nutrient availability in ETP during the LGM, especially for the Cocos Ridge study region, where the offset between proxies was greatest. However, on the Carnegie Ridge, there may not have been a decrease in LGM productivity, as suggested by the smaller offset between proxies and

the potential seasonal bias in *G. ruber* Mg/Ca temperatures. This finding suggests that caution should be applied when interpreting TEX_{86} records based solely on the relationship between core-top/Holocene TEX_{86} temperatures and modern observational temperatures, as TEX_{86} temperatures may be tied to productivity variability. In addition, we have compared glacial cooling estimates based on both temperature proxies and found estimates based on TEX_{86}^{H} temperatures to be too high (greater degree of cooling), especially on the Cocos Ridge, in comparison with other regional records. Therefore, TEX_{86}^{H} temperatures should not be used for computing glacial cooling, especially in the ETP.

CHAPTER IV

THERMOCLINE TEMPERATURE VARIABILITY REVEALS SHIFTS IN THE TROPICAL PACIFIC MEAN STATE ACROSS MARINE ISOTOPE STAGE 3

IV.1. Introduction

The current climatic mean state of the equatorial Pacific Ocean is characterized by trade wind induced upwelling of cold water in the east and the accumulation of warm surface waters in the west, resulting in a strong east-west sea surface temperature (SST) gradient. This SST gradient is reflected in the subsurface by a deeper thermocline in the western Pacific that shoals to near the surface in the eastern equatorial Pacific (EEP) upwelling region. The initiation and propagation of El Niño-Southern Oscillation (ENSO) events are due to perturbations to this ocean-atmosphere system, as trade wind strength and the zonal SST gradient are intrinsically linked. Although ENSO originates in the tropical Pacific, it affects global weather and climate events, such as drought/flooding and tropical storms, through teleconnections.

A number of modeling studies suggest that ENSO interacts with the mean state of the tropical Pacific (Guilyardi, 2006). For example, a reduced east-west SST gradient is associated with a weakened Walker circulation and reduced trade wind strength. If an external forcing introduces east-west asymmetry, this asymmetry can be amplified in the same way as interannual perturbations are, through the positive ocean-atmosphere Bjerknes feedback (DiNezio et al., 2010). This then would lead to an altered mean state

of the tropical Pacific resembling El Niño or La Niña (Dijkstra and Neelin, 1995). Such changes in the mean state can influence ENSO-related processes and feedbacks, and have the potential to modify ENSO properties (Choi et al., 2012 and Guilyardi et al., 2009). Nevertheless, it remains unclear how ENSO feedbacks interact as the mean state changes, and these questions will become increasingly important as our current climate continues to warm, potentially altering the mean state (Latif and Keenlyside, 2009).

Using a model capable of resolving ENSO variability, Clement and Cane (1999) investigated the effect of a uniform heating applied to tropical Pacific. Heating applied during late summer/early fall, when the Intertropical Convergence Zone (ITCZ) migrates north over the EEP, will result in larger atmospheric heating of the convergent western Pacific relative to the divergent eastern Pacific, driving easterly wind anomalies at the equator (Clement and Cane, 1999). In turn, this results in a cooler east Pacific, or more La Niña-like conditions. A uniform cooling applied to the tropical Pacific in late summer/early fall yields the opposite response, with westerly wind anomalies on the equator, which can develop into a more El Niño-like response (Clement and Cane 1999). These changes to the tropical Pacific mean state under varying climate forcings, termed the ocean dynamical thermostat, have been invoked to explain a number of paleoclimate records attempting to reconstruct past mean state changes (e.g. Koutavas et al., 2002 and Stott et al., 2002).

A recent study by Schmidt et al. (2014) analyzed CMIP5 (Coupled Model Intercomparison Project 5) model simulations to try to understand future climate variability (under future projections with varying greenhouse gas radiative forcings)

based on the models ability to hindcast paleoclimate changes. The study noted that although trends in the mean state and ENSO-related variance within the tropical Pacific were highly variable over the 20th century among model runs, the CMIP5 projections converged upon a more El Niño-like (warmer EEP) mean state change by the year 2100 (Schmidt et al., 2014). This finding, however, would be at odds with the dynamical thermostat theory, as it predicts a more La Niña-like mean state under increased warming, suggesting the tropical Pacific ocean-atmosphere system has more complex feedbacks then previously thought. Thus, having constraints on past mean state changes, especially under past periods of abrupt warming, may be key to understanding future climate change.

Modeling efforts such as those performed by Schmidt et al. (2014) commonly use benchmark time periods of the Last Glacial Maximum (LGM), the mid-Holocene, and the last millennium to measure model skill. Indeed, numerous studies have attempted to reconstruct the tropical Pacific mean state across these time intervals, but often come to disagreeing results. For example, Koutavas et al. (2002) and Koutavas and Joanides (2012) characterized the LGM as more El Niño-like with amplified ENSO variability, while a recent study by Ford et al. (2015) found a deeper EEP thermocline during the LGM that resulted in reduced ENSO variability compared to the late Holocene.

Here, we use the abrupt climate warming events of Marine Isotope Stage 3 (MIS 3), termed Dansgaard-Oeschger (D-O) events, from 32 – 64 kyr, as a natural experiment for understanding how the tropical Pacific mean state changed across past periods of

rapid climate warming. D-O events are periods of abrupt warming and gradual cooling that punctuated the climate of the last glacial period (Schmidt and Hertzberg, 2011). These abrupt warmings are thought to be due to sudden reinvigorations of Atlantic Meridional Overturning Circulation from a more subdued glacial state (Clement and Peterson, 2008). We measure the Mg/Ca ratios of a thermocline dwelling planktonic foraminifera, *Neogloboquadrina dutertrei*, as a proxy for thermocline temperature variability from a sediment core recovered from the heart of the EEP cold-tongue upwelling region. Reconstructing subsurface temperature change in this region removes the large seasonal cycle imprint on surface temperatures, and instead, thermocline temperatures vary with ENSO conditions. We interpret variability in thermocline temperatures as shifts in the tropical Pacific mean state whereby increases or decreases in subsurface temperature are indicative of a more El Niño-like or La Niña-like mean state, respectively. These results can then be used in modeling studies to determine whether perturbations in the mean state of the tropical Pacific may effect future changes in ENSO dynamics and associated teleconnections.

IV.2. Oceanographic Setting

The EEP is a highly dynamic oceanographic region characterized by strong vertical and meridional gradients. The easterly trade winds blowing along the equator result in Ekman induced divergence of surface waters and consequent upwelling along the equator. The resultant shallow thermocline leads to the upwelling of cool, nutrient rich waters, giving rise to the eastern Pacific equatorial cold-tongue, extending east of 120ºW to the South American continent (Fiedler and Talley, 2006). Just beneath the

surface along the equator, lies the strong, eastward flowing Equatorial Undercurrent (EUC). The EUC lies at the base of the equatorial thermocline between 30 – 300 m and is the source of the water that upwells into the thermocline (Kessler, 2006). As the source waters of the EUC are derived from sub-Antarctic Mode Water/Antarctic Intermediate Waters that form in the Southern Ocean off Antarctica, the EEP serves as an important region linking the tropics to the high latitudes (Toggweiler et al., 1991). The three main surface currents of the EEP are the eastward flowing North Equatorial Countercurrent between 5 and 10ºN and the westward flowing North and South Equatorial Currents, which flow on either side of the countercurrent (Kessler, 2006). The equatorial front, located at around 3ºN, separates the cold tongue region to the south from the east Pacific warm pool to the north (Kessler, 2006)

Piston core MV1014-02-17JC (17JC hereafter; 0°10.8'S, 85°52.0'W; 2870 m water depth) was recovered from the EEP aboard the *R/V Melville* in 2010 on cruise MV1014 (Figure 4.1). The core location is on the northwest edge of the Carnegie Ridge and located directly within the cold tongue equatorial upwelling region (Fiedler and Talley, 2006). At the surface, temperatures range annually between 23.0°C (September) and 26.1°C (March), with an average annual temperature of 24.1°C (Locarnini et al., 2013). The surface mixed layer extends down to ~25 m, with the thermocline between 25 and 75 m. Average annual salinity at the surface is 34.1 (Zweng et al., 2013). The region is characterized by high concentrations of nutrients brought to the surface from upwelling, which fuels high primary productivity along the equator (Pennington et al., 2006).

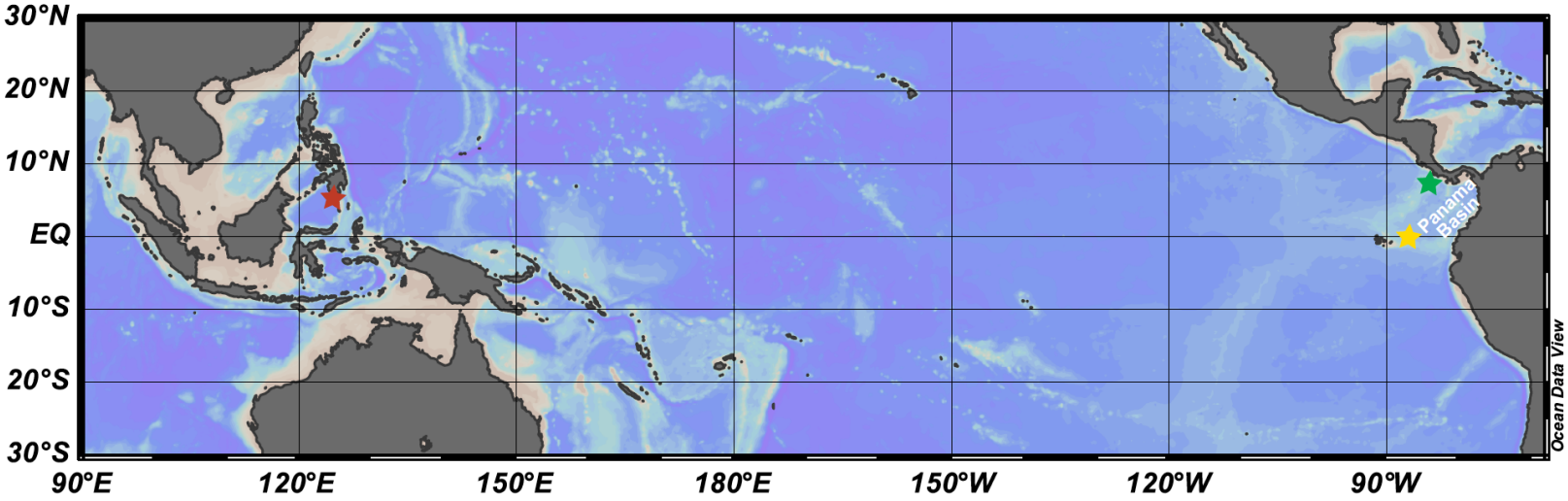

Figure 4.1 Locations of cores referred to throughout this study. Location of cores MV1014-02-17JC (yellow star; 0°10.8'S, 85°52.0'W; 2870 m water depth; this study), Ocean Drilling Program (ODP) Site 1240 (yellow star; 0°01.31'S, 86°27.76'W; 2921 m water depth; Pena et al., 2008), ME-24JC (yellow star; 0°01'N, 86°27'W; 2941 m water depth; Dubois et al., 2014), MD02-2529 (green star; 08°12.33'N, 84°07.32'W; 1619 m water depth; Leduc et al., 2007), and MD98-2181 (red star; 6.3°N, 125.83°E; 2114 m water depth; Saikku et al., 2009 and Stott et al., 2002). Note that cores 17JC, ODP 1240, and 24JC are all located in the general region of the yellow star marker. Also noted is the location of the Panama Basin in the Eastern Equatorial Pacific. Map created with Ocean Data View (Schlitzer, 2013).

IV.2.1. Subsurface Temperature Change as an Indicator of ENSO State

One of the major limitations to reconstructing climate variability in the EEP is the strong imprint of the seasonal cycle on surface ocean parameters (Leduc et al., 2009). While the surface mixed layer of our study region experiences high seasonality (3.1°C range), the subsurface experiences limited seasonality. The planktonic foraminifera *N. dutertrei* inhabits the lower thermocline region of the EEP between 50 and 75 m water depth, corresponding to the depth of highest primary productivity and the associated deep chlorophyll maximum (Fairbanks et al., 1982). At 75 m water depth at our study location, the seasonal range of temperatures is ~1.3°C, less than half of the sea surface seasonality (Figure 4.2).

The location of 17JC is also directly influenced by ENSO variability. During El Niño events, the easterly trade winds weaken, warm sea surface temperature anomalies migrate towards the EEP, upwelling in the EEP is drastically reduced, and the thermocline deepens (Wang et al., 2006). As a result, warm sea surface temperature anomalies are felt in the subsurface of the EEP upper-water column. Primary productivity is also greatly diminished as a result of the changes in upwelling, as cool, nutrient rich waters are no longer being brought to the surface. The opposite effects are felt during La Niña events, when intensification of the trade winds results in intensified upwelling, cooler surface and subsurface temperature anomalies, and a shoaling of the EEP thermocline to near the sea surface. These changes are best exemplified in buoy data from the Tropical Atmosphere Ocean (TAO) array. Figure 4.3 shows water column temperature data from the sea surface down to 120 m from the TAO buoy located at

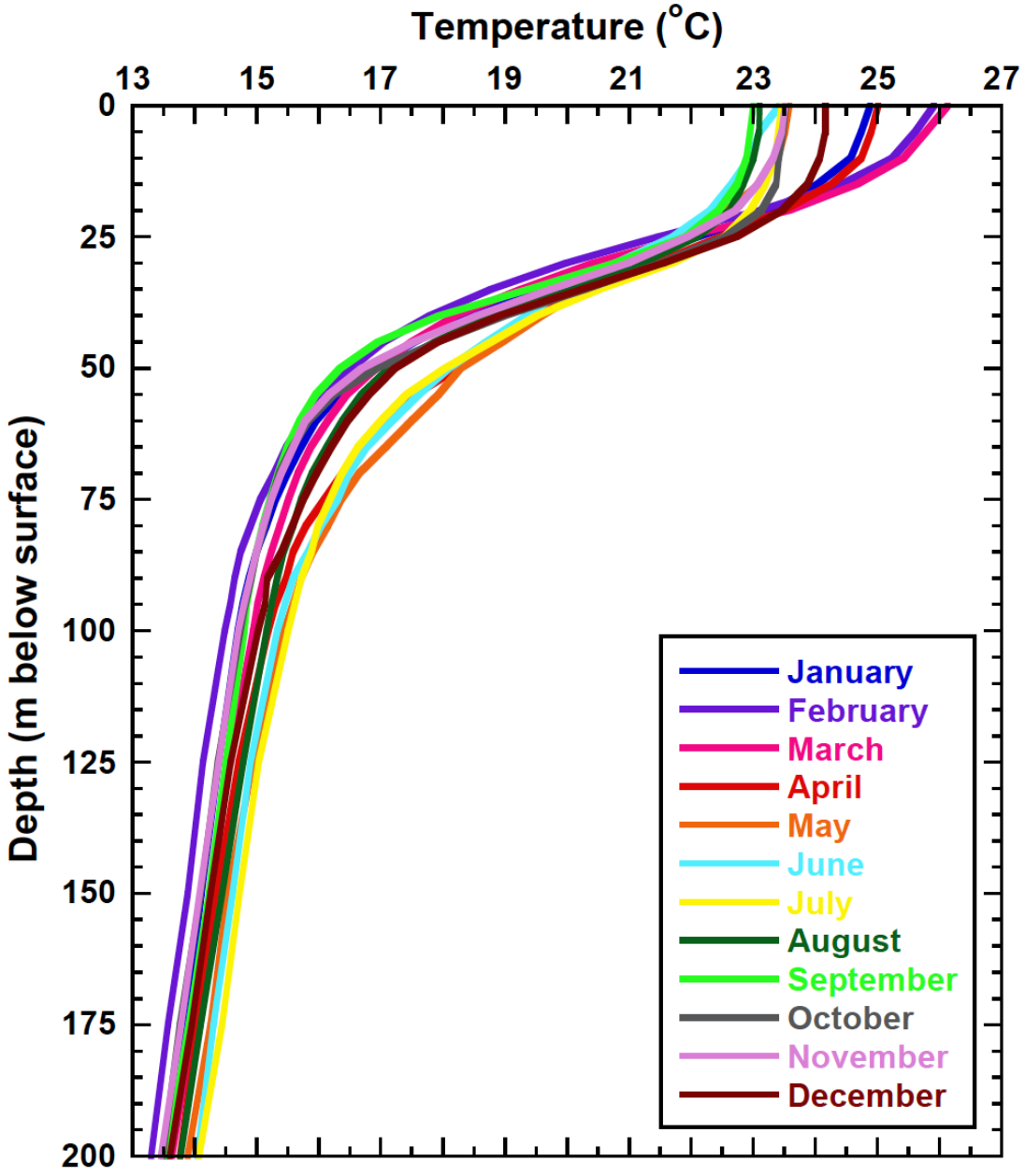

Figure 4.2 Monthly water column temperature profiles from the location of core 17JC. Colors are noted in the key on the figure. The temperatures are derived from the World Ocean Atlas 13 (Locarnini et al., 2013). The planktonic foraminifera *N. dutertrei* inhabits the lower thermocline region between 50 and 75 m water depth. Note the large seasonal range of temperatures at the surface that decreases with depth.

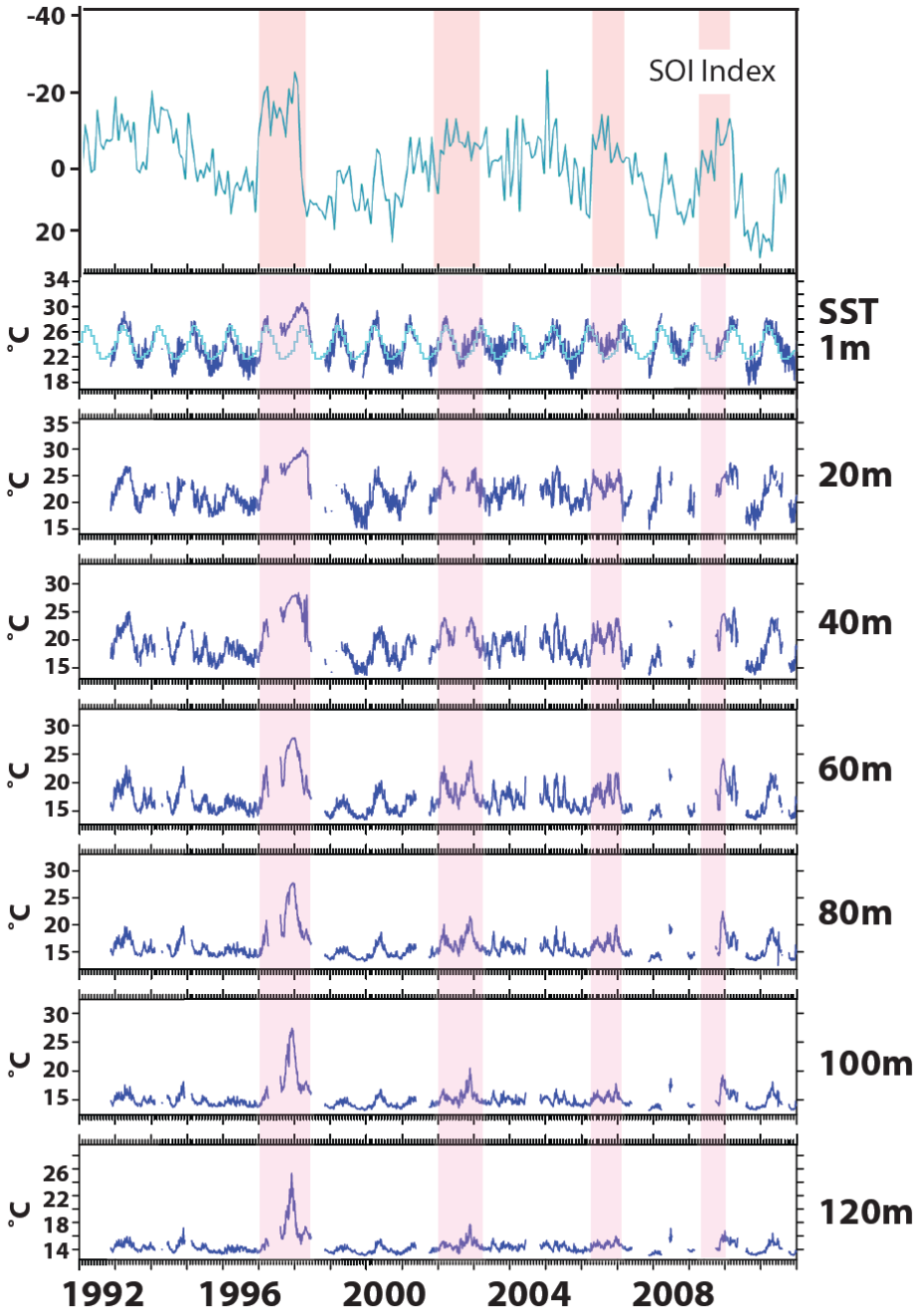

Figure 4.3 TAO array temperature data from 1992-2011 from the buoy located at 95°W. Upper panel shows the Southern Oscillation Index (SOI) over the same time period. The 1 m sea surface temperature (SST) panel also shows the seasonal cycle plotted in light blue. Pink intervals mark the times of El Niño events. SST variability is dominated by seasonal cycle variability whereas temperature variability at depth reflects ENSO activity. At the depth *N. dutertrei* inhabits in the water column (~60 m), the influence of the seasonal cycle is minimal, and variability shows stronger correspondence to the SOI index of ENSO variability. Data from TAO project website (http://pmel.noaa.gov/tao/index.shtml).

95°W from 1992–2011 (http://pmel.noaa.gov/tao/index.shtml). Variability of sea surface temperature is dominated by the seasonal cycle, whereas temperature variability at deeper depths reflects ENSO activity with only a small contribution of the seasonal cycle. Subsurface anomalies of up to 10°C are noted during some of the strongest El Niño events. By extrapolating the hydrographic variability associated with individual ENSO events into longer-term mean state changes, periods characterized as more El Niño-like should record strong subsurface temperature increases, with the opposite holding true for La Niña-like conditions. *N. dutertrei* is ideally suited to record this variability due to its habitat depth in the water column. Based on stable carbon and oxygen isotope records, Spero et al. (2003) found that *N. dutertrei* consistently records thermocline properties in this region and does not show any evidence of vertical migration through the water column over at least the last three glacial cycles.

IV.3. Materials and Methods

IV.3.1. Age Model Development

The age model for 17JC is based on a combination of radiocarbon dates determined from the planktonic foraminifera *N. dutertrei*, the presence of the Los Chocoyos ash layer at 856 cm, and tie points between the percent $CaCO_3$ records of 17JC and nearby core ME-24JC (24JC hereafter). Radiocarbon ages were obtained for 3 intervals of 17JC at 220 cm, 356.5 cm, and 441.5 cm, and converted to calendar age using Calib 7.1 with a marine reservoir correction 400 years (Table 4.1; Figure 4.4). The Los Chocoyos ash layer, which has been dated to 84 kyr (Drexler et al., 1980), is present in 17JC at 854 cm. This datum marker serves as our maximum age constraint for 17JC.

Depth (cm)	Accession #	F_m	F_m error	$\delta^{13}C$	^{14}C Age (yr)	SD (yr)	Calendar Age (yr BP)	Error - (yr BP)	Error + (yr BP)
220	OS-98923	0.16710	0.00120	1.26	14350	60	16900	290	230
356.5	OS-117129	0.05160	0.00110	2	23800	180	27600	270	260
441.5	OS-117130	0.02820	0.00110	1.26	28700	310	32200	800	870

Table 4.1 17JC AMS-^{14}C data

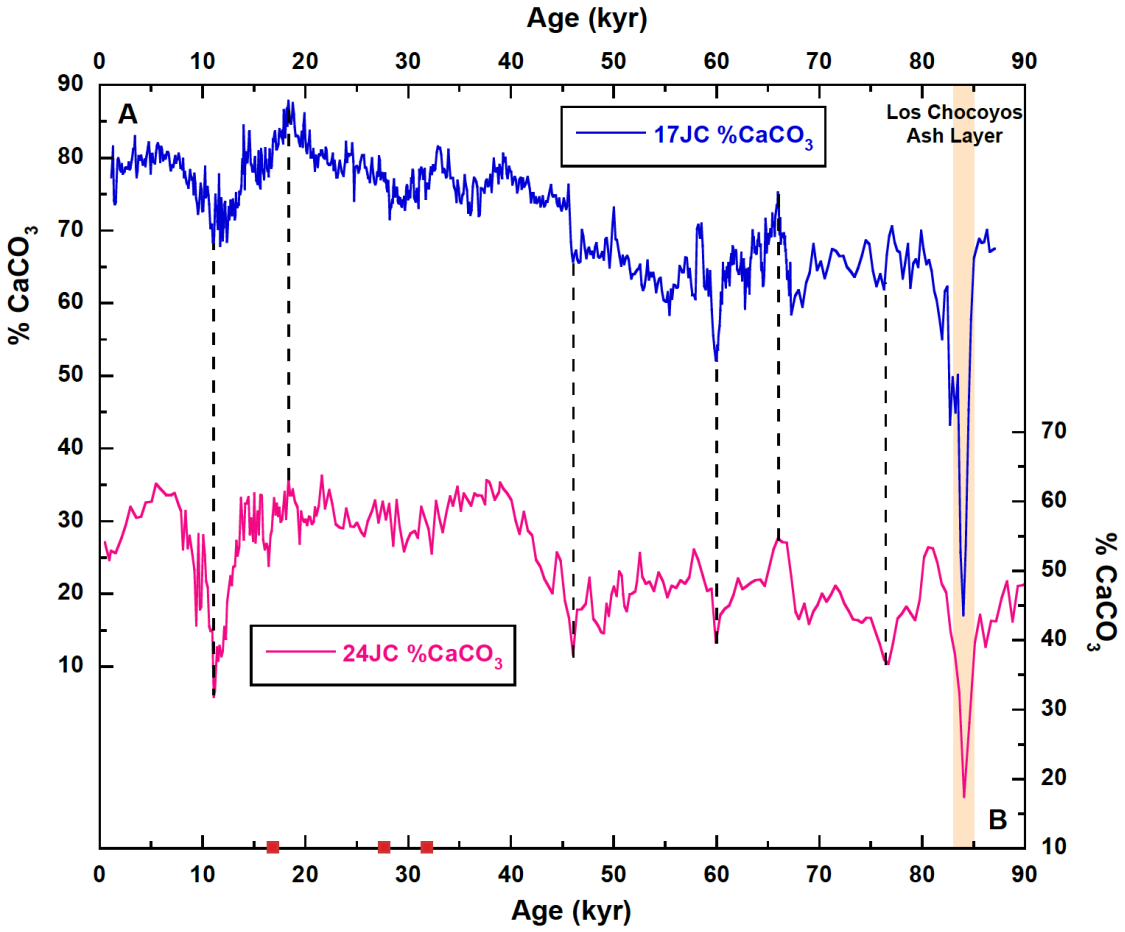

Figure 4.4 Percent calcium carbonate (% $CaCO_3$) records. (A) 17JC (blue line; data courtesy of M. Lyle) and (B) 24JC (pink line; Dubois et al., 2010). Tie points used to create the 17JC age model from the 24JC % $CaCO_3$ record are shown with dotted lines. The presence of the Los Chocoyos ash layer at 84 kyr is noted as abrupt declines in % $CaCO_3$ in both records, and is also noted with the beige bar. Shown on the bottom axis are the three radiocarbon dates based on *N. dutertrei* obtained for this study. See Table 4.1 for radiocarbon date information. Dates are based on most probably age distributions from Calib 7.1.

The remainder of the age model is based on tie points between the percent $CaCO_3$ records of 17JC (data courtesy of M. Lyle) and nearby core 24JC (Dubois et al., 2010) (Figure 4.4). The age model for 24JC, which has been updated since the publication of the 24JC percent $CaCO_3$ record (Dubois et al., 2010), is discussed in detail in Dubois et al. (2014). Briefly, the 24JC age model is based on 6 radiocarbon-dated intervals based on *N. dutertrei* and a benthic foraminiferal $\delta^{18}O$ record tied to the LR04 (Lisiecki and Raymo, 2005) stack (Dubois et al, 2014). The tight match between percent $CaCO_3$ records indicates the strong spatial coherency of regional productivity variability. Tie points between the two percent $CaCO_3$ records were chosen as distinct minimum and maximum values in both records (Figure 4.4). In both records, the minimum percent $CaCO_3$ values at 854 cm in 17JC and 980 cm in 24JC correspond to the interval containing the Los Chocoyos ash layer. Across the time period of interest in this study from 32 to 64 kyr, the average sedimentation rate is 9.3 cm/kyr (Figure 4.5). As our study does not aim to recognize leads or lags between our records and records of climate variability in the high-latitude North Atlantic, we believe that our age model is sufficient to capture multi-centennial scale mean state changes in the EEP relative to warming and cooling events recorded in Greenland ice cores.

IV.3.2. Foraminiferal Analyses

Samples were obtained between 439 cm and 742 cm in 17JC at 2 cm resolution, and freeze-dried. Based on an average sedimentation rate of 9.3 cm/kyr, the 2 cm sampling resolution equates to approximately 215 years. Samples were then weighed, rehydrated and disaggregated in ultra-pure water, wet-sieved through a 63 μm mesh, and

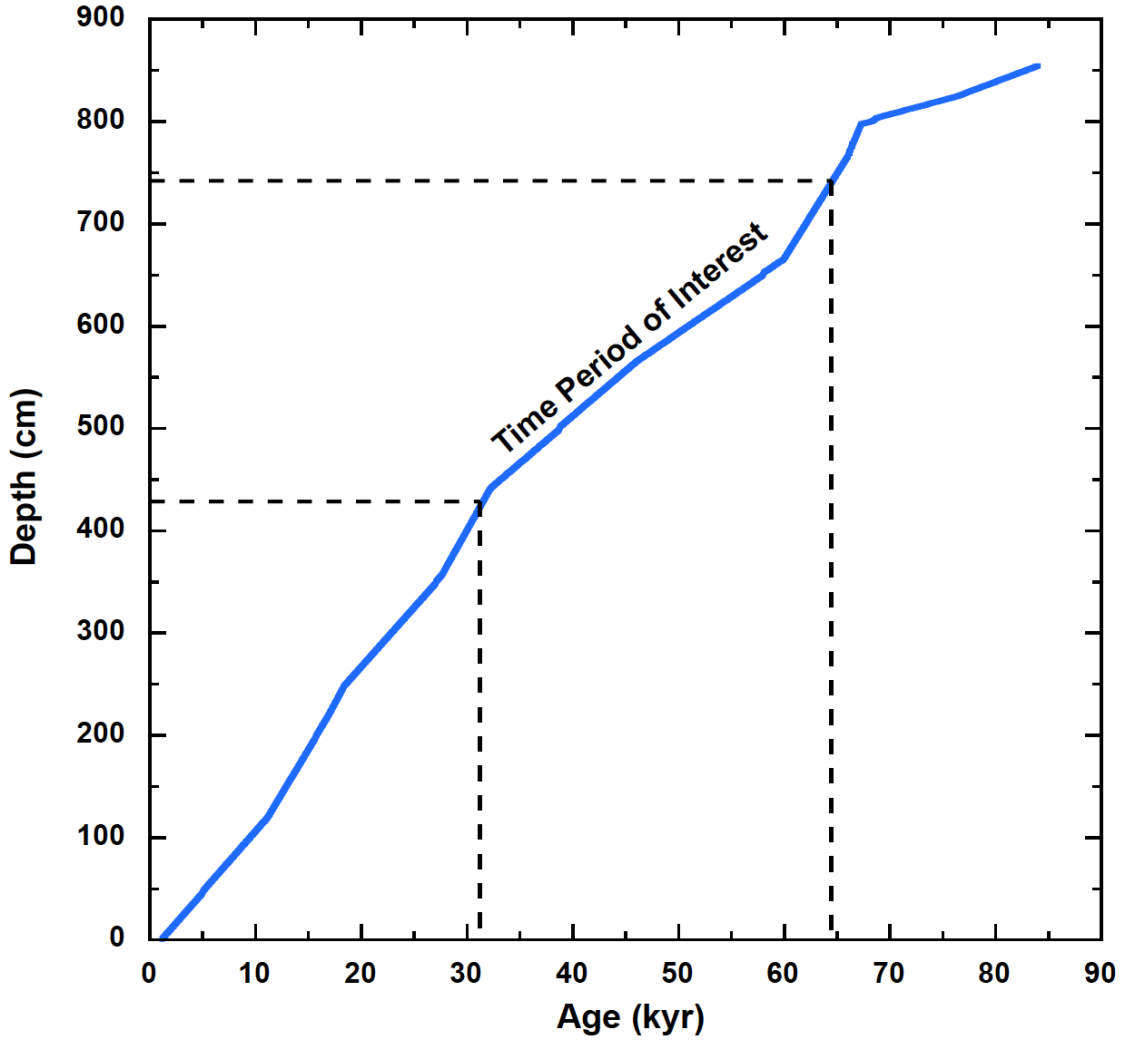

Figure 4.5 Depth in 17JC versus age based on the age model created in this study. Note the overall linear sedimentation rates. The time period of interest for this study spans from 32 kyr to 64 kyr across Marine Isotope Stage 3, and based on our age model, has an average sedimentation rate of 9.3 cm/kyr.

dried in an oven at 50°C. To minimize intraspecific variations in geochemistry, specimens of *N. dutertrei* were collected from the 400-450 μm size fraction. All tests were measured against a calibrated reticle to verify the size restriction. This is especially important to do when selecting tests from a narrow size range. Using a narrow size range while selecting *N. dutertrei* tests for analyses minimizes any habitat depth related variability that may affect test geochemistry. Approximately 70 tests of *N. dutertrei* were picked from each interval, gently crushed between glass plates under a microscope, and homogenized. From this pool, two aliquots of ~320 μg each were selected for analysis. This methodology differs from that employed most often for foraminiferal trace metal analyses, where a number of tests are picked to a desired weight. The tests are then crushed, homogenized, and split into two even aliquots. However, when analyzing larger test sizes as we are doing in this study, the number of foraminifera needed to achieve a desired weight is often small (around 10 tests). Given the lower thermocline depth habitat of *N. dutertrei*, this species may experience a wider range of temperatures than those, for example, that dwell in the upper mixed layer over an individual foraminifera's 2-4 week life span. Thus, analyzing samples based on a small number of tests may not be fully representative of the entire population.

To maintain trace metal clean conditions, the samples were then cleaned according to the procedures described by Schmidt et al. (2012b) in a laminar flow clean bench. The cleaning process included sonication in both ultra clean water and methanol to remove clays, a hot water bath in reducing agents to remove metal oxides, and a hot water bath in an oxidizing solution to remove organic matter. Finally, the samples were

transferred to new acid-leached micro-centrifuge vials and leached with a dilute ultra-pure nitric acid solution. The samples were dissolved and analyzed at Texas A&M University on a Thermo Scientific Element XR High Resolution Inductively Coupled Plasma Mass Spectrometer (HR-ICP-MS) using isotope dilution, as outlined in Lea and Martin (1996). A suite of elements including Na, Mg, Ca, Sr, Ba, U, Al, Fe and Mn, were analyzed.

Analyses were monitored for anomalously high Al/Ca, Fe/Ca, and Mn/Ca ratios. High Al/Ca ratios indicate the presence of detrital clays that were not removed during the cleaning process, while elevated levels of Fe/Ca or Mn/Ca indicate the presence of diagenetic coatings that were not removed during the cleaning process. Boyle (1983) noted that the presence of Mn-rich carbonate overgrowths can be problematic for trace metal analyses of foraminifera because Mn-carbonate may contain high levels of other trace elements, significantly altering the composition of 'pure' foraminifera carbonates. Furthermore, Pena et al. (2005) found that foraminifera tests recovered from the Panama Basin are especially susceptible to Mn-rich carbonate overgrowths due to the delivery of relatively large amounts of both biogenic reactive organic carbon and hydrothermal Mn to the sea floor. The high flux of organic carbon promotes redox reactions in the upper sediment column, including manganese reduction, which can lead to the upward diffusion of dissolved Mn(II) ions and the reprecipitation of Mn(IV) as oxides near the sediment-water interface (Pena et al., 2005). Together, these conditions can generate surface enrichments in sediments. Given the location of 17JC within the confines of the Panama Basin, monitoring for Mn/Ca ratios is especially critical. Finally, Lea et al.

(2006) noted distinct intervals of elevated Fe/Ca ratios in a nearby core closer to the Galapagos Islands, caused by the presence of volcanic shards in the sediments. Thus, monitoring for anomalous Fe/Ca ratios is also essential.

IV.4. Results

IV.4.1. Thermocline Temperatures

The *N. dutertrei* Mg/Ca temperature calibration from Anand et al. (2003) was used to calculate lower thermocline temperatures (T) from *N. dutertrei* Mg/Ca ratios.

$$Mg/Ca = .342 \exp 0.09(T) \quad (\text{error } \pm 1.2°C) \quad \text{Eq. (4.1)}$$

This calibration equation has been used by previous studies that measured Mg/Ca ratios on *N. dutertrei* in the EEP (Pena et al., 2008 and Sadekov et al., 2013). Figure 4.6 shows the raw, uncalibrated *N. dutertrei* Mg/Ca ratios (Figure 4.6A), along with the temperatures calibrated using equation (4.1) (Figure 4.6B). Each data point represents the average of the two separate analyses for the aliquots of each homogenized sample. Over the course of this study, the long-term precision of a matrix-matched synthetic standard was 1.78% (2-sigma), which is equivalent to ±0.16°C based on an average *N. dutertrei* Mg/Ca ratio of .96 mmol/mol. The record displays multi-decadal to millennial-scale variability in thermocline temperatures, overlain on an overall trend of decreasing thermocline temperatures from 64 kyr to 32 kyr. This trend is shown in figure 4.6B, and corresponds to an overall average decline in thermocline temperature of 2.8°C over the time period. The intervals of our record with the warmest thermocline temperatures occur at 60 kyr and 64 kyr, with temperatures of 16.0°C and 16.45°C, respectively, and are slightly warmer than the ~15°C temperature of the modern depth habitat of *N.*

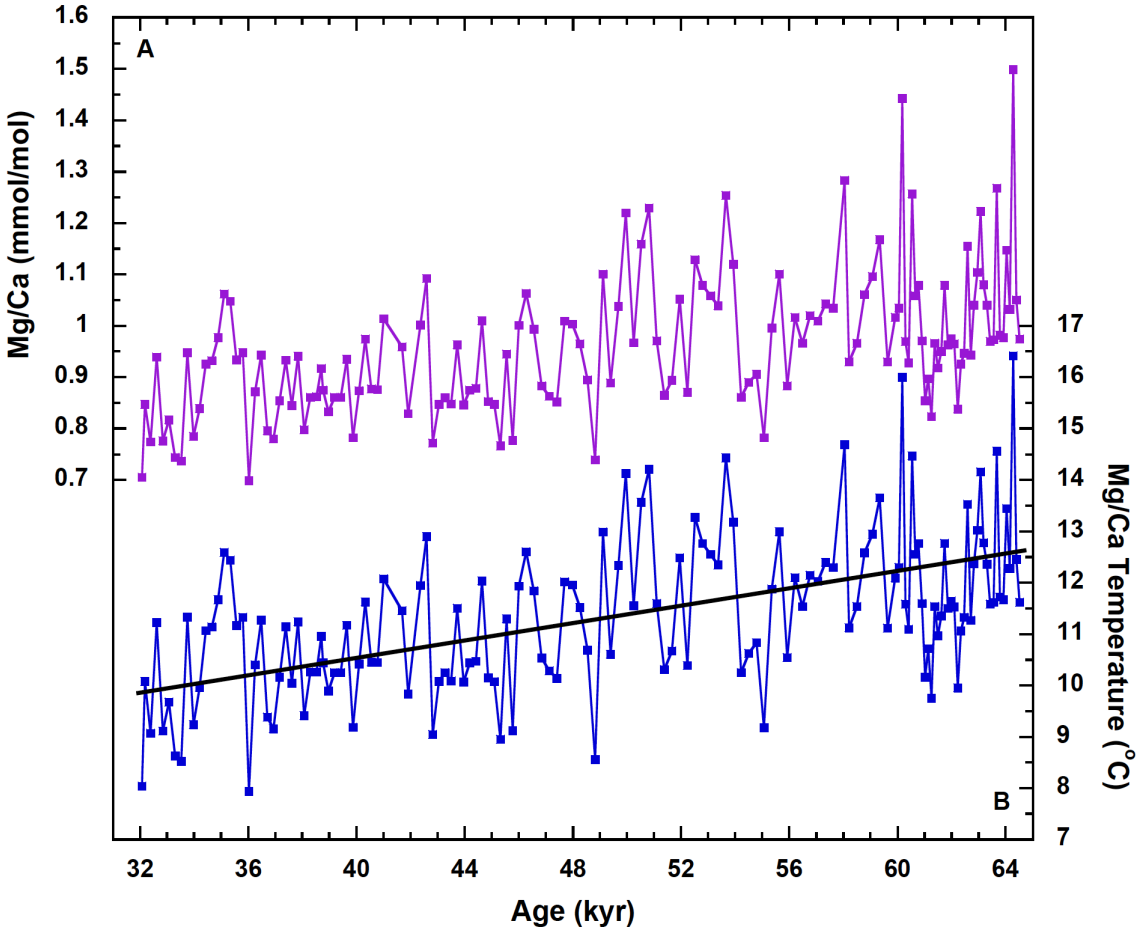

Figure 4.6 *N. dutertrei* Mg/Ca data and calibrated temperatures. Raw *N. dutertrei* Mg/Ca ratios (A, purple line) analyzed in this study. Each point is based on the average of two analyses for each interval. Mg/Ca ratios were calibrated to temperature (B, blue line) using the *N. dutertrei* species-specific equation from Anand et al. (2003). Also shown is the average trend line through the calibrated Mg/Ca temperatures (B, black line).

dutertrei at our study location. The coolest thermocline temperatures of the record occur at 32 kyr and 36 kyr, with both intervals recording thermocline temperatures of ~8°C.

The record is punctuated by numerous multi-decadal to millennial-scale warming and cooling events from 64 kyr to 32 kyr. The largest magnitude of warming occurs between 61 kyr and 60 kyr, with thermocline temperatures warming by 6.25°C. Although not as large in magnitude, similar warmings occur between 55 kyr and 53.8 kyr (5.4°C), and 36 kyr and 35 kyr (4.7°C). Other abrupt warming events occur throughout the record, with magnitudes of warming closer to 4°C. Cooling events occur more gradually, although 5°C of cooling is recorded between both 60 kyr and 59 kyr, and 50 kyr and 49 kyr. In addition, thermocline temperatures display an increased range of variability in the earlier portion of the record from 64 kyr to 46 kyr compared to the later period.

IV.4.2. Monitoring of Secondary Effects

Mn/Ca ratios were closely monitored throughout the duration of this study for evidence of Mn-rich carbonate overgrowths that may have not been removed during the foraminiferal cleaning process. An average Mn/Ca value of 21 μmol/mol was calculated over 300 individual analyses. Only three analyses returned anomalously high (>100 μmol/mol) Mn/Ca values, and the associated Mg/Ca values were removed from our dataset. Although the remainder of analyses returned low Mn/Ca values, we wanted to determine if there was any relationship between our Mg/Ca and the Mn/Ca ratios, to see if our Mg/Ca ratios might be affected by any remaining Mn-rich carbonates. To do this,

we plotted Mg/Ca ratios versus Mn/Ca ratios, and calculated an r^2 value of 0.013, indicating that there is no discernable trend between the two parameters (Figure 4.7). The highest Mn/Ca ratios are actually found around the mid-range of Mg/Ca values, suggesting that any Mn-rich carbonate overgrowths still present are not resulting in increased Mg/Ca values. We also found no anomalously elevated Fe/Ca values, which may have indicated the presence of volcanic shards in our samples.

Another important secondary effect that may influence Mg/Ca ratios is calcite dissolution, especially in the EEP where the lysocline is estimated to occur at ~2900 m (Thunell et al., 1981). The effects of dissolution on planktonic foraminifera tests generally becomes evident in EEP sediments between ~2500 – 3000 m water depth (Kowsmann, 1973). The partial dissolution of foraminifera tests can significantly bias Mg/Ca ratios due to the heterogeneous distribution of Mg within the test and the higher solubility of Mg-rich calcite (Brown and Elderfield, 1996 and Dekens et al., 2002). Thus, given that core 17JC was recovered from 2870m, very close to the lysocline depth, it is imperative to assess whether dissolution is affecting our samples. Previous studies have noted that foraminifera tests recovered from a similar depth in the EEP (2830 m) contained tests with superior preservation during glacial periods (Lea et al., 2006). Two independent potential indicators of dissolution are available for 17JC: percent coarse fraction >63 μm, and average *N. dutertrei* (400 – 450 μm) shell weight (Figure 4.8A and B, respectively). A visual comparison between these two indicators shows high correspondence, which may suggest dissolution is a common control on both parameters. However, the *N. dutertrei* Mg/Ca record has weak negative correlations with both

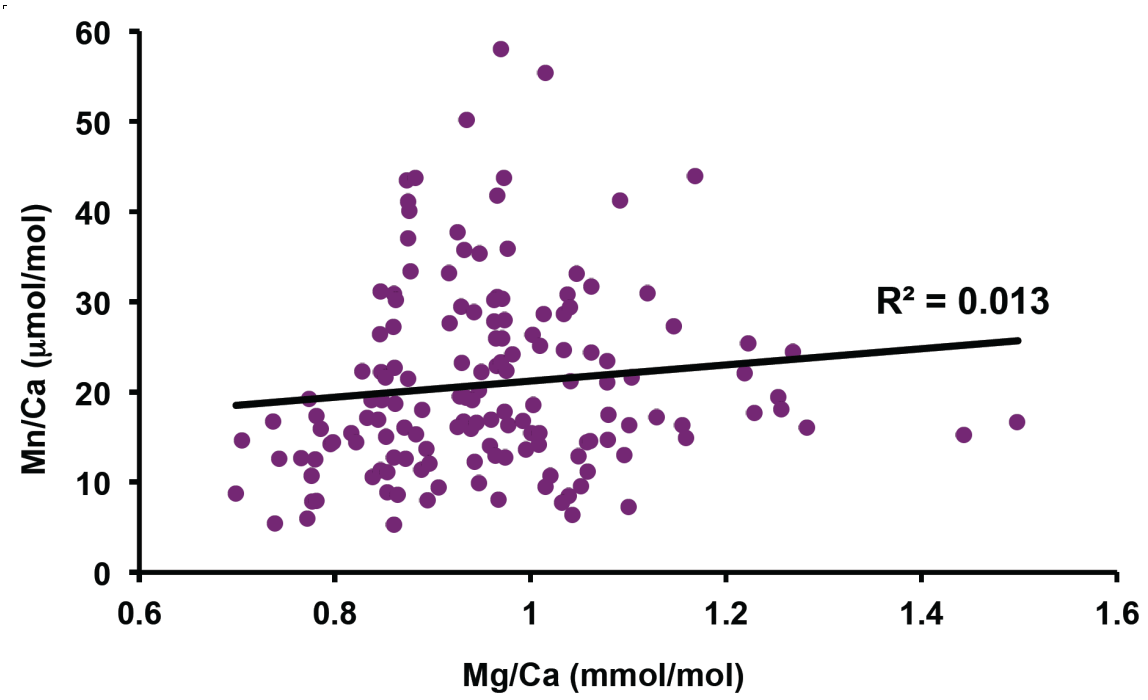

Figure 4.7 Mn/Ca versus Mg/Ca ratios for each *N. dutertrei* analysis. A trend line through the data (black line) yields an r^2 of 0.013, indicating that there is no discernable trend between the Mn/Ca and Mg/Ca ratios.

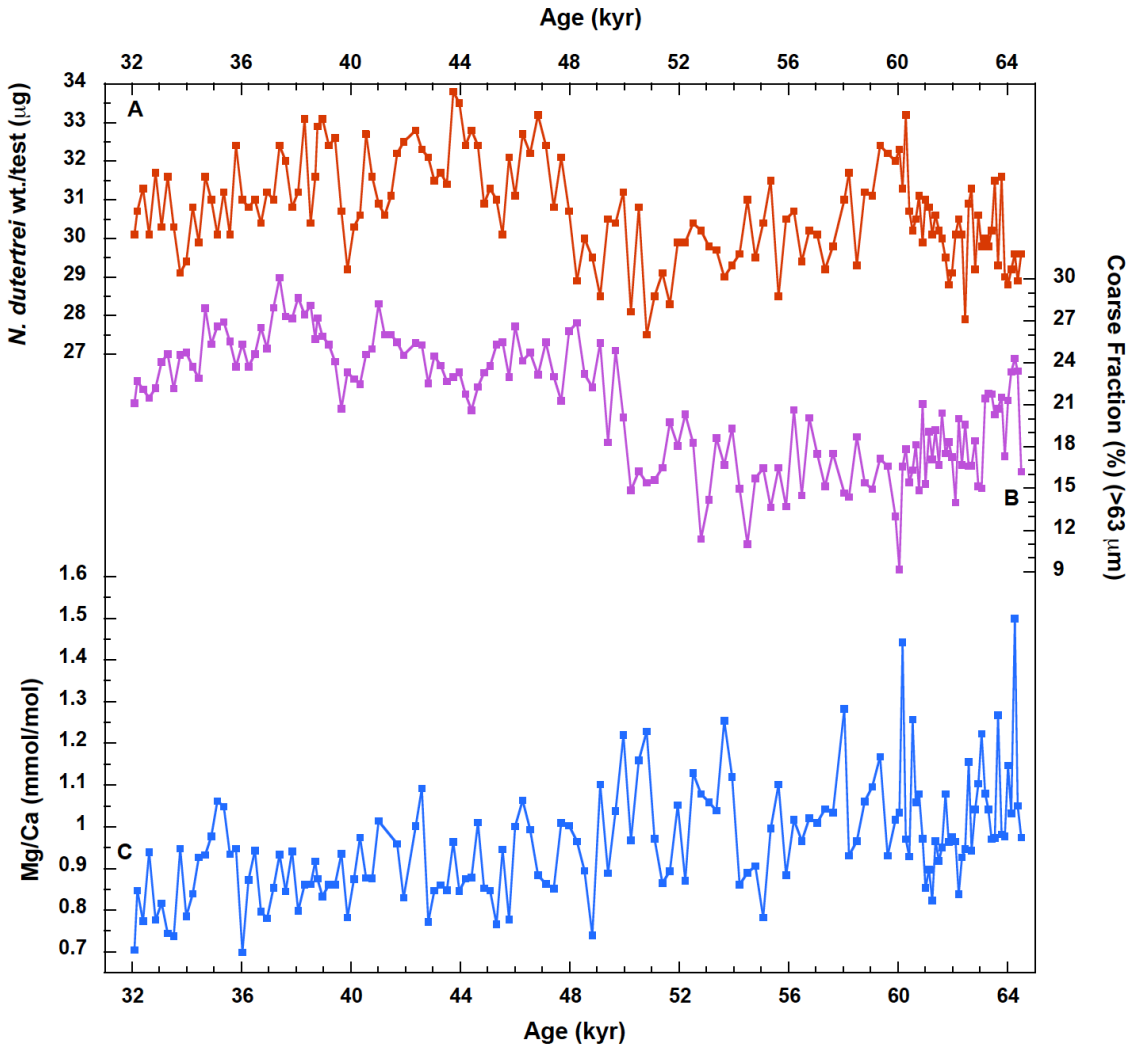

Figure 4.8 Indicators of dissolution in 17JC. (A) Average *N. dutertrei* test weight from the ~70 tests analyzed from each interval from the 400 – 450 µm size fraction (red line). (B) Percent coarse fraction (> 63 µm) for each interval (purple line). (C) *N. dutertrei* Mg/Ca ratios (blue line). The dissolution indicators shown in (A) and (B) are plotted with increased preservation upward and increased dissolution downward.

percent coarse fraction (r^2 = 0.12) and *N. dutertrei* shell weight (r^2 = 0.06), indicating that dissolution is not a significant down-core influence in 17JC. In addition, the correlations are negative (negative r values), which is the opposite direction to that expected if dissolution were to be a control on Mg/Ca ratios. If anything, the increased dissolution in the older portion of our record might be dampening the warming signal suggested by the Mg/Ca ratios.

Lastly, we do not believe that salinity is impacting our Mg/Ca ratios. Although a recent study of core-top sediments in the Atlantic Ocean claimed that salinity had a much stronger control on foraminiferal Mg/Ca ratios than temperature (Arbuszewski et al., 2010), a new study showed that this conclusion likely resulted from latitudinal differences in foraminiferal dissolution resulting from regional productivity variability in surface waters and the incorrect application of a single depth-corrected Mg/Ca-sea surface temperatre calibration across the entire Atlantic basin (Hertzberg and Schmidt, 2013). In addition, the average annual sea surface salinity at our site is 34.1 (Zweng et al., 2013), well below the 35.5 and above cut off suggested by Arbuszewski et al. (2010) for salinity affecting Mg/Ca ratios.

IV.5. Discussion

IV.5.1. Changes in the Tropical Pacific Mean State Across MIS 3

The goal of the present study is to characterize the mean state of the tropical Pacific across the abrupt warming events of MIS 3, known as D-O events. To this end, we plotted our *N. dutertrei* Mg/Ca temperature record, which displays numerous millennial-scale warming events across MIS 3, along with the Greenland NGRIP ice

core $\delta^{18}O$ record to determine the relationship between climate change in the high-latitude North Atlantic and the mean state of the tropical Pacific (Figure 4.9). We find that many of the millennial-scale warming events noted in the EEP thermocline temperature record are in phase with the abrupt warming events in the NGRIP $\delta^{18}O$ record. Specifically, D-O events 17, 16, 15, 14, 12, and 7 all show significant thermocline warmings of ~4°C. These warming events are more prominent in the older portion of our record, and decrease in magnitude after ~44 kyr. Many of the cold stadials across MIS 3 also correspond to periods of cooler thermocline temperatures in the EEP.

Based on the modern relationship between thermocline temperatures and ENSO variability at our study site, we interpret our findings to indicate that the tropical Pacific was in a more El Niño-like mean state during interstadial periods, especially for the portion of our record from 64 kyr to 44 kyr. We find the opposite during cold stadials, with cooler thermocline temperatures indicative of a more La Niña-like mean state. We interpret intervals with El Niño-like mean states in the sense of reflecting states in which El Niño conditions are more frequent and/or more intense, with the opposite for La Niña-like mean states. Overall, the older portion of our record from 64 kyr to 44 kyr displays warmer thermocline temperatures, suggesting that this period was generally a more El Niño-like period. We hypothesize that this is due to the longer, more sustained warming during interstadials throughout this portion of our record. A prolonged period of El Niño-like conditions would inhibit the development of strong La Niña events due to a weaker east-west SST gradient across the tropical Pacific. After 44 kyr until the end

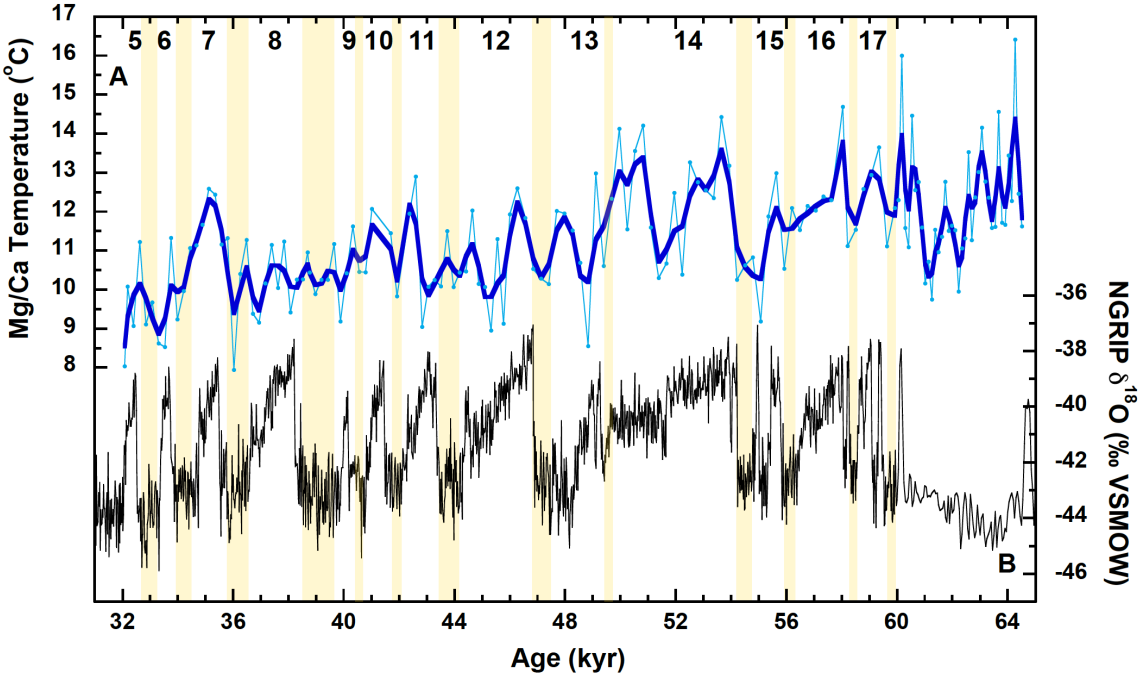

Figure 4.9 Comparison of thermocline temperatures and NGRIP ice core record. Comparison of (A) *N. dutertrei* Mg/Ca temperatures and (B) the Greenland NGRIP ice core $\delta^{18}O$ record (North Greenland Ice Core Project Members, 2004 and NGRIP Dating Group, 2008). The Mg/Ca temperatures (light blue) are shown with a 3-point smoothing function (dark blue). The NGRIP $\delta^{18}O$ record is plotted such that upward is warmer and downward is cooler. Dansgaard-Oeschger interstadial warm periods are labeled with numbers along the upper axis and cool stadial periods are marked with yellow bars.

of our record at 32 kyr, conditions are more La Niña-like with overall cooler thermocline temperatures. The D-O events after 44 kyr tend to be shorter in length, with more sustained cooling during stadial periods than warming during interstadial periods. The D-O interstadial warmings during this period often do not correspond to warmer thermocline temperatures in 17JC, suggesting that there was a stronger east-west SST gradient prohibiting the development of El Niño events. Overall, our new record of EEP thermocline temperatures across MIS 3 suggests that there is a relationship between high-latitude North Atlantic climate variability and the mean state of the tropical pacific.

There is one existing record of thermocline temperatures from the EEP across MIS 3 from a sediment core recovered from ODP Site 1240, generated using the same thermocline dwelling foraminifera utilized by our study (Figure 4.10B) (Pena et al., 2008). Although the record shows the same overall thermocline cooling trend from 64 kyr to 32 kyr, there are no large warming events like those evident in our record. There are two distinct differences in the methodologies used to create both records. Pena et al. (2008) used a 315 – 355 μm size fraction for *N. dutertrei* while we utilized a 400 – 450 μm size fraction. Unfortunately, little data exists on the relationship between test size and Mg/Ca ratios in *N. dutertrei*, especially over these two different size fractions (Elderfield et al., 2002). For mixed-layer dwelling foraminifera, larger test sizes often correspond to higher Mg/Ca ratios, and thus warmer temperatures (Elderfield et al., 2002 and Spero et al., 2003). However, for deeper, thermocline-dwelling species, there is no clear relationship between test size and Mg/Ca ratios, and the relationship is often different between species (Elderfield et al., 2002). The size fraction differences between

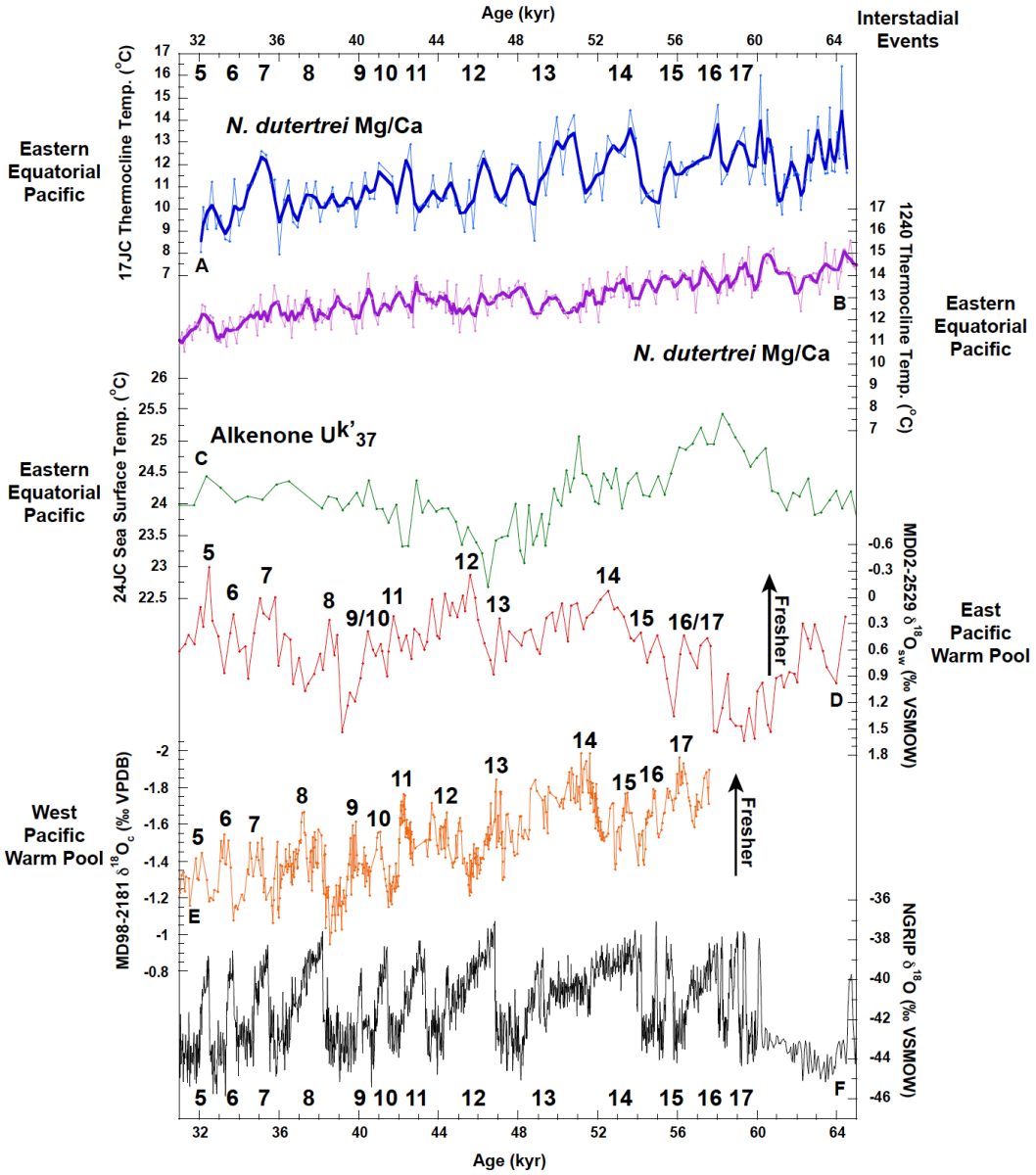

Figure 4.10 Comparison of thermocline temperature record with other temperature and hydrologic records. Comparison of (A) *N. dutertrei* Mg/Ca temps (light blue, 3-point smoothing function in dark blue) with other records of tropical Pacific temp and hydrologic variability. (B) *N. dutertrei* Mg/Ca temp record of Pena et al. (2008) (light purple) with 3-point smoothing function (dark purple) from ODP site 1240 in the EEP. (C) Alkenone $U^{k'}_{37}$ SST record of Dubois et al. (2011 and 2014) from core ME-24JC in the EEP (green). (D) $\delta^{18}O_{sw}$ record of Leduc et al. (2007) from core MD02-2529 in east Pacific warm pool (red), plotted with fresher conditions up / saltier conditions down. (E) $\delta^{18}O_c$ record of Saikku et al. (2009) (modified after Stott et al., 2002) from core MD98-2181 in west Pacific warm pool (orange), plotted with fresher conditions up / saltier conditions down. D-O events labeled in (D) and (E) derived from labeling systems in original references. (F) Greenland NGRIP ice core $\delta^{18}O$ record (North Greenland Ice Core Project Members, 2004 and NGRIP Dating Group, 2008). NGRIP $\delta^{18}O$ record plotted with warmer up / cooler down. D-O events on top / bottom axes labeled with reference to NGRIP $\delta^{18}O$ record.

our studies may be responsible for the overall differing ranges of *N. dutertrei* temperatures recorded at both sites. Additionally, we pooled a larger number of *N. dutertrei* shells for each analysis, which may have increased the variability of the population for each interval. Lastly, the two core sites are located in slightly different regions along the Carnegie Ridge and at different depths, and thus may record varying sensitivities to changes in water column temperatures. Although the Pena et al. (2008) *N. dutertrei* thermocline temperature record does not show the same millennial-scale patterns as 17JC, the overall cooling trend from 64 kyr to 32 kyr agrees with our record and interpretation of a change from an overall more El Niño-like mean state prior to 44 kyr to a La Niña-like mean state after 44 kyr. Interestingly, however, Pena et al. (2008) interpreted their record in the opposite fashion based on a record of thermocline *N. dutertrei* $\delta^{18}O_{seawater}$ ($\delta^{18}O_{sw}$) values as a proxy for thermocline salinity variability, and records of surface and thermocline $\delta^{13}C$ variability as a proxy for upwelling strength. Their $\delta^{18}O_{sw}$ and $\delta^{13}C$ records suggest that periods of warmer thermocline temperatures correspond to periods of more positive $\delta^{18}O_{sw}$, indicative of saltier thermocline water, and more negative $\delta^{13}C$, indicating upwelling from the thermocline to the surface. Taken together, Pena et al. (2008) hypothesized that these records suggest that the periods of thermocline warming were more La Niña-like, which in inconsistent with our interpretation based solely on thermocline temperature. $\delta^{13}C$ variability is often difficult to interpret, as numerous factors can influence the $\delta^{13}C$ of foraminifera tests (Spero et al., 2003), and thermocline salinity is not a direct indicator of ENSO variability in the EEP.

Although thermocline temperature change is a more direct indicator of ENSO related variability in the EEP than SST change, we wanted to compare our thermocline temperature record with an existing record of SSTs derived from the alkenone $U^{k'}_{37}$ proxy from core 24JC (Figure 10C) (Dubois et al., 2011 and Dubois et al., 2014). Recall that core 24JC was utilized to create our 17JC age model, thus comparing these two records is more direct than using SST records that may be derived from foraminiferal Mg/Ca records from other cores (e.g. Pena et al., 2008). The 24JC SST record does not display the same variability as seen in the 17JC thermocline temperature record, and instead shows longer-term warming and cooling trends of ~1.5 to ~2.5°C. There is an interval of prolonged warmth from 60 kyr to 56 kyr that corresponds to a prolonged warm period in 17JC, but overall the records display few similarities. It is likely that the 24JC SST record may be responding to longer-term orbital scale changes that are influencing the seasonal cycle, or that the alkenone $U^{k'}_{37}$ proxy may be strongly seasonally biased. Timmerman et al. (2014) found that alkenone production peaks in boreal winter, thus the 24JC record may be seasonally biased. Interestingly, El Niño events are thought to be phase locked into the seasonal cycle, peaking in boreal winter (Rasmusson and Carpenter, 1982). Therefore, the warmer SST conditions noted in the older portion of the 24JC alkenone SST record may reflect warmer winter SSTs if this was a period of a more El Niño-like mean state.

IV.5.2. Comparison with Records of Hydrologic Variability Across MIS 3

In addition to records of temperature variability across MIS 3, records of hydrologic variability may help characterize changes in the tropical Pacific mean state.

Stott et al. (2002) created a record of $\delta^{18}O$ variability of a surface dwelling planktonic foraminifera *Globigerinoides ruber* from a sediment core located in the west Pacific warm pool (MD98-2181; Figure 4.1, red star). In this region, sea surface salinity is strongly affected by ENSO variability, with a decrease in summer precipitation by as much as 60% during major El Niño events as the convective region of western pacific migrates east (Stott et al., 2002). The record of *G. ruber* $\delta^{18}O$ variability shows more negative values (fresher surface waters) during D-O interstadial warm events, and more positive values (saltier surface waters) during stadial cold events of MIS 3 (Stott et al., 2002). Stott et al. (2002) interpreted these changes based on modern ENSO analogues, with fresher D-O interstadials characterized by La Niña-like conditions, and saltier D-O stadials characterized by El Niño-like conditions. More recently, Saikku et al. (2009) increased the resolution of the Stott et al. (2002) $\delta^{18}O$ record (Figure 4.10E), and reinterpreted the record in terms of latitudinal shifts in the ITCZ across D-O events, leading to variability in sea surface salinity during interstadials and stadials. Cooler surface waters in the western Pacific during stadials would be consistent with a southerly bias in the annual migration of the ITCZ, resulting in saltier conditions recorded at the site of MD98-2181 (Saikku et al., 2009). While they did not rule out the influence of ENSO mean state variability, as suggested by Stott et al. (2002), they noted that SST records from the east and west Pacific made it difficult to discern whether stadials were more El Niño- or La Niña-like (Saikku et al., 2009).

A record of hydrologic variability from the EEP supports the interpretation of a shifting ITCZ across D-O events in the tropical Pacific, as well. Leduc et al. (2007)

combined alkenone $U^{k'}_{37}$ SSTs and *G. ruber* $\delta^{18}O$ to calculate $\delta^{18}O_{sw}$ variability in a sediment core from the northern EEP in the east Pacific warm pool (MD02-2529; Figure 4.1 green star) (Figure 4.10D). They found fresher conditions at their study location during D-O interstadials, consistent with a northern shift in the ITCZ (Leduc et al., 2007). Saltier conditions were noted during cool D-O stadials, suggesting a southward migration of the ITCZ away from their site (Leduc et al., 2007). When taken together, the records of hydrologic variability from both the western and eastern equatorial Pacific appear to be recording latitudinal shifts in the ITCZ across the tropical Pacific, rather than changes in the mean ENSO state as suggested by Stott et al. (2002). The records do not provide clear support for either El Niño-like or La Niña-like conditions during interstadials warming or stadial cooling.

IV.6. Conclusions

We have attempted to reconstruct past changes in the tropical Pacific mean state across the abrupt warming events of MIS 3 by measuring Mg/Ca ratios in the thermocline dwelling foraminifera *N. dutertrei*. Our thermocline temperature record reveals that interstadial warming events are characterized by a more El Niño-like mean state, with increases in thermocline temperatures up to 6°C. The thermocline warming events are more pronounced in our record from 64 kyr to 44 kyr when overall global climate was in a warmer state. Moving from 44 kyr to 32 kyr, our record shows cooler thermocline temperatures, suggesting a shift to a more La Niña-like mean state, as climate began transitioning into the glacial maximum. Overall, our new record of thermocline temperatures across Marine Isotope Stage 3 suggests that there is a

relationship between high-latitude North Atlantic climate variability and the mean state of the tropical pacific, although the complex feedback mechanisms are still not fully understood.

It is hoped that a record of SST based on *G. ruber* Mg/Ca ratios from the same sediment core intervals analyzed for *N. dutertrei* Mg/Ca ratios for this study will provide additional insight into the questions addressed here. This record will enable the calculation of a surface-thermocline temperature gradient, which may help us to further understand the water column dynamics across MIS 3. Additionally, single test *N. dutertrei* Mg/Ca analyses may shed light on ENSO variability in relation to the changes in the mean state we have predicted here.

CHAPTER V

CONCLUSIONS

The goal of this dissertation was to better understand two widely used paleotemperature proxies, and to apply one in a novel way to try to reconstruct past changes in tropical Pacific climate variability. The following is a summary of the findings of the major studies in this dissertation.

The goal of Chapter II was to reinvestigate a proposed large salinity effect on Mg/Ca ratios in the planktonic foraminifera *Globigerinoides ruber*. Foraminifera test weights and scanning electron microscopy were used to examine the potential effects of dissolution on test Mg/Ca ratios that may have influenced the results of the study that proposed the large salinity effect (Arbuszewski et al., 2010). These analyses showed that *G. ruber* tests from the equatorial region are highly dissolved compared to those from the subtropical North and South Atlantic gyres, significantly impacting their Mg/Ca-sea surface temperatures (SSTs). Shell weights from the higher productivity equatorial region of the Atlantic are on average 20% and 15% lower than those from the oligotrophic North and South Atlantic gyres, respectively. These results suggest that application of a single dissolution-corrected Mg/Ca-SST calibration equation for *G. ruber* (Dekens et al., 2002) is not valid across the entire Atlantic Basin, given the excellent preservation of shells in the oligotrophic gyre regions. Basin-wide application of a dissolution-corrected calibration equation leads to artificially high Mg/Ca-SSTs in

the subtropical gyre regions. However, a dissolution-corrected calibration equation for *G. ruber* is needed in the high-productivity equatorial upwelling region where there is evidence for significant shell dissolution, even at core depths above the lysocline. In addition, for core depths below the lysocline in the subtropics, a dissolution-corrected calibration equation for *G. ruber* still appears to be required. After taking into account usage of appropriate calibration equations and comparison to temperatures based on realistic *G. ruber* growth seasons and depth habitats, a strong correlation was calculated between observational SSTs and calculated *G. ruber* Mg/Ca-SSTs. Thus, invoking a large salinity effect on *G. ruber* Mg/Ca ratios is unnecessary. This study provides evidence that regional differences in preservation, rather than salinity, significantly affects *G. ruber* Mg/Ca-SSTs in the Atlantic, and supports culturing experiments that found salinity only has a minor influence on foraminiferal Mg/Ca ratios.

The aim of Chapter III was to investigate the TEX_{86} temperature proxy in the eastern tropical Pacific (ETP) by utilizing Mg/Ca paleothermometry on multiple species of planktonic foraminifera across the Holocene and Last Glacial Maximum (LGM). The use of the TEX_{86} temperature proxy has thus far come to disagreeing results as to whether TEX_{86} temperatures are representative of surface or subsurface conditions. In addition, although TEX_{86} temperatures might reflect sea surface temperatures based on core-top (Holocene) values, this relationship might not hold further back in time. The study compared TEX_{86} temperatures and Mg/Ca temperatures of three species of planktonic foraminifera that inhabit the upper mixed layer and thermocline for two regions of the ETP, the Cocos Ridge and the Carnegie Ridge. The results show that

while TEX_{86}^{H} temperatures agree well, within error, with *G. ruber* Mg/Ca temperatures for the Holocene, there is a significant cold bias in TEX_{86}^{H} temperatures at the LGM for both study regions, whereby TEX_{86}^{H} temperatures are more representative of upper thermocline temperatures than SSTs. The offset between *G. ruber* Mg/Ca temperatures and TEX_{86}^{H} temperatures cannot be reconciled with the use of different TEX_{86} temperature calibrations. The best explanation for the offset between proxies is a decrease in nutrient availability in the ETP during the LGM, especially for the Cocos Ridge study region, where the offset between proxies was greatest (6.3°C). However, on the Carnegie Ridge, there may not have been a decrease in LGM productivity, as suggested by the smaller offset between proxies (2.9°C) and the potential seasonal bias in *G. ruber* Mg/Ca temperatures. Overall, these findings suggest that caution should be applied when interpreting TEX_{86} records based solely on the relationship between core-top/Holocene TEX_{86} temperatures and modern observational temperatures, as TEX_{86} temperatures may be tied to productivity variability. In addition, glacial cooling estimates were compared based on both temperature proxies and found estimates based on TEX_{86}^{H} temperatures to be too high (greater degree of cooling), especially on the Cocos Ridge, in comparison with other regional records. Therefore, TEX_{86}^{H} temperatures should not be used for computing glacial cooling, especially in the ETP.

Finally, Chapter IV utilized Mg/Ca paleothermometry to create a record of thermocline temperature variability in the eastern equatorial Pacific (EEP) across Marine Isotope Stage 3 (MIS 3) in an effort to understand how the mean climate state of the tropical Pacific varied during past periods of abrupt warming. By analyzing Mg/Ca

ratios in the thermocline dwelling foraminifera *Neogloboquadrina dutertrei,* a record of thermocline temperature was reconstructed from a sediment core located in the EEP cold tongue upwelling region, where subsurface temperatures vary strongly with ENSO. Changes in thermocline temperatures were interpreted based on modern ENSO analogues, with periods of warmer or cooler thermocline temperatures indicative of a more El Niño-like or La Niña-like mean state, respectively. The new thermocline temperature record reveals that interstadial warming events were characterized by a more El Niño-like mean state, with increases in thermocline temperatures up to 6°C. The thermocline warming events are more pronounced in the record from 64 kyr to 44 kyr when overall global climate was in a warmer state. Moving from 44 kyr to 32 kyr, the record shows cooler thermocline temperatures, suggesting a shift to a more La Niña-like mean state, as climate began transitioning into the glacial maximum. Overall, the new record of thermocline temperatures across MIS 3 suggests that there is a relationship between high-latitude North Atlantic climate variability and the mean state of the tropical pacific, although the complex feedback mechanisms are still not fully understood.

There are a number of ways that these studies can be expanded on in future work. It is hoped that a transect of surface and subsurface water from the Northern subtropical and tropical Atlantic will yield tighter constraints on the $\delta^{18}O_{sw}$ – salinity relationship of the region. This may enable more accurate calculations of isotopic calcification temperatures based on the newly recalibrated Mg/Ca temperatures from Chapter II. Completing the time series of Mg/Ca and TEX_{86}^{H} temperatures investigated for the

Holocene and LGM in Chapter III may yield insight into export productivity and nutrient availability in the eastern equatorial Pacific across the last deglaciation. Finally, it is hoped that a record of SST based on *G. ruber* Mg/Ca ratios from the same sediment core intervals of 17JC analyzed for *N. dutertrei* Mg/Ca ratios in Chapter IV will provide additional insight into the mean state of the tropical Pacific across MIS 3. This record will enable the calculation of a surface-thermocline temperature gradient, which may help to further understand the water column dynamics across MIS 3. Additionally, single test *N. dutertrei* Mg/Ca analyses may shed light on ENSO variability in relation to the changes in the mean state predicted in Chapter IV.

REFERENCES

Adelseck, C.G., 1978. Dissolution of deep-sea carbonate: preliminary calibration of preservational and morphologic aspects. Deep-Sea Research 25, 1167-1185.

Anand, P., Elderfield, H., Conte, M.H., 2003. Calibration of Mg/Ca thermometry in planktonic foraminifera from a sediment trap time series. Paleoceanography 18, PA0846.

Arbuszewski, J., deMenocal, P., Kaplan, A., Farmer, E.C., 2010. On the fidelity of shell-derived $\delta^{18}O_{sw}$ estimates. Earth and Planetary Science Letters 300, 185-196.

Archer, D., Emerson, S., Reimers, S., 1989. Dissolution of calcite in deep-sea sediments: pH and O_2 microelectrode results. Geochimica et Cosmochimica Acta 53, 2831-2845.

Barker, S., Greaves, M., Elderfield, H., 2003. A study of cleaning procedures used for foraminiferal Mg/Ca paleothermometry. Geochemistry Geophysics Geosystems 4, GC0559.

Barker, S., Kiefer, T., Elderfield, H., 2004. Temporal changes in North Atlantic circulation constrained by planktonic foraminiferal shell weights. Paleoceanography 19, PA3008.

Barker, S., Cacho, I., Benway, H., Tachikawa, K., 2005. Planktonic foraminiferal Mg/Ca as a proxy for past oceanic temperatures: a methodological overview and data compilation for the Last Glacial Maximum. Quaternary Science Reviews 24, 821-834.

Bé, A.W.H., 1960. Ecology of recent planktonic foraminifera: part 2 – bathymetric and seasonal distributions in the Sargasso Sea off Bermuda. Micropaleontology 6, 373-392.

Bé, A. W., 1977. An ecological, zoogeographic and taxonomic review of recent planktonic foraminifera. Academic Press, London.

Bé, A. W., 1980. Gametogenic calcification in a spinose planktonic foraminifer, *Globigerinoides sacculifer* (Brady). Marine Micropaleontology 5, 283-310.

Beer, C.J., Schiebel, R., Wilson, P.A., 2010a. Technical note: on methodologies for determining the size-normalized weight on planktic foraminifera. Biogeosciences 7, 2193-2198.

Beer, C.J., Schiebel, R., Wilson, P.A., 2010b. Testing planktic foraminiferal shell weight as a surface water [CO_3^{2-}] proxy using plankton net samples. Geology 38, 103-106.

Bemis, B.E., Spero, H.J., Bijma, J., Lea, D.W., 1998. Reevaluation of the oxygen isotopic composition of planktonic foraminifera: experimental results and revised paleotemperature equations. Paleoceanography 13, 150-160.

Berger, W.H., Bonneau, M.C., Parker, F.L., 1982. Foraminifera on the deep-sea floor: lysocline and dissolution rate. Oceanolgica Acta 5, 249-258.

Berger, W.H., 1968. Planktonic foraminifera: selective solution and paleoclimatic interpretation. Deep-Sea Research 15, 31-43.

bin Shaari, H., Yamamoto, M., Irino, T., 2013. Enhanced upwelling in the eastern equatorial Pacific at the last five glacial terminations. Palaeoceanography, Palaeoclimatology, Palaeoecology 386, 8-15.

Bolton, A., Baker, J.A., Dunbar, G.B., Carter, L., Smith, E.G.C., Neil, H.L., 2011. Environmental versus biological controls on Mg/Ca variability in *Globigerinoides ruber* (white) from core top and plankton tow samples in the southwest Pacific Ocean. Paleoceanography 26, PA2219.

Boussetta, S., Bassinot, F., Sabbatini, A., Caillon, N., Nouet, J., Kallen, N., Rebaubier, H., Klinkhammer, G., Labeyrie, L., 2011. Diagenetic Mg-rich calcite in Mediterranean sediments: quantification and impact on foraminiferal Mg/Ca thermometry. Marine Geology 208, 195-204.

Boyle, E.A., 1983. Manganese carbonate overgrowths on foraminifera tests. Geochimica et Cosmochimica Acta 47, 1815-1819.

Brassell, S.C., Eglinton, G., Marlowe, I.T., Pflaumann, U., Sarnthein, M., 1986. Molecular stratigraphy: a new tool for climatic assessment. Nature 320, 129–133.

Broecker, W.S., Clark, E., 2001. An evaluation of Lohmann's foraminifera weight dissolution index. Paleoceanography 16, 531-534.

Broecker, W.S., Clark, E., 2002. A major dissolution event at the close of MIS 5e in the western equatorial Atlantic. Geochemistry Geophysics Geosystems 3, GC000210.

Brown, S.J., Elderfield, H., 1996. Variations in Mg/Ca and Sr/Ca ratios of planktonic foraminifera caused by postdepositional dissolution: evidence of shallow Mg-dependent dissolution. Paleoceanography 11, 543-551.

Brzezinski, M., 1988. Vertical distribution of ammonium in stratified oligotrophic waters. Limnology and Oceanography 33, 1176-1182.

Caron, D. A., Anderson, O.R., Lindsey, J.L., Faber, W.W.J., Lim, E.L., 1990. Effects of gametogenesis on test structure and dissolution of some spinose planktonic foraminifera and implications for test preservation. Marine Micropaleontology 16, 93-116.

Cartapanis, O., Tachikawa, K., Bard, E., 2011. Northeastern Pacific oxygen minimum zone variability over the past 70 kyr: Impact on biological production and oceanic ventilation. Paleoceanography 26, PA2126.

Chen, W., Mohtadi, M., Schefuß, E., Mollenhauer, G., 2014. Organic-geochemical proxies of sea surface temperature in surface sediments of the tropical eastern Indian Ocean. Deep Sea Research I 88, 17-29.

Choi, J., An, S-I., Yeh, S.-W., 2012. Decadal amplitude modulation of two types of ENSO and its relationship to the mean state. Climate Dynamics 38, 2631-2644.

Chong, P., 2010. Archaebacterial bipolar tetraether lipids: Physio-chemical and membrane properties. Chemistry and Physics of Lipids 163, 253-265.

Clement, A.C., Cane, M., 1999. A role for the tropical Pacific coupled ocean-atmosphere system on Milankovitch and millennial timescales. Part I: a modeling study of the tropical Pacific variability. Mechanisms of Global Climate Change at Millennial Time Scales, 363-371.

Cléroux, C., Cortijo, E., Anand, P., Labeyrie, L., Bassinot, F., Caillon, N., Duplessey, J-C., 2008. Mg/Ca and Sr/Ca ratios in planktonic foraminifera: proxies for upper water column temperature reconstruction. Paleoceanography 23, PA3214.

CLIMAP Project Members, 1976. The surface of the ice-age Earth. Science 191, 1131-1137.

de Rosa, M., Esposito, E., Gambacorta, A., Nicolaus, B., Bu'Lock, J., 1980. Effects of temperature on ether lipid compositions of *Caldariella acidophila*. Phytochemistry 19, 827-831.

de Villiers, S., 2005. Foraminiferal shell-weight evidence for sedimentary calcite dissolution above the lysocline. Deep-sea Research I 52, 671-680.

Dean, W.E., Gardner, J.V., Piper, D.Z., 1997. Inorganic geochemical indicators of glacial-interglacial changes in productivity and anoxia on the California continental margin. Geochimica et Cosmochimica Acta 61, 4507-4518.

Dekens, P.S., Lea, D.W., Pak, D.K., Spero, H.J., 2002. Core top calibration of Mg/Ca in tropical foraminifera: refining paleotemperature estimation. Geochemistry Geophysics Geosystems 3, GC0200.

Deuser, W.G., 1987. Seasonal variations in isotopic composition and deep-water fluxes of the tests of perennially abundant planktonic foraminifera of the Sargasso Sea: results from sediment-trap collections and their paleoceanographic significance. Journal of Foramimiferal Research 17, 14-27.

Dijkstra, H.A., Neelin, J.D., 1995. Ocean-atmosphere interaction and the tropical climatology: part II. Why the Pacific cold tongue is in the east. Journal of Climate 8, 1343-1359.

DiNezio, P.N., Clement, A., Vecchi, G.A., 2010. Reconciling differing views of tropical Pacific climate change. EOS Transactions 91, 141-142.

Drexler, J. W., Rose, W.I.J., Sparks, R.S.J., Ledbetter, M.T., 1980. The Los Chocoyos Ash, Guatemala: a major stratigraphic marker in middle America and in three ocean basins, Quaternary Research 13, 327-345.

Dubois, N., Kienast, M., Kienast, S., Calvert, S.E., Francois, R., Anderson, R., 2010. Sedimentary opal records in the eastern equatorial Pacific: it is anot all about leakage. Global Biogeochemical Cycles 24, GB3821.

Dubois, N., Kienast, M., Kienast, S., Normandeau, C., Calvert, S.E., Herbert, T.D., Mix, A., 2011. Millennial-scale variations in hydrography and biogeochemistry in the Eastern Equatorial Pacific over the last 100 kyr. Quaternary Science Reviews 30, 210-223.

Dubois, N., Kienast, M., Kienast, S., Timmermann, A., 2014. Millennial-scale Atlantic/East Pacific sea surface temperature linkages during the last 100,000 years. Earth and Planetary Science Letters 396, 134-142.

Eggins, S., De Deckker, P., Marshall, J., 2003. Mg/Ca variation in planktonic foraminifera tests: implications for reconstructing palaeo-seawater temperature and habitat migration. Earth and Planetary Science Letters 212, 291-306.

Elderfield, H., Ganssen, G., 2000. Past temperature and $\delta^{18}O$ of surface ocean waters inferred from foraminiferal Mg/Ca ratios. Nature 405, 442-445.

Elderfield, H., Vautravers, M., Cooper, M., 2002. The relationship between shell size and Mg/Ca, Sr/Ca, $\delta^{18}O$, and $\delta^{13}C$ of species of planktonic foraminifera. Geochemistry Geophysics Geosystems 3, GC0194.

Emerson, S., Bender, M., 1981. Carbon fluxes at the sediment-water interface of the deep-sea: calcium carbonate preservation. Journal of Marine Research 39, 139-162.

Erez, J., Luz, B., 1983. Experimental paleotemperature equation for planktonic foraminifera. Geochimica et Cosmochimica Acta 47, 1025–1031.

Fairbanks, R.G., Wiebe, P.H., Bé, A.W.H., 1980. Vertical distribution and isotopic composition of living planktonic foraminifera in the Western North Atlantic. Science 207, 61-63.

Fairbanks, R.G., Sverdlove, M., Free, R., Wiebe, P.H., Bé, A.W.H., 1982. Vertical distribution and isotopic fractionation of living planktonic foraminifera from the Panama Basin. Nature 298, 841-844.

Fairbanks, R.G., Charles, C.D., Wright, J.D., 1992. Origin of global meltwater pulses. Radiocarbon after four decades, pp 473-500.

Faul, K., Ravelo, A.C., Delaney, M.L., 2000. Reconstructions of upwelling, productivity, and photic zone depth in the eastern equatorial Pacific Ocean using planktonic foraminiferal stable isotopes and abundances. Journal of Foraminiferal Research 30, 110-125.

Ferguson, J.E., Henderson, G.M., Kucera, M., Rickaby, R.E.M., 2008. Systematic change of foraminiferal Mg/Ca ratios across a strong salinity gradient. Earth and Planetary Science Letters 265, 153-166.

Fiedler, P. C., Talley, L.D., 2006. Hydrography of the eastern tropical Pacific: A review. Progress in Oceanography 69, 143-180.

Ford, H.L., Ravelo, A.C., Hovan, S., 2012. A deep Eastern Equatorial Pacific thermocline during the early Pliocene warm period. Earth and Planetary Science Letters 355-356, 152-161.

Ford, H.L., Ravelo, A.C., Polissar, P.J., 2015. Reduced El Niño-Southern Oscillation during the Last Glacial Maximum. Science 347, 255-258.

Frazel, D.W., Berberian, G., 1990. Distributions of chlorophyll and primary productivity in relation to water column structure in the eastern North Atlantic Ocean, Global Biogeochemical Cycles 4, 241-251.

Ganeshram, R.S., Pedersen, T.F., 1998. Glacial-interglacial variability in upwelling and bioproductivity off NW Mexico: implications for quaternary paleoclimate. Paleoceanography 13, 634-645.

Guilyardi, E., 2006. El Niño-mean state-seasonal cycle interactions in a multi-model ensemble. Climate Dynamics 26, 329-348.

Guilyardi, E., Wittenberg, A., Fedorov, A., Collins, M., Wang, C., Capotondi, A., Oldenborgh, G.J., Stockdale, T., 2009. Understanding El Niño in ocean-atmosphere general circulation models: progress and challenges. Bulletin of the American Meteorological Society 90, 325-340.

Hales, B., Emerson, S., 1996. Calcite dissolution in sediments on the Ontong-Java Plateau: in situ measurements of porewater O_2 and pH. Global Biogeochemical Cycles 10, 527-541.

Hales, B., Emerson, S., 1997. Calcite dissolution in sediments of the Ceara Rise: in situ measurements of porewater O_2, pH, and $CO_{2(aq)}$. Geochimica et Cosmochimica Acta 61, 501-514.

Hastings, D.W., Russell, A., Emerson, S., 1998. Foraminiferal magnesium in *G. sacculifer* as a paleotemperature proxy in the equatorial Atlantic. Paleoceanography 13, 161-169.

Hemleben, C., Spindler, M., Anderson, O.R., 1989. Modern Planktonic Foraminifera. Springer-Verlag, New York, 363 pp.

Herndl, G., Reinthaler, T., Teira, E., van Aken, H., Veth, C., Pernthaler, A., Pernthaler, J., 2005. Contribution of Archaea to total prokaryotic production in the deep Atlantic Ocean. Applied and Environmental Microbiology 71, 2303-2309.

Hertzberg, J.E., Schmidt, M.W., 2013. Refining *Globigerinoides ruber* Mg/Ca paleothermometry in the Atlantic Ocean. Earth and Planetary Science Letters 383, 123-133.

Ho, S., Yamamoto, M., Mollenhauer, G., Minagawa, M., 2011. Core top TEX_{86} values in the south and equatorial Pacific. Organic Geochemistry 1, 94-99.

Ho, S., Laepple, T., 2015. Glacial cooling as inferred from marine temperature proxies TEX_{86}^{H} and $U^{k'}_{37}$. Earth and Planetary Science Letters 409, 15-22.

Hönisch, B., Allen, K.A., Lea, D.W., Spero, H.J., Eggins, S.M., Arbuszewski, J., deMenocal, P., Rosenthal, Y., Russell, A.D., Elderfield, H., 2013. The influence of salinity on Mg/Ca in planktic foraminifers – evidence from cultures, core-top sediments and complimentary $\delta^{18}O$. Geochimica et Cosmochimica Acta 121, 196-213.

Hoogakker, B.A.A., Klinkhammer, G.P., Elderfield, H., Rohling, E.J., Hayward, C., 2009. Mg/Ca paleothermometry in high salinity environments. Earth and Planetary Science Letters 284, 583-589.

Huguet, C., Schimmelmann, A., Thunell, R., Lourens, L., Sinninghe Damsté, J.S., Schouten, S., 2007. A study of the TEX_{86} paleothermometer in the water column and sediments of the Santa Barbara Basin, California. Paleoceanography 22, PA3203.

Huguet, C., de Lange, G.J., Gustafsson, O., Middelburg, J.J., Sinninghe Damsté, J.S., Schouten, S., 2008. Selective preservation of soil organic matter in oxidized marine sediments (Madeira Abyssal Plain). Geochemica et Cosmochimica Acta 72, 6061-6068.

Huguet, C., Kim, J., de Lange, G., Sinninghe Damsté, J.S., Schouten, S., 2009. Effects of long term oxic degradation on the TEX_{86} and BIT organic proxies. Organic Geochemistry 40, 1188-1194.

Huot, Y., Babin, M., Bruyant, F., Grob, C., Twardowski, M.S., Claustre, H., 2007. Relationship between photosynthetic parameters and different proxies of phytoplankton biomass in the subtropical ocean. Biogeosciences 4, 853-868.

Hut, G., 1987. Stable isotope reference samples for geochemical and hydrological investigations. Report on Consultant's Group Meeting. International Atomic Agency, Vienna, Austria, p. 42.

Imbrie, J., N.G. Kipp, N.G., 1971. A new micropaleontological method for quantitative paleoclimatology: Application to a late Pleistocene Caribbean core. K.K. Turekian (Ed.), The Late Cenozoic Glacial Ages, Yale University Press, New Haven, CT, 71–181.

Ingalls, A., Shah, S., Hansman, R., Aluwihare, L.I., Santos, G.M., Druffell, E.R.M., Pearson, A., 2006. Quantifying archaeal community autotrophy in the mesopelagic ocean using natural radiocarbon. Proceedings of the National Academy of Sciences of the United States of America 103, 6442-6447.

Jahnke, R.A., Craven, D.B., Gaillard, J.-F., 1994. The influence of organic matter diagenesis on $CaCO_3$ dissolution at the deep-sea floor. Geochemica et Cosmochimica Acta 58, 2799-2809.

Jones, G.A., Johnson, D.A., Curry, W.B., 1984. High-resolution stratigraphy in Late Pleistocene/Holocene sediments of the Vema Channel. Marine Geology 58, 59-87.

Karner, M., DeLong, E., Karl, D., 2001. Archaeal dominance in the mesopelagic zone of the Pacific Ocean. Nature 409, 507-510.

Kessler, W.S., 2006. The circulation of the eastern tropical Pacific: A review. Progress in Oceanography 69, 181-217.

Kim, J.-H., Schouten, S., Hopmans, E., Donner, B., Sinninghe Damsté, J.S., 2008. Global sediment core-top calibration of the TEX_{86} paleothermometer in the ocean. Geochimica et Cosmochimica Acta 72, 1154–1173.

Kim, J.-H., Huguet, C., Zonneveld, K.A.F., Versteegh, G.J.M., Roeder, W., Sinninghe Damsté, J.S., Schouten, A., 2009a. An experimental field study to test the stability of lipids used for the TEX_{86} and $U^{k'}_{37}$ palaeothermometers. Geochimica et Cosmochimica Acta 73, 2888-2898.

Kim, J.-H., Crosta, X., Michel, E., Schouten, S., Duprat, J., Sinninghe Damsté, J.S., 2009b. Impact of lateral transport on organic proxies in the Southern Ocean. Quaternary Research 41, 246-250.

Kim, J.-H., van der Meer, J., Schouten, S., Helmke, P., Willmott, V., Sangiorgi, F., Koc, N., Hopmans, E., Sinninghe Damsté, J.S., 2010. New indices and calibrations derived from the distribution of crenarchaeal isoprenoid tetraether lipids: Implications for past sea surface temperature reconstructions. Geochimica et Cosmochimica Acta 74, 4639-4654.

Kisakürek, B., Eisenhauer, A., Böhm, G., Garbe-Schönberg, D., Erez, J., 2008. Controls on shell Mg/Ca and Sr/Ca in cultured planktonic foraminiferan, *Globigerinoides ruber* (white). Earth and Planetary Science Letters 273, 260-269.

Könneke, M., Bernhard, A.E., de la Torre, J.R., Walker, C.B., Waterbury, J.B., Stahl, D.A., 2005. Isolation of an autotrophic ammonia-oxidizing marine archaeon. Nature 437. 543-546.

Kontakiotis, G., Mortyn, P.G., Antonarakou, A., Martínez-Botí, M.A., Triantaphyllou, M.V., 2011. Field-based validation of a diagenetic effect on *G. ruber* Mg/Ca paleothermometry: core top results from the Aegean Sea (eastern Mediterranean). Geochemistry Geophysics Geosystems 12, Q09004.

Koutavas, A., Lynch-Stieglitz, J., Marchitto, T.M., Sachs, J.P., 2002. El Niño-like pattern in ice age tropical Pacific sea surface temperature. Science 297, 226-230.

Koutavas, A., Joanides, S., 2012. El Niño-Southern Oscillation extrema in the Holocene and Last Glacial Maximum. Paleoceanography 27, PA4208.

Kowsmann, R.O., 1973. Coarse components in surface sediments of the Panama Basin, eastern equatorial Pacific. Journal of Geology 81, 473-491.

Latif, M., Keenlyside, N.S., 2009. El Niño/Southern Oscillation response to global warming. Proceedings of the National Academy of Sciences of the United States of America 106, 20578-20583.

Lea, D.W., Martin, P.A., 1996. A rapid mass spectrometric method for the simultaneous analysis of barium, cadmium, and strontium in foraminifera shells. Geochimica et Cosmochimica Acta 60, 3143-3149.

Lea, D.W., Mashiotta, T.A., Spero, H.J., 1999. Controls on magnesium and strontium uptake in planktonic foraminifera determined by live culturing. Geochimica et Cosmochimica Acta 63, 2369-2379.

Lea, D.W., Pak, D.K., Spero, H.J., 2000. Climate impact of Late Quaternary Equatorial Pacific sea surface temperature variations. Science 289, 1719 – 1724.

Lea, D. W., Martin, P.A., Pak, D.K., Spero, H.J., 2002. Reconstructing a 350 ky history of sea level using planktonic Mg/Ca and oxygen isotope records from a Cocos Ridge core. Quaternary Science Reviews 21, 283-293.

Lea D. W., Pak, D.K., Belanger, C.L., Spero, H.J., Hall, M.A., Shackleton N.J., 2006. Paleoclimate history of the Galápagos surface waters over the last 135,000 yr. Quaternary Science Reviews 25, 1152-1167.

Leduc, G., Vidal, L., Tachikawa, K., Rostek, F., Sonzogni, C., Beaufort, L., Bard, E., 2007. Moisture transport across Central America as a positive feedback on abrupt climatic changes. Nature 445, 908-911.

Leduc, G., Vidal, L., Cartapanis, O., Bard, E., 2009. Modes of eastern equatorial Pacific thermocline variability: Implications for ENSO dynamics over the last glacial period. Paleoceanography 24, PA3202.

Lee, K.-E., Kim, J.-H, Wilke, I., Helmke, P., Schouten, S., 2008. A study of the alkenone, TEX_{86}, and planktonic foraminifera in the Benguela Upwelling System: implications for past sea surface temperature estimates. Geochemistry Geophysics Geosystems 9, Q10019

LeGrande, A.N., Schmidt, G.A., 2006. Global gridded data set of the oxygen isotopic composition of seawater. Geophysical Research Letters 33, 5.

Lincoln, S.A., Wai, B., Eppley, J.M., Church, M.J., Summons, R.E., DeLong, E.F., 2014. Planktonic euryarchaeota are a significant source of archaeal tetraether lipids in the ocean. Proceedings of the National Academy of Sciences of the United States of America 111, 9858-9863.

Lisiecki, L.E., Raymo, M.E., 2005. A Pliocene-Pleistocene stack of 57 globally distributed benthic $\delta^{18}O$ records. Paleoceanography 20, PA1071.

Locarnini, R.A., Mishonov, A.V., Antonov, J.I., Boyer, T.P., Garcia, H.E., 2006. World Ocean Atlas 2005, volume 1: temperature. Ed. by S. Levitus, 182 pp., NOAA, Silver Spring, MD.

Locarnini, R.A., Michonov, A.V., Antonov, J.I., Boyer, T.P., Garcia, H.E., Baranova, O.K., Zweng, M.M., Paver, C.R., Reagan, J.R., Johnson, D.R., Hamilton, M., Seidov, D., 2013. World Ocean Atlas 2013, volume 1: temperature. Ed. by S. Levitus and A. Michonov, 40 pp., NOAA Atlas NESDIS 73.

Lomas, M.W., Lipschultz, F., 2006. Forming the primary nitrite maximum: Nitrifiers or phytoplankton? Limnology and Oceanography 51, 2453-2467.

Lopes dos Santos, R., Prange, M., Castañeda, I.S., Schefuß, E., Mulitza, S., Schulz, M., Niedermeyer, E.M., Sinninghe Samsté, J.S., Schouten, S., 2010. Glacial-interglacial variability in Atlantic meridional overturning circulation and thermocline adjustments in the tropical North Atlantic. Earth and Planetary Science Letters 300, 407-414.

Loubere, P., Fariduddin, M., 2008. Tropical Pacific-Atlantic climate-driven switching of thermocline nutrient content and export productivity. Global Biogeochemical Cycles 22, GB3117.

Lund, D.C., Curry, W., 2006. Florida Current surface temperature and salinity variability during the last millennium. Paleoceanography 21, PA2009.

Lyle, M., Murray, D.M., Finney, B.P., Dymond, J., Robbins, J.M., Brooksforce, K., 1988. The record of late Pleistocene biogenic sedimentation in the eastern tropical Pacific Ocean. Paleoceanography 3, 39-59.

Lynch-Stieglitz, J., Adkins, J.F., Curry, W.B., Dokken, T., Hall, I.R., Herguera, J.C., Hirschi, J., Ivanova, E.V., Kissel, C., Marchal, O., Marchitto, T.M., McCave, I.N., McManus, J.F., Mulitza, S., Ninnemann, U., Peeters, F., Yu, E-F., Zahn, R., 2007. Atlantic meridional overturning circulation during the Last Glacial Maximum. Science 316, 66-69.

Marcantonio, F., Lyle, M., Ibrahim, R., 2013. Particle sorting during sediment redistribution processes and the effect on ^{230}Th-normalized mass accumulation rates. Geophysical Research Letters 41, 5547-5554.

MARGO Project Members, 2009. Constraints on the magnitude and patterns of ocean cooling at the Last Glacial Maximum. Nature Geoscience 2, 127-132.

Martin, W.R., Sayles, F.L., 2006. Organic matter oxidation in deep-sea sediments: distribution in the sediment column and implications for calcite dissolution. Deep-Sea Research Part II 53, 771-792.

Massana, R., Murray, A., Preston, C., DeLong, E., 1997. Vertical distribution and phylogenetic characterization of marine planktonic Archaea in the Santa Barbara Basin. Applied and Environmental Microbiology 63, 50-56.

Mathien-Blard, E., Bassinot, F., 2009. Salinity bias on the foraminifera Mg/Ca thermometry: correction procedure and implications for past ocean hydrographic reconstructions. Geochemistry Geophysics Geosystems 10, Q12011.

Medina-Elizalde, M., Lea, D.W., Fantle, M.S., 2008. Implications of seawater Mg/Ca variability for Plio-Pleistocene tropical climate reconstruction. Paleoceanography 22, PA3127.

Meeder, E, Mackey, K.R.M., Paytan, A., Shaked, Y., Iluz, D., Stambler, N., Rivlin, T., Post., A.F., Lazar, B., 2012. Nitrite dynamics in the open ocean – clues from seasonal and diurnal variations. Marine Ecology Progress Series 453, 11-26.

Milliman, J.D., Troy, P.J., Balch, W.M., Adams, A.K., Li, Y.-H., Mackenzie, F.T., 1999. Biologically mediated dissolution of calcium carbonate above the chemical lysocline? Deep-Sea Research Part I 46, 1653-1669.

Mollenhauer, G., Schneider, R.R., Jennerjahn, T., Müller, P.J., Wefer, G., 2004. Organic carbon accumulation in the South Atlantic Ocean: its modern, mid-Holocene and last glacial distribution. Global Planetary Change 40, 249-266.

Mollenhauer, G., Eglinton, T.I., Hopmans, E.C., Sinninghe Damsté, J.S., 2008. A radiocarbon-based assessment of the preservation characteristics of crenarchaeol and alkenones from continental margin sediments. Organic Geochemistry 39, 1039-1045.

NGRIP dating group, 2008. IGBP PAGES/Wprld Data Center for Paleoclimatology. Data contribution series # 2008-034. NOAA/NCDC Paleoclimatology Program, Boulder CO, USA.

North Greenland Ice Core Project Members, 2004. High-resolution record of Northern Hemisphere climate extending into the last interglacial period. Nature 431, 147-151.

Nürnberg, D., Bijma, J., Hemleben, C., 1996. Assessing the reliability of magnesium in foraminiferal calcite as a proxy for water mass temperatures. Geochimica et Cosmochimica Acta 60, 803-814.

Nürnberg, D., Müller, A., Schneider, R.R., 2000. Paleo-sea surface temperature calculations in the equatorial east Atlantic from Mg/Ca ratios in planktic formaninifera: A comparison to sea surface temperature estimates from $U^{K'}_{37}$, oxygen isotopes, and foraminiferal transfer function. Paleoceanography 15, 124-134.

Oppo, D.W., Rosenthal, Y., Linsley, B.K., 2009. 2,000-year-long temperature and hydrology reconstructions from the Indo-Pacific warm pool. Nature 460, 1113-1116.

Pedersen, T.F., 1983. Increased productivity in the eastern equatorial Pacific during the last glacial maximum (19,000 to 14,000 yr. b.p.). Geology 11, 16-19.

Pedersen, T.F., Nielsen, B., Pickering, M., 1991. Timing of late Quaternary productivity pulses in the Panama Basin and implications for atmospheric CO_2. Paleoceanography 6, 657-677.

Pena, L.D., Calvo, E., Cacho, I., Eggins, S., Pelejero, C., 2005. Identification and removal of Mn-Mg-rich contaminant phases on foraminiferal tests: implications for Mg/Ca past temperature reconstructions. Geochemistry Geophysics Geosystems 6, Q09P02.

Pena, L. D., Cacho, I., Ferretti, P., Hall, M.A., 2008. El Niño–Southern Oscillation–like variability during glacial terminations and interlatitudinal teleconnections. Paleoceanography 23, PA3101.

Pennington, T., Mahoney, K., Kuwahara, V., Kolber, D., Calienes, R., Chavez, F., 2006. Primary production in the eastern tropical Pacific: A review. Progress in Oceanography 69, 285-317.

Prahl, F.G., Wakeham, S.G., 1987. Calibration of unsaturation patterns in long-chain ketone compositions for paleotemperature assessment. Nature 330, 367-369.

Premuzic, E.T., Benkovitz, C.M., Gaffney, J.S., Walsh, J.J., 1982. The nature and distribution of organic matter in the surface sediments of world oceans and seas. Organic Geochemistry 4, 63-77.

Rasmusson, E.M., Carpenter, T.H., 1982. Variations in tropical sea surface temperature and surface wind fields associated with the Southern Oscillation/El Niño. Monthly Weather Review 110, 354-384.

Ravelo A., Fairbanks, R., 1992. Oxygen isotopic composition of multiple species of planktonic foraminifera: Recorders of the modern photic zone temperature gradient. Paleoceanography 7, 815–831.

Regenberg, M., Nürnberg, D., Steph, S., Groeneveld, J., Garbe-Schönberg, D., Tiedemann, R., Dullo, W.C., 2006. Assessing the effect of dissolution on planktonic foraminiferal Mg/Ca ratios: evidence from Caribbean core tops. Geochemistry Geophysics Geosystems 7, Q07P15.

Regenberg, M., Steph, S., Nürnberg, D., Tiedemann, R., Garbe-Schönberg D., 2009. Calibrating Mg/Ca ratios of multiple planktonic foraminiferal species with $\delta^{18}O$-calcification temperatures: Paleothermometry for the upper water column. Earth and Planetary Science Letters 278, 324-336.

Regenberg, M., Regenberg, A., Garbe-Schönberg, D., Lea, D.W., 2014. Global dissolution effects on planktonic foraminiferal Mg/Ca ratios controlled by the calcite-saturation state of bottom waters. Paleoceanography 29, 127-142.

Richey, J., Hollander, D., Flower, B., Eglinton, T., 2011. Merging late Holocene molecular organic and foraminiferal-based geochemical records of sea surface temperature in the Gulf of Mexico. Paleoceanography 26, PA1209.

Robinson, R.S., Martinez, P., Pena, L.D., Cacho, I., 2009. Nitrogen isotopic evidence for deglacial changes in nutrient supply in the eastern equatorial Pacific. Paleoceanography 24, PA1702.

Rosenthal, Y., Lohmann, G.P., Lohmann, K.C., Sherrell, R.M., 2000. Incorporation and preservation of Mg in *Globigerinoides sacculifer*: implications for reconstructing the temperature and $^{18}O/^{16}O$ of seawater. Paleoceanography 15, 135-145.

Rosenthal, Y., Lohmann, G.P., 2002. Accurate estimation of sea-surface temperatures using dissolution corrected calibrations for Mg/Ca paleothermometry. Paleoceanography 17, PA0749.

Rosenthal, Y., Perron-Cashman, S.L.C.H., Bard, E., Barker, S., Billups, K., Bryan, M., Delaney, M.L., deMenocal, P.B., Dwyer, G.S., Elderfield, H., German, C.R., Greaves, M., Lea, D.W., Marchitto, T.M., Pak, D.K., Paradis, G.L., Russell, A.D., Schneider, R.R., Scheiderich, K., Stott, L., Tachikawa, K., Tappa, E., Thunel, R., Wara, M., Weldeab, S., Wilson, P.A., 2004. Interlaboratory comparison study of Mg/Ca and Sr/Ca measurements in planktonic foraminifera for paleoceanographic research. Geochemistry Geophysics Geosystems 5, GC0650;

Rueda, G., Rosell-Melé, A., Escala, M., Gyllencreutz, R., Backman, J., 2009. Comparison of instrumental and GDGT-based estimates of sea surface and air temperatures from the Skagerrak. Organic Geochemistry 40, 287-291.

Russell, A.D., Hönisch, B., Spero, H.J., Lea, D.W., 2004. Effects of seawater carbonate ion concentration and temperature on shell U, Mg, and Sr in cultured planktonic foraminifera. Geochimica et Cosmochimica Acta 68, 4347-4361.

Sabbatini, A., Bassinot, F., Boussetta, S., Negri, A., Rebaubier, H., Dewilde, F., Nouet, J., Caillon, N., Morigi, C., 2011. Further constraints on the diagenetic influences and salinity effect on *Globigerinoides ruber* (white) Mg/Ca thermometry: implications in the Mediterranean Sea. Geochemistry Geophysics Geosystems 12, GC3675.

Sadekov, A., Eggins. S.M., De Deckker, P., 2005. Characterization of Mg/Ca distributions in planktonic foraminifera species by electron microprobe mapping. Geochemistry Geophysics Geosystems 6, Q12P09.

Sadekov, A., Eggins. S.M., De Deckker, P., Kroon, D., 2008. Uncertainties in seawater thermometry deriving from intratest and intertest Mg/Ca variability in *Globigerinoides ruber*. Paleoceanography 23, PA1215.

Sadekov, A.Y., Ganeshram, R., Pichevin, L., Berdin, R., McClymont, E., Elderfield, H., Tudhope, A.W., 2013. Palaeoclimate reconstructions reveal a strong link between El Niño-Southern Oscillation and Tropical Pacific mean state. Nature Communications 4, 1-8.

Saikku, R., Stott, L., Thunell, R., 2009. A bi-polar signal recorded in the western tropical Pacific: Northern and Southern Hemisphere climate records from the Pacific warm pool during the last Ice Age. Quaternary Science Reviews 28, 2374-2385.

Schlitzer, R., Ocean Data View, http://odv.awi.de, 2013.

Schmidt, G.A., Bigg, G.R., Rohling, E.J., 1999. Global seawater oxygen-18 database. http://data.giss.nasa.gov/o18data/

Schmidt, M.W., Vautravers, M.J., Spero, H.J., 2006. Rapid subtropical North Atlantic salinity oscillations across Dansgaard-Oeschger cycles. Nature 443, 561-564.

Schmidt, M.W., Lynch-Stieglitz, J., 2011. Florida Straits deglacial temperature and salinity change: implications for tropical hydrologic cycle variability during the Younger Dryas. Paleoceanography 26, PA4205.

Schmidt, M.W., Hertzberg, J.E., 2011. Abrupt climate change during the last ice age. Nature Education knowledge 3.

Schmidt, M.W., Chang, P., Hertzberg, J.E., Them, T.R., Ji, L., Otto-Bliesner, B.L., 2012a. Impact of abrupt deglacial climate change on tropical Atlantic subsurface temperatures. Proceedings of the National Academy of Sciences of the United States of America 109, 14348-14352.

Schmidt, M.W., Weinlein, W.A., Marcantionio, F., Lynch-Stieglitz, J., 2012b. Solar forcing of Florida Straits surface salinity during the early Holocene. Paleoceanography 27, PA3204.

Schmidt, G.A., Annan, J.D., Bartlein, P.J., Cook, B.I., Guilyardi, E., Hargreaves, J.C., Harrison, S.P., Kageyama, M., Lovejoy, S., Mann, M.E., Masson-Delmotte, V., Risi, C., Thompson, D., Timmermann, A., Tremblay, L., Yiou, P., 2014. Using palaeo-climate comparisons to constrain future projections in CMIP5. Climate of the Past 10, 221-250.

Schmittner, A., Urban, N.M., Shakun, J.D., Mahowald, N.M., Clark, P.U., Bartlein, P.J., Mix, A.C., Rosell-Melé, A., 2011. Climate sensitivity estimated from temperature reconstructions of the Last Glacial Maximum. Science 334, 1385-1388.

Schmuker, B., Schiebel, R., 2002. Planktic foraminifers and hydrography of the eastern and northern Caribbean Sea. Marine Micropaleontology 46, 387-403.

Schouten, S., Hopmans, E.C., Schefuß, E., Sinninghe Damsté, J.S., 2002. Distributional variations in marine crenarchaeotal membrane lipids: a new tool for reconstructing ancient sea water temperatures? Earth and Planetary Science Letters 204, 265-274.

Schouten, S., Hopmans, E.C., Sinninghe Damsté, J.S., 2004. The effect of maturity and depositional redox conditions on archaeal tetraether lipid palaeothermometry. Organic Geochemistry 35, 567-571.

Schouten, S., Forster, A., Panoto, F.E., Sinninghe Damsté, J.S., 2007a. Towards calibration of the TEX_{86} palaeothermometer for tropical sea surface temperatures in ancient greenhouse worlds. Organic Geochemistry 38, 1537-1546.

Schouten, S., Huguet, C., Hopmans, E.C., Kienhuis, M.V.M., Sinninghe Damsté, J.S., 2007b. Analytical methodology for TEX_{86} paleothermometry by high-performance liquid chromatography/atmospheric pressure chemical ionization-mass spectrometry. Analytical Chemistry 79, 2940-2944.

Schouten, S., Hopmans, E.S., Rosell-Melé, A., Pearson, A., Bauersachs, P.A.T., Bard, E., Bernasconi, S.M., Bianchi, T.S., Brocks, J.J., Carlson, L.T., Castañeda, I.S., Derenne, S., Selver, A.D., Dutta, K., Eglinton, T., Fosse, C., Galy, V., Grice, K., Hinrichs, K.-U., Huang, Y., Huguet, A., Huguet, C., Hurley, S., Ingalls, A., Jia, G., Keely, B., Knappy, C., Kondo, M., Krishnan, S., Lincoln, A., Lipp, S., Mangelsdorf, K., Martínez-García, A., Ménot, G., Mets, A., Mollenhauer, G., Ohkouchi, N., Ossebaar, J., Pagani, M., Pancost, R.D., Pearson, E.J., Peterse, F., Reichart, G.-J., Schaeffer, P., Schmitt, G., Schwark, L., Shah, S.R., Smith, R.W., Smittenberg, R.H., Summons, R.E., Takano, Y., Talbot, H.M., Taylor, K.W.R., Tarozo, R., Uchida, M., Dongen, B.E.V., Van Mooy, B.A.S., Wang, J., Warren, C., Weijers, J.W.H., Werne, J.P., Woltering, M., Xie, S., Yamamoto, M., Yang, H., Zhang, C.L., Zhang, Y., Zhao, M., Sinninghe Damsté, J.S., 2009. An interlaboratory study of TEX_{86} and BIT analysis of sediments, extracts, and standard mixtures. Geochemistry Geophysics Geosystems 14, 5263-5285.

Seki, O., Schmidt, D., Schouten, S., Hopmans, E., Sinninghe Damsté, J., Pancost, R., 2012. Paleoceanographic changes in the eastern Equatorial Pacific over the last 10 Myr. Paleoceanography 27, PA3224.

Sinninghe Damsté, J.S., Hopmans, E.C., Schouten, S., van Duin, A.C.C., Geenevasen, J.A.J., 2002a. Crenarchaeol: The characteristic core glycerol dibiphytanyl glycerol tetraether membrane lipid of cosmopolitan pelagic crenarchaeota. Journal of Lipid Research 43, 1641-1651.

Sinninghe Damsté, J.S., Rijpstra, W., Reichart, G., 2002b. The influence of oxic degradation on the sedimentary biomarker record II. Evidence from Arabian Sea sediments. Geochimica et Cosmochimica Acta 66, 2737-2754.

Spero, H., Mielke, K.M., Kalve, E.M., Lea, D.W., Pak, D.K., 2003. Multispecies approach to reconstructing eastern equatorial Pacific thermocline hydrography during the past 360 kyr. Paleoceanography 18, PA000814.

Steph, S., Tiedemann, R., Prange, M., Groeneveld, J., Schulz, M., Timmermann, A., Nürnberg, D., Rühlemann, C., Saukel, C., Haug, G.H., 2010. Early Pliocene increase in thermohaline overturning: A precondition for the development of the modern equatorial cold tongue. Paleoceanography 25, PA2202.

Stott, L., Poulsen, C., Lund, S., Thunell, R.C., 2002. Super ENSO and global climate oscillations at millennial time scales. Science 297, 222-226.

Thunell, R.C., Honjo, S., 1981. Calcite dissolution and the modification of planktonic foraminiferal assemblages. Marine Micropaleontology 6, 169-182.

Thunell, R.C., Curry, W.B., Honjo, S., 1983. Seasonal variation in the flux of planktonic foraminifera: time series sediment trap results from the Panama Basin. Earth and Planetary Science Letters 64, 44-55.

Timmermann, A., Sachs, J., Timm, O.E., 2014. Assessing divergent SST behavior duing the last 21 ka derived from alkenones and *G. ruber*-Mg/Ca in the equatorial Pacific. Paleoceanography 29, 680-696.

Tierney, J.E., 2014. Biomarker-based inferences of past climate: The TEX_{86} paleotemperature proxy. Holland, H.D., Turekian, K.K. (Eds.). Treatise on Geochemistry (Second Edition), Elsevier, 379-393.

Tierney, J.E., Tingley, M.P., 2014. A Bayesian, spatially-varying calibration model for the TEX_{86} proxy. Geochinica et Cosmochimica Acta 127, 83-107.

Toggweiler, J.D., Dixon, K., Broecker, W.S., 1991. The Peru upwelling and the ventilation of the South Pacific thermocline. Journal of Geophysical Research 96, 20467-20497.

Tolderlund, D.S., and Bé, A.W.H., 1971. Seasonal distribution of planktonic foraminifera in the western North Atlantic. Micropaleontology 17, 297-329.

Turich, C., Freeman, K.H., Bruns, M.A., Conte, M.H., Jones, A.D., Wakeham, S.G., 2007. Lipids of marine archaea: Patterns and provenance in the water-column and sediments. Geochimica et Cosmochimica Acta 71, 3272-3291.

Turich, C., Schouten, S., Thunell, R.C., Varela, R., Astor, Y., Wakeham, S., 2013. Comparison of TEX_{86} and U^{K}_{37} temperature proxies in sinking particles in the Cariaco Basin. Deep-Sea Research I 78, 115-133.

Uda, I., Sugai, A., Itoh, Y., Itoh, T., 2001. Variation in molecular species of polar lipids from *Thermoplasma acidophilum* depends on growth temperature. Lipids 36, 103-105.

Wada, E., Hattori, A., 1971. Nitrite metabolism in the euphotic layer of the central North Pacific Ocean. Limnology and Oceanography 16, 766-772.

Wang, C., Enfield, D.B., 2001. The tropical Western Hemisphere warm pool. Geophysical Research Letters 28, 1635-1638.

Wang, C., Fiedler, P.C., 2006. ENSO variability and the eastern tropical Pacific: A review. Progress in Oceanography 69, 239-266.

Wakeham, S.G., Lewis, C., Hopmans, E.C., Schouten, S., Sinninghe Damsté, J.S., 2003. Archaea mediated anaerobic oxidation of methane in deep euxinic waters of the Black Sea. Geochimica et Cosmochimica Acta 67, 1359-1374.

Wei, Y., Wang, J., Liu, J., Dong, L., Li, L., Wang, H., Wang, P., Zhao, M., Zhang, C., 2011. Spatial variations in archaeal lipids of surface water and core-top sediments in the South China Sea and their implications for paleoclimate studies. Applied Environmental Microbiology 77, 7479-7489.

Weldeab, S., Lea, D.W., Schneider, R.R., Andersen, N., 2007. 155,000 years of West African Monsoon and ocean thermal evolution. Science 316, 1303-1307.

Wuchter, C., Shouten, S., Coolen, M.J.L., Sinninghe Damsté, J.S., 2004. Temperature-dependent variation in the distribution of tetraether membrane lipids of marine Crenarchaeota: Implications for TEX_{86} paleothermometry. Paleoceanography 19, PA4028.

Wuchter, C., Schouten, S., Wakeham, S.G., Sinninghe Damsté, J.S., 2005. Temporal and spatial variation in tetraether membrane lipids of marine crenarchaeota in particulate organic matter: implications for TEX_{86} paleothermometry. Paleoceanography 21, PA4208.

Wuchter, C., Schouten, S., Wakeham, S.G., Sinninghe Damsté, J.S., 2006. Archaeal tetraether membrane lipid fluxes in the northeastern Pacific and the Arabian Sea: Implications for TEX_{86} paleothermometry. Paleoceanography 21, PA4208.

Zhang, Y.G., Pagani, M., Liu, Z., 2014. A 12-million year temperature history of the topical Pacific Ocean. Science 344, 84-87.

Zhu, C., Weijers, J.W.H., Wagner, T., Pan, J.-M., Chen, J.-F., Pancost, R.D., 2011. Sources and distributions of tetraether lipids in surface sediments across a large river-dominated continental margin. Organic Geochemistry 41, 376-386.

Zweng, M.M., Reagan, J.R., Antonov, J.I., Locarnini, R.A., Mishonov, A.V., Boyer, T.P., Garcia, H.E., Baranova, O.K., Johnson, D.R., Seidov, D., Biddle, M.M., 2013. World Ocean Atlas 2013, volume 2: salinity. Ed. by A. Mishonov. NOAA Atlas NESDIS 74, 39 pp.